DEVELOPMENT OF RECYCLED FRIENDLY ALUMINIUM ALLOYS FOR AUTOMOTIVE AND STRUCTURAL APPLICATIONS

DANIEL NG'ERA WANG'OMBE

DOCTOR OF PHILOSOPHY
(Mechanical Engineering)

JOMO KENYATTA UNIVERSITY OF AGRICULTURE AND TECHNOLOGY

2022

Development of Recycled Friendly Aluminium Alloys for Automotive and Structural Applications

Daniel Ng'era Wang'ombe

A Thesis Submitted in Partial Fulfilment of the Requirements for the Doctor of Philosophy in Mechanical Engineering of the Jomo Kenyatta University of Agriculture and Technology

2022

DECLARATION

This thesis is my original work and has not been presented for a degree in any other university.

Signature..... Date...../...../.....

Daniel Ng'era Wang'ombe

This thesis has been submitted for examination with our approval as university supervisors:

Signature..... Date...../...../.....

Prof. S. M. Maranga, PhD

JKUAT, Kenya

Signature..... Date...../...../.....

Dr. Bruno Robert Mose, PhD

JKUAT, Kenya

Signature..... Date...../...../.....

Dr. Thomas Ochuku Mbuya, PhD

UoN, Kenya

DEDICATION

This work is dedicated to those at the centre of my being: God, late dad, mum, Alice, Mercy, Grace and Prudence.

ACKNOWLEDGMENT

The research work presented herein, while full of challenges, turned out to be an adventurous, exciting, instructive and joyful experience that benefited; first, from the appropriate direction of my supervisors; Prof. S.M. Maranga, Dr. Bruno and Dr. Ochuku. I am extremely grateful for their patience, encouragement and guidance throughout the entire research period.

Secondly, I would also like to express my gratitude to Technical University of Mombasa (TUM), National Research Fund (NRF) and Jomo Kenyatta University of Agriculture and Technology (JKUAT) Research Production and Extension (RPE) division for funding this research.

Thirdly, experiments were carried out in laboratories in different institutions, whereby their personnel contributed immensely to the success of this work. I wish to thank Messrs. Mwai, Kathulima, Ombui and Amira of Engineering Workshops of JKUAT for their assistance during casting, extrusion and friction stir welding (FSW) respectively. Additionally I do acknowledge the support of Messrs. Kahiro and Maina of Department of Mechanical and Manufacturing Engineering of University of Nairobi (UoN) during microhardness testing and microstructural analysis. Further I wish to thank University of Southampton for offering their facility for high pressure torsion (HPT).

Last but not least, I am grateful to my wife and children for their constant support and encouragement. Their moral and spiritual support, encouraged me to push on with the research even during desperate times. Thanks a lot.

TABLE OF CONTENTS

LIST OF TABLES

LIST OF FIGURES

LIST OF APPENDICES

LIST OF ABBREVIATIONS

ARB	Accumulative Roll Bending
ASTM	American Society for Testing and Materials
BEI	Backscatter Electron Imaging
BM	Base Metal
BS	British Standards
CDRX	Continuous Dynamic Recrystallization
CHPT	Continuous High Pressure Torsion
CT	Computed Tomography
DAS	Dendrite Arm Spacing
DKU	Dedan Kimathi University
DRX	Dynamic Recrystallization
EBSD	Electron Backscattered Diffraction
ECAP	Equal Channel Angular Pressing
EDM	Electric Discharge Machine
EDX	Energy Dispersive X-ray Spectrography
EoL	End of Life
FSP	Friction Stir Processing
FSW	Friction Stir Welding
HAZ	Heat Affected Zone
HPT	High Pressure Torsion
HPTE	High Pressure Torsion Extrusion
HV	Vicker's Microhardness
JIS	Japanese Industrial Standard
JKUAT	Jomo Kenyatta University of Agriculture and Technology
KAM	Kenya Association of Manufacturers

KNBS	Kenya National Bureau of Statistics
KPA	Kenya Ports Authority
KPLC	Kenya Power and Lighting Company
KRA	Kenya Revenue Authority
MFA	Material Flow Analysis
NMC	Numerical Machining Complex
PJL	Plate Joint Line
RPE	Research Production and Extension
RPM	Revolutions Per Minute
SAD	Selected Area Difraction
SAED	Selected Area Electron Diffraction
SDAS	Secondary Dendrite Arm Spacing
SEI	Secondary Electron Imaging
SEM	Scanning Electron Microscope
SFE	Stacking Fault Energy
SPD	Severe Plastic Deformation
SZ	Stirred Zone
TEM	Transmission Electron Microscope
TMAZ	Thermal Mechanically Affected Zone
TUK	Technical University of Kenya
TUM	Technical University of Mombasa
TWI	The Welding Institute
UFG	Ultra-fine Grain
UoN	University of Nairobi

LIST OF SYMBOLS

F	Extrusion force [N]
Fe_{crit}	Critical iron level
K	Extrusion constant
N	Number of revolutions per minute
P	Extrusion pressure [MPa]
R	Extrusion ratio
T_m	Melting temperature [^{o}C]
V	Extrusion velocity [m/min]
Y_s	Yied strength [MPa]

LIST OF GREEK SYMBOLS

ϵ	Torsional strain
γ	Shear strain
ε	Equivalent strain
α-Al	Aluminium matrix
α-Fe	Alpha phase of iron intermetallics.
β-Fe	Beta phase of iron intermetallics
π-Fe	Pi phase of iron intermetallics
σ	Stress
σ_f	Nominal stress at fracture
σ_{uts}	Ultimate tensile strength
σ_y	Yield stress

LIST OF ELEMENTS

Al	Aluminum
B	Boron
Ca	Calcium
Cl	Chlorine
Cr	Cromium
Cu	Copper
Fe	Iron
Mg	Magnesium
Mg	Manganese
Na	Sodium
Ni	Nickel
O	Oxygen
Sc	Scandium
Si	Silicon
Sn	Tin
Ti	titanium
Zn	Zinc

ABSTRACT

Use of aluminium alloys for structural applications in Kenya is expected to be preferred to steel; due to their high resistance to corrosion, large strength-to-weight ratio and recyclability. However, it has not been the case because; first, availability of raw material (wrought aluminium structural scrap) has not been established. Secondly, processing of standard wrought alloys using mix scrap categories is costly, since it requires dilution with primary aluminium and alloying element adjustment. Finally, the alloys produced have low strength for broader structural applications. To overcome the challenges, recycling strategies that sort aluminium structural scrap component by component were investigated. Testing performance characteristics of the recycled sorted scrap melt was carried out to ascertain its structural acceptability. Therefore, this research aimed at developement of recycled friendly aluminium alloys for automotive and structural applications. An industry survey was conducted to establish the availability and consumption of aluminium scrap in Kenya. Data was collected from scrap dealers, foundries and agencies that handled either aluminium or aluminium data using a questionnaire, site visits and interviews. A mass flow analysis (MFA) was performed on the data collected. Mass flow analysis established that 9,948.4 tons of scrap were collected in year 2017. The scrap originated from automotive, construction, household, processing and electrical industries; in proportions of 41, 29.6, 19.1, 7.7 and 2.8 % respectively. The scrap consumed locally was 7,615 tons; and consisted of 3000, 6000 and 300 alloy series in ratios of 66.2, 25.2 and 8.6 % respectively. Aluminium structural scrap originated mainly from automotive and construction industries. 2,880 tons of pure aluminium were used to dilute the scrap. Based on the MFA results, four batches of wrought aluminium structural scrap from Nairobi dealers were sorted component by component. Each batch was melted and subjected to spectro-chemical analysis. Sorting considerably reduced cost associated with melting mixed scrap, followed by dilution with primary aluminium and adjusting alloying elements composition. The batches yielded secondary wrought alloys of 6000 series that were equivalent to 6005, 6061, 6063 and 6070 standard alloys. However, impurities of iron and zinc rose slightly while magnesium and manganese faded marginally. The secondary 6061 alloy was selected for further processing through extrusion, high pressure torsion (HPT) and friction stir welding (FSW). The selection was informed by its composition that matched its equivalent standard alloy; and its broad application in manufacture of automotive and structural components. Further, its behaviour was to be generalized to the other three alloys of the same series. The processes were expected to improve its microstructure and mechanical properties for better structural performance. As extruded 6061 secondary alloy had a strength of 214 MPa which matched with standard alloy. This showed that sorting scrap component by componet was a

cheaper alternative to use of mixed scrap and use of primary aluminium while developing the alloy. The extrudates were further processed by HPT at a pressure of 6.0 GPa, while varying turns from 0.25 to 10. HPT processing of the as extruded material broke down and homogenized the second phase particles. Average Vickers microhardness of HPT processed samples increased from 50 to 110 $HV_{0.3}$; while tensile strength increased from 214 MPa to 381 MPa. The extruded alloy was friction stir welded at spindle speed and feed rate varying from 530 to 1320 rev/min and 40 to 100 mm/min respectively. Microstructure, micro hardness, strength and ductility of samples were analysed at every stage. Friction stir welding refined grains of the alloy in the stirred zone. Maximum average microhardness of 70 $HV_{0.3}$ in stirred zone was obtained at lowest speed of 530 rev/min and highest feed of 100 mm/min. Therefore, microhardness was inversely proportional to spindle speed and directly proportional to feed rate. A maximum joint strength of 84 MPa was obtained at a speed of 915 rev/min and a feed of 100 mm/min. Through the research, it was found that available wrought Al scrap quantities can be recycled through alternative and cheaper methodology namely component by component to yield cheaper secondary alloys such as Al 6005, 6061, 6063 and 6070 alloys which are widely used for structural applications. This eliminated the need for expensive Laser assisted sorting machines which require huge investment. The mechanical properties and weldability of the extruded secondary wrought Al 6061 alloy were enhanced through HPT and FSW. However, FSW parameters including tool rotational speed,tool geometry and feed rate need to be optimized further in order to produce a much stronger joint.

CHAPTER ONE

INTRODUCTION

1.1 Background

Aluminium is the second most used metal after steel (Ayogu & Eze, 2019). Aluminium and its alloys have wide applications in transport, construction, food processing and electrical industries (Gao, Yi, Lee, & Lindley, 2004; D. S. Jiang, Lui, & Chen, 1999; Kaufman, 2006). The popularity arises from its superior properties; including: light weight, resistance to corrosion, high specific strength, high alloy tensile strength, good electrical conductivity and thermal conductivity (Nturanabo, Masu, & Kirabira, 2019).

Aluminium and its alloys are developed through smelting (primary processing) to produce standard alloys and recycling (secondary processing) to produce either standard or secondary alloys. Smelting bauxite yields pure aluminium, with low tensile strength between 90 to 140 N/mm^2 (Kraisat & Jadyil, 2010). Alloying the pure aluminium produces standard alloys that have improved mechanical properties. Further, depending on the alloying element present, the alloys can be strengthened by either heat treatment or strain hardening. Aluminium standard alloys are classified as wrought or cast alloys. Aluminium cast wrought alloys are futher processed through extrusion, rolling and forging to produce finished or semi-finished products. The products are scrapped at the end of their useful life.

Aluminium scrap is recyclable. Developing aluminium alloys through recycling of scrap is friendly due to its:- economic benefits, environment conservation and higher repeatablity. First, aluminium recycling is preferable to smelting because it is

cheaper since it saves 95% of the energy required during primary processing (Kumari, Pillai, Nogita, Dahle, & Pai, 2006). In addition, mining and processing of bauxite degrades the environment by changing the landscape and emitting carbon dioxide (Das, Green, & Kaufman, 2010).

Several studies on recycling of cast Al alloys have reported on improvement of castability and mechanical properties of recycled cast alloys (Kumari et al., 2006; Mbuya, Bruno, Ng'ang'a, & Maranga, 2010; Ng'ang'a, Odera, Mbuya, & Oduori, 2010; Wangombe, 2014). Other studies report that cast alloys are popular among the recycled products, since they have higher concentration of alloying elements and higher tolerance limits for impurities as opposed to wrought alloys (Das, 2006; Kevorkijan, 2010). As a result cast products can be made from a combination of either wrought and cast scrap or just only cast scrap (Green, 2007). On the other hand, development of standard wrought aluminium alloys from recycled scrap is challenging because they require tight compositional limits. Development of standard structructural wrought aluminium alloys from scrap is carried out in three steps (Das, 2006; Kevorkijan, 2010). First, mixed scrap is identified. Secondly, the scrap melt is diluted with primary aluminium. Finally, alloying elements are added to the melt, in order to correct its composition to the required tight limit. The actual composition is confirmed by use of a spectrometer. This procedure is very costly. After casting, the wrought alloys are processed through metal forming. Structural wrought aluminium alloys are mostly processed through extrusion.

An attempt to overcome the tight compositional limits of standard wrought aluminium alloys during recycling has been made by proposing production of secondary aluminium alloys that contain moderately wider specification limits on alloying elements, while being lenient on higher limits of impurities and without substantial restriction on performance characteristics (Das, 2006; Kevorkijan, 2010, 2013). This can be achieved by avoiding use of mixed scrap through meticulus scrap sorting. Sorting criterion is usually based on the scrap physical properties, its former

application, and its reaction with corosive chemicals. Physical properties include density and colour. The practice will allow direct consumption of the sorted scrap; and thus avoid use of costly pure aluminium for dilution and addition of elements to adjust to correct compositional levels and mitigate advese effects of impurities. Avoiding the two steps of dillution and alloy adjustment through scrap sorting will reduce the cost of the recycled alloy. The resultant wrought secondary structural alloy is usually processed through extrusion. The performance charasteristics of the extruded structural material can be enhanced further by application of severe plastic deformation processes including high pressure torsion (HPT) and friction stir welding (FSW).

HPT is an emerging technology that has been found to improve mechanical properties of material (Sakai et al., 2005). It involves application of high pressure and a twisting moment on a material. Thus introducing severe plastic deformation on a material without changing its shape. Such deformation increases the hardness and tensile strength of a material. Initially the size of HPT components was 10mm diameter and 0.8mm thickness (Sakai et al., 2005). Over time the HPT components have increased in size to a discs 40mm diameter and rings of 100mm diameter (Edalati & Horita, 2009). Improved continuous high pressure torsion (CHPT) has created a room for processing long materials inform of wires or sheets (Edalati, Lee, & Horita, 2012).

Riveting and welding are used to join wrought aluminium alloys. Fusion welding methods that are used to join aluminium are arc, laser beam and electron beam welding. Challenges associated with fusion welding of aluminium alloys include high thermal conductivity, porosity, oxide inclusions and solidification cracking (Olabode, Kah, & Martikainen, 2013). FSW is solid state welding technique that can overcome the fusion welding challenges (Kwon et al., 2002; Sen & Sharma, 2016). During FSW, a rotating tool with a shoulder and terminating in a pin, moves along the butting or lapping surfaces of two rigidly clamped plates placed on a backing plate. The

tool motion first, produces frictional heat that plasticizes the material and secondly stirs the metal until a welded joint is formed. The joint is formed at temperatures below the melting temperature, thus avoiding flaws associated with high heat input (Vimalraj & Kah, 2021).

1.2 Problem Statement

Aluminium recycling industry is promising since it conserves processing energy and environment. However, it has not thrived as expected since it is facing challenges associated with scrap trading and melting (Wangombe, 2014). Kenyan scrap dealers collect aluminium scrap and either export it or sell it to local foundries. Data about availability and consumption of the scrap is vague and is therefore, one of the activities to be studied in this work. The cheap scrap is exported to European and Asian markets where it is used to make costly products that are imported back. Opportunities for job creation, availability of cheaper products and higher foreign earnings are lost when large proportion of scrap is exported without value addition. The initaial stages of development of the recycled friendly structural alloy requires establishment of availability of the required scrap through a survey.

Previous industry survey found that the micro-foundries utilized inferior technology, which resulted in predominant production of low-grade castings (Mose, 2009). The products include house ware (pans and pots), machine components (pulleys and gears), automobile parts (spacers) and decorations for welded steel grills. A number of researchers have conducted studies on secondary cast aluminium alloys (Mbuya et al., 2010; Mose, 2009; Njuguna, 2007; Wangombe, 2014; Zeru, 2014). From the studies it was found that adjustment of minor alloying elements improved castability, microstructure and mechanical properties of the ensuing alloys. The research emphasis on secondary cast alloys have encourage the growth of aluminium casting industry. However, research on production of secondary wrought aluminium alloys has not been done fully since the products are costly due to the use of costly

production procedures. This study will explore on development of structural wrought alloys that will use sorted scrap directely, and thus avoid addition of alloying elements which is a costly procedure.

Recycling of scrap to produce structural wrought alluminium alloys requires addition of costly pure aluminium followed by adjustment of alloying elements. This practice makes the resultant secondary alloys and their associated products to be costly. Consequently, the products face competition from cheaper materials like iron and imported aluminium structural materials. There is a need to develop cheaper wrought aluminium secondary alloys that can directly consume the structural scrap Al from Kenyan market. The variant structural alloys produced by direct consumption of scrap may have broader concentration of alloying elements and higher level of impurities. The effect of variation on concentration of alloying elements and higher level of impurities in the recycled wrought alloys need to be investigated.

Use of sorted scrap either directly or with minimum modification will avoid use of costly primary aluminium.However, the secondary wrought aluminium alloys will be of low grade. Their performance characteristics will be lowered due to variation of alloying elements and raised limit of impurities. Extrusion alone will not be sufficient to improve their mechanical properties to levels required for structural applications. After sorting and melting the scrap, the novel material being developed from the scrap need to be subjected to to microstructure analysis and mechanical tests in order to compare its response with the equivalent standard alloy.

Further processing of the extruded structural wrought aluminium alloys using emerging SPD techniques of HPT and FSW is expected to improve their microstructural properties, mechanical properties and weldability. HPT has been found to improve the microstructural and mechanical properties of materials. The process has been used to produce mini-components such as screws and washers. Over time the size of the components has increased to rods and sheets. This

will allow for the production of bigger structural components. HPT processing is expected to minimize defects in the microstructure of the secondary wrought alloys; thus increasing their strength and hardness. Fusion welding of structural wrought aluminium alloy structures faces challenges associated with melting of aluminium. However, FSW is a solid state welding process. The welding temperature is below the melting temperature of the wrought aluminium alloys. The low temperature is expected to overcome the challenges associated with fusion welding and thus improve the weldability of a material the recycled wrought Al alloys.

1.3 Objectives

The key objective of this study was to develop recycled friendly aluminium alloys for automotive and structural applications derived from sorted wrought aluminium structural scrap. This was achieved by carrying out the following specific objectives:

1. To establish the availability of suitable scrap for development of recycled wrought aluminium structral alloy.
2. To characterize performance characteristics of extruded structural wrought aluminium alloys derived from the sorted scrap.
3. To investigate performance characteristics of the extruded structural secondary wrought alloy through HPT.
4. To determine weldability of the extruded structural secondary wrought alloy through FSW.

1.4 Justification and Significance of the Study

Kenyan aluminium industry relies heavily on scrap. The meticulus scrap sorting methodology will be a major boost to this industry. Introduction of the alloy

in the market will enhance Kenyan goverment emphasis on growth of industerial manufacting by 2030.

Development of aluminium structural wrought alloy from scrap is friendly environmentally and economically. Since, it recycle materials that are difficult to dispose and does not disturb environment as in the case of minning aluminium ore. Aluminium recycling compared to primary processing is cheaper by 95 % interms of energy consumption. Recycling scrap is an economic activity that creates employment and generates income. The recycled structural alloy obtained directly from melting sorted scrap is cheaper than the standard alloy as it avoided dilution of scrap melt with primary aluminium, adjustment of the level of alloying elements and mitigating the adverse effects of impurities which are costly. Enhancement of the recycled alloy's properties through HPT will strengthen it. The weldability of the structural wrought aluminium alloy will be improved by FSW. All the benefits of this study will contribute immensely towards production of cheaper secondary wrought aluminium alloys that will compete with steel and standard aluminium wrought alloys in structural applications. The alloy developed will find wide application in the fabrication of aotomotive body panels and structures; rail coach structures; building structures including windows, doors, partitions and civil works including bridge railings.

1.5 Thesis Structure

This thesis is organized into five chapters. The first chapter covers the background, problem statement, objectives and justification of the study. Chapter two consists of literature review on fundamentals, applications and material flow analysis (MFA) of aluminium and its alloys with particular attention to its recycling. Further post cast processing techniques including extrusion and SPD have been reviewed. Chapter three outlines the methodology used in collecting data for this research. The fourth chapter gives the results, their analysis and discussions. The fifth chapter enumerates

the conclusions and recommendations, emanating from this study.

CHAPTER TWO

LITERATURE REVIEW

2.1 Overview

Rise in demand of structural aluminium alloys in industries including: automobile, electrical transmission, building and construction has been noted. The demand has been triggered by light weight and high strength to weight ratio of aluminium and its alloys, which make them better alternatives to ferrous materials. The demand can be met through recycling local aluminium scrap. Tight compositional limit of primary aluminium alloys has been a major challenge during recycling. However, a knowledge of aluminium alloys, applications, material flow analysis (MFA) and meticulous selection of readily available scrap during melting is required so as to yield recycled structural alloys that can compete with standard alloys. Evaluation of the properties of the recycled alloys is key in determination of threshold for their application.

This section reviews on aluminium recycling with respect to understanding aluminium and its alloys, effects of minor alloying elements, applications of the alloys, MFA and recycling challenges. Recent post cast processing technologies such as HPT and FSW, will be reviewed. The methods have been found promising in enhancing mechanical properties of aluminum alloys.

2.2 Aluminium, Aluminium Alloys and their Applications

Aluminium products at the end of their useful life become a source of recyclable scrap. Aluminium recycling can be understood properly by first looking at aluminium, its alloys and their applications.

2.2.1 Aluminium

Pure aluminium has high formability, corrosion resistance and can be strain hardened (Askeland, Phulé, Wright, & Bhattacharya, 2003). Its mechanical properties are mainly enhanced by alloying with major and minor alloying elements. However, some elements exist in the alloys as impurities. Resultant alloys are broadly classified into wrought and cast alloys; and each class is further categorized into series based on major alloying elements such as Cu, Mn, Mg, Mg and Si, and Zn (Kevorkijan, 2010; King, 1987). Each series has properties that make it best suited for particular application(s). Scrap from products that are no longer in use is recyclable.

2.2.2 Classification of Wrought Aluminum Alloys

Wrought Al alloys are mainly produced from primary aluminium and accommodate small quantities of impurities. They find use in a wide range of engineering applications depending upon the alloy series as summarized in Table 2.1. Basically, the alloy series are classified as non-heat treatable (1xxx, 3xxx and 5xxx) and heat treatable alloys (2xxx, 6xxx and 7xxx).

2.2.2.1 Non-heat Treatable Wrought Al Alloys

The non-heat treatable wrought Al alloys include 1xxx, 3xxx and 5xxx series. Most 4xxx alloys are non heat treatable except 4032 and 4145 alloys. Non-heat

Table 2.1: Categories, Properties and Applications of Wrought Aluminium Alloys.

Alloy	Properties and Applications
1xxx (pure Al)	Properties: ultimate tensile Strength (70 - 185 MPa); strain hardened; extremely high corrosion resistance, formability and electrical conductivity. Applications: electrical cables (1350), food wrappings (1105), chemical piping(1060), sheet, tanks, chemical containers, space mirrors
2xxx (Cu based)	Properties: ultimate tensile strength (185 - 430 MPa); heat treatable; susceptible to corrosion; difficult to weld. applications: Aircraft wings (2024, 2124 and 2314), engine (2618) and fuselage; truck beams (2014) and automotive wheels (2014)
3xxx (Mn based)	Properties: ultimate tensile Strength (110 - 285 MPa); strain hardened; ductile; high resistance to corrosion. Applications: cook ware (3003); heat exchanger tubing; chemical piping (3003); can bodies (3004 and 3104); building and construction (3005, 3104 and 3105)
4xxx (Si based)	Properties: ultimate tensile strength (170 - 380 MPa); heat treatable; Applications: Forged aircraft pistons (4032); welding rods for 6xxx alloys (4043)
5xxx (Mg based)	Properties: ultimate tensile strength (125- 350 MPa); heat treatable; ductile; and non-corrosive. Applications: sheets and plates for building and construction, bridges (5083), storage tanks; automotive body frames and inner panels(5754); rail car body (5454; and ends of cans (5182)
6xxx (Mg and Si based)	properties: ultimate tensile strength (125 - 400 MPa); heat treatable; non corrosive; and less ductile. Applications: Extrusions for automotive body frames (6063), body panels (6022, 6111), truck beams (6070); construction and structural elements (6005, 6061 and 6063); electrical wire (6201), bus conductor (6101), electrical cable towers (6061 and 6063); 6061 is a general purpose alloy used in air craft, marine yachts, piping, automotive body
7xxx (Zn based)	Properties: ultimate tensile strength (220 - 605 MPa); heat treatable; low resistance to corrosion; difficult to weld, and requires skill to produce and fabricate. Applications: Automotive bumpers (7116 and 7129), armored vehicles; air craft parts (7045 and 7075), fuselage (7050); and bridges (7045 and 7075)

treatable alloys are strengthened by strain hardening or microstructure refining. Strain hardening occur during cold working processes like forging rolling, drawing and extrusion. Cold working increases tensile strength, yield strength and hardness, at the expense of ductility.

The tensile strength of 1xxx and 3xxx alloys after strain hardening rises to a maximum of 185 MPa. Such strength is not suitable for structural applications. The 5xxx series alloys contain Mg as a major alloying element. Their tensile strength is maximum at 350 MPa, after strain hardening during cold working. They withstand corrosion even in salty environments and maintain their toughness even at cryogenic temperature(Smallman & Bishop, 1999). They are easily welded by a variety of techniques. The properties allow the 5xxx series alloys sheets and plates to be used in structures.

2.2.2.2 Heatreatable Wrought Al Alloys

Wrought Al alloy series that are heat treatable include 2xxx, 6xxx and 7xxx). The alloy series are strengthened by precipitation hardening due to the presence of strengthening second phase particles. The heat treatable structural alloys gain their maximum strength when subjected to T6 thermal treatment. A standard T6 heat treatment consists of solutionizing, quenching and ageing. Solutionizing involves holding an alloy at a temperature slightly below the eutectic point so as to break down the precipitates, homogenize the alloying element concentration in the α-phase and modification of the morphology of second phases. Quenching is rapid cooling of the solutionized alloy in order to preserve the solute in a super-saturated solid solution. Ageing involves subjecting the supersaturated solution to a room temperature or a slightly higher temperature over a period of time so as to separate strengthening phases from the supersaturated solid solution. The heat treatment improves the mechanical properties of the alloy.

The 2xxx wrought aluminium alloys chiefly contain Cu. Addition of Cu increases ultimate tensile strength to a range of 185 - 430 MPa; and makes them heat treatable (A. W. Zhu, Gable, Shiflet, & Starke Jr, 2002). Phases containing Cu, Si and Mg which include Al_2Cu, Mg_2Si and $Al_5Mg_8Si_6Cu_2$ enhance the precipitation hardening the alloys (Elgallad, Samuel, Samuel, & Doty, 2010). Heat treatment of 2014 and 2024 alloys during extrusion has been found to improve mechanical properties at the lowest possible concentrations of Cu and Mg (Lesniak & Woznicki, 2012). Products of these alloys are susceptible to corrosion and are difficult to weld. However, cladding or coating of the products reduces corrosion. Usually the products are joined by riveting, screws and fasteners. The alloys are available in form of rolled sheets or extruded sections.

Table 2.2: Composition (%) of Alloying Elements in Common 6xxx Alloys (Davis, 1993).

Alloy	Si	Fe	Cu	Mn	Mg	Cr	Zn	Ti	Others
6005	0.6 - 0.9	0.35	0.10	0.10	0.4 - 0.6	0.1	0.1	0.15	0.15
6016	1.0 - 1.5	0.5	0.2	0.2	0.25 - 0.6	0.1	0.2	0.15	0.15
6061	0.4 - 0.8	0.7	0.15 - 0.4	0.15	0.8 - 1.2	0.04 - 0.35	0.25	0.15	0.15
6063	0.2 - 0.6	0.35	0.1	0.1	0.45 - 0.9	0.1	0.1	0.1	0.15
6463	0.2 - 0.6	0.15	0.2	0.05	0.45 - 0.9	-	0.05	-	0.15
6070	1.0 - 1.7	0.5	0.15 - 0.4	0.4 - 1.0	0.5 - 1.2	0.1	0.2	0.15	0.15
6082	0.7 - 1.3	0.5	0.1	0.4 - 1.0	0.6 - 1.2	0.1	0.25	0.15	0.15
6101	0.3 - 0.7	0.5	0.1	0.03	0.35 - 0.8	0.03	0.1	-	0.15
6201	0.5 - 0.9	0.5	0.1	0.03	0.6 - 0.9	0.03	0.1	-	0.15
6111	0.6 - 1.1	0.4	0.5 - 0.9	0.1 - 0.45	0.5 - 1.0	0.1	0.15	0.2	0.15

Al 6xxx alloy series shown in Table 2.2, contain Mg and Si as the major alloying elements. The alloying elements enable them to respond well to heat treatment with a maximum strength in T6 temper. The alloys derive their strength from the precipitation hardening phase, Mg_2Si. Swaged 6066 alloy was found to have optimum strength and hardness when solutionized for 95 minutes at 530 ^{0}C followed by ageing at 175 ^{0}C for 8 hours (Tan & Ogel, 2007). Presence of the alloying elements increase strength at the expense of ductility. Ultimate tensile strength of the alloys

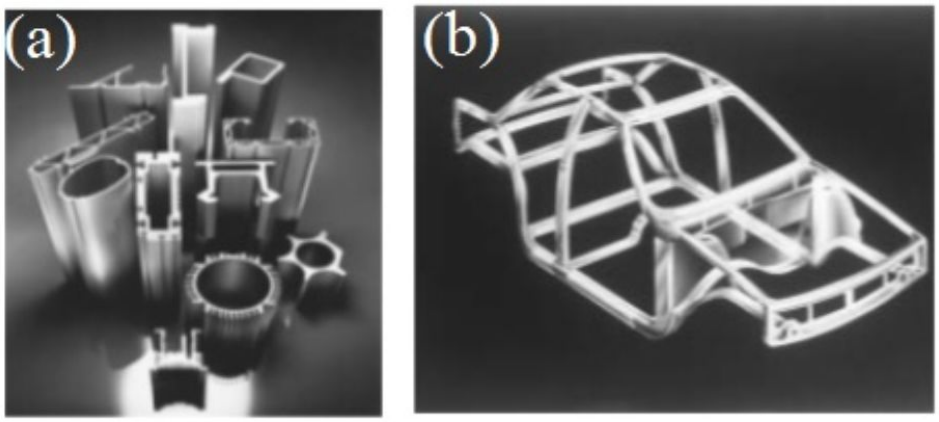

Figure 2.1: 6xxx (a) Extruded Sections and (b) Audi Space Frame (Kaufman & Rooy, 2004).

ranges from 125 - 400 MPa. The 6xxx series compared to other structural alloys have medium strength, high formability, excellent weldability, exceptional corrosion resistance, and low cost (Troeger & Starke, 1999). Fabrication of products from these alloys involves extrusion,rolling and at times forging. Examples of extruded products are shown in Figure 2.1. The alloys can be used in aircraft and automotive to replace the more expensive 2xxx and 7xxx alloys.

The 7xxx series alloys contain Zn as the major alloying element. These alloys contain the highest ultimate tensile strength ranging from 220 - 605 MPa, are heat treatable, have low corrosion resistance, are difficult to weld and requires a lot of skill during production and fabrication(Muller, 2011).

The 6xxx series alloys compared to 2xxx, 5xxx and 7xxx series are attractive as they have wide range of engineering uses because of their relatively low cost, high resistance to corrosion, medium strength, ease of welding and formability through extrusion, rolling and forging. A high proportion of extruded materials are produced from the 6xxx series.

2.2.3 Cast Aluminum Alloys

Cast aluminum alloys have bigger percentages of alloying elements and impurities than wrought alloys. Their five series are based on chief alloying elements that include Cu, Si, Mg and Zn as shown in Table 2.3. The alloys range from 2xx.x to 7xx.x series. The 2xx.x, 3xx.x and 7xx.x alloys are heat treatable while the 4xx.x and 5xx.x are non-heat treatable.

Table 2.3: Categories, Properties and Applications of Cast Aluminum Alloys.

Alloy	Properties and applications of cast alloys
2xx.x (Cu based)	Properties: high ultimate tensile strength (130 - 450 MPa) at room and elevated temperatures; heat treatable and poor castability. Applications: automotive cylinder heads, engine blocks, and piston heads (203.0); aerospace industry (201.0 and 204.0)
3xx.x (Si based with Mg and Cu)	Properties: ultimate tensile strength (130 - 275 MPa); heat treatable, excellent castability. Applications: cylinder heads (319, 354, 355, 356 and 380); pistons (332, 336 and 339); engine blocks (319, 332 and 390); alloy wheels (356), gear boxes and housing (357 and 380)
4xx.x (Si based)	Properties: ultimate tensile strength (115 - 170 MPa), non-heat treatable. Applications: engine blocks and pistons.
5xx.x (Mg based)	Properties: strength (115 - 170 MPa); non heat treatable. Applications: door and window fittings, marine applications (512.0 and 514.0)
7xx.x (Zn based)	Properties: ultimate tensile strength (205 - 380 MPa); heat treatable. Applications: aircraft, garden tools, office machines, farming implements and plant machinery parts

2xx.x alloys contain copper in concentrations of 4 to 8%; and are heat treatable. Addition of copper increases their strength by solid solution and precipitation hardening(Mohamed, Samuel, & Kahtani, 2013). They have high ultimate tensile strength at room and elevated temperature in the range of 130 - 450 MPa. However; they have poor castability. The alloys are used in automobile industry to cast cylinder heads, engine blocks and piston heads (203.0); and in aerospace industry (201.0 and

204.0).

Table 2.4: Composition (%) of Common Commercial 3xx.x alloys (Kaufman & Rooy, 2004).

Alloy	Si	Cu	Mg	Fe	Mn	Ni	Zn	Ti
319.0	5.5 - 6.5	3.0 - 4.0	0.10	1.0	0.5	0.35	1.0	0.25
332.0	8.5 - 10.5	2.0 - 4.0	0.5 - 1.5	1.3	0.5	0.5	1.0	0.25
336.0	12.0	1.0	1.0	1.2	-	2.5	0.35	-
339.0	12.0	2.25	1.0	1.2	-	1.0	1.0	-
354	9	1.8	0.5					
355	5	1.25	0.5					
A356.0	6.5 - 7.5	0.25	0.25 - 0.45	0.2	0.1	-	0.1	0.2
A357.0	6.4 - 7.5	0.2	0.45 - 0.7	0.2	0.1	-	0.1	0.2
A380.0	7.5 - 9.5	3.0 - 4.0	0.1	1.2	0.5	0.5	3.0	-
A390.0	16.0 - 18.0	4.0 - 5.0	0.45 - 0.65	1.3	0.5	0.1	1.5	0.2
A413.0	11.0 - 13.0	1.0	0.1	1.3	0.35	0.5	0.5	-

3xx.x alloys are also called aluminum silicon (Al-Si) alloys, since they have silicon as the major alloying element as shown in Table 2.4. Concentration of silicon in these alloys is between 5 to 17 % (Sabatino & Arnberg, 2009). These are the most common commercial casting alloys because of their superior casting properties including: ultimate tensile strength ranges from 130 - 275 MPa, high fluidity, excellent feedability and freedom from hot shortness (Kaufman & Rooy, 2004). The heat of fusion of silicon is about five times that of aluminium and therefore significantly improves the fluidity of aluminium silicon alloys(Kaufman & Rooy, 2004). Expansion of silicon upon solidification counteracts the solidification shrinkage of aluminum from 6.7 % to 4.5 % depending on the amount of silicon. In mildly acidic environments silicon increases the corrosion resistance of pure aluminum (Kaufman & Rooy, 2004). Magnesium concentration of about 0.1 to 0.7 % in aluminum silicon alloys allow them to respond well to T6 heat treatment. Aluminum silicon alloys are used to cast: cylinder heads (319, 356, 380, 355 and 354), Pistons (332, 336, 339), engine blocks [380 ($AlSi_8Cu_3$), 319 ($AlSi_6Cu_4$), 332 ($AlSi_9Cu_3Fe$) and 390 ($AlSi_{17}Cu_4Mg$)], alloy wheels (A356), Gear boxes and housing (357 and 380),

and rear axle housing (380).

The 4xx.x alloys are composed of mainly 5 - 12 % silcon. They are non-heat treatable; and have high fluidity, weldability and strength. They are used to cast pump casing, cook wares and railings.

Magnesium which forms the basis of the 5xx.x series, is added to aluminum foundry alloys in concentrations of 4 to 8 %. The alloys are non-heat treatable. Without silicon, the magnesium aluminum foundry alloys have poor castability. Their applications include: door and window fittings; and marine applications 512.0 and 514.0.

The 7xx.x series alloys are based on the aluminum-zinc system and have relatively narrow freezing ranges and moderate castability (Sabatino & Arnberg, 2009). Their ultimate tensile strength ranges from 205 - 380 MPa and are heat treatable. Zinc forms intermetallic compounds such as $MgZn_2$ that promote precipitation hardening (Callister, 2007; Rana, Purohit, & Das, 2012). Their applications include: bushing and bearings, office machines, farming equipment and mining equipment.

Both aluminum and its alloys have found applications in a number of the major markets. Consequently, the local scrap is expected to be generated from these industries.

2.2.4 Effects of Minor Alloying Elements and Impurities

Minor alloying elements are added as modifiers, grain refiners and iron correctors. Modifying agents like sodium, strontium and calcium alter the shape of eutectic silicon from acicular to a fibrous form; which improves significantly the mechanical properties of the alloy(Kumari et al., 2006). Addition of modifiers in aluminum alloys have been found to improve strength, increase elongation, toughness and fatigue properties (Kaufman & Rooy, 2004; Kumari et al., 2006; Lui, Samuel, &

Samuel, 2003; Njuguna, 2007; Wangombe, 2014). However, optimum concentration of the modifier is essential to avoid the associated defects like porosity and oxide inclusions(Mbuya et al., 2010; Mose, 2009).

Fine equiaxed grains in aluminium alloys are usually achieved either through increased solidification rate (direct chill casting) and/or addition of grain refiners that mainly contain titanium and boron (Kashyap & Chandrashekar, 2001; Zhang, Chen, & Poirier, 2000). A completely fine-grained structure is preferred, since it is stronger and more ductile. The structure has been found to result in several advantages in the casting stage, and subsequent mechanical (extrusion, rolling and forging), thermal and surface treatment steps (Lumley, 2011; Ramachandran, Sharma, & Balasubramanian, 2008). Grain refinement during casting enhance feeding, minimize segregation, mitigate the micro porosity and alleviate cracking (hot tearing and cracking). Trace additions of nickel improves hot hardness of aluminum alloys (Rana et al., 2012). During further processing of the grain refined cast alloys; formability, machinability, heat treatment and anodizing become better.

Elements like iron may be present as impurities with deleterious effects on the properties of the alloy Kraisat and Jadyil (2010). It forms hard and brittle intermetallics in aluminium alloys (Taghaddos, Hejazi, Taghiabadi, & Shebestari, 2009). The Fe-rich phases have three distinct shapes as shown in Figure 2.2; and include needles (β-Fe), Chinese script (α-Fe), globular rosettes (π-Fe), hexagonal, star-like and indefinite forms (Taylor, 2004; Wang, Jones, & Osborne, 2003). Presence of β-Fe, particularly as large platelets, cause a significant reduction in fatigue, impact, fracture toughness, tensile strength, ductility and corrosion resistance arising from their brittle nature (Kraisat & Jadyil, 2010; Mrówka-Nowotnik, Sieniawski, & Wierzbiñska, 2007; Murali, Arvind, & Raman, 1997; Taylor, 2004). The brittle phase initiate mini cracks and also lay an avenue for propagation of big cracks during fatigue failure. The α-Fe particles are more resistant to crack initiation and propagation than the β-Fe. Presence of iron in

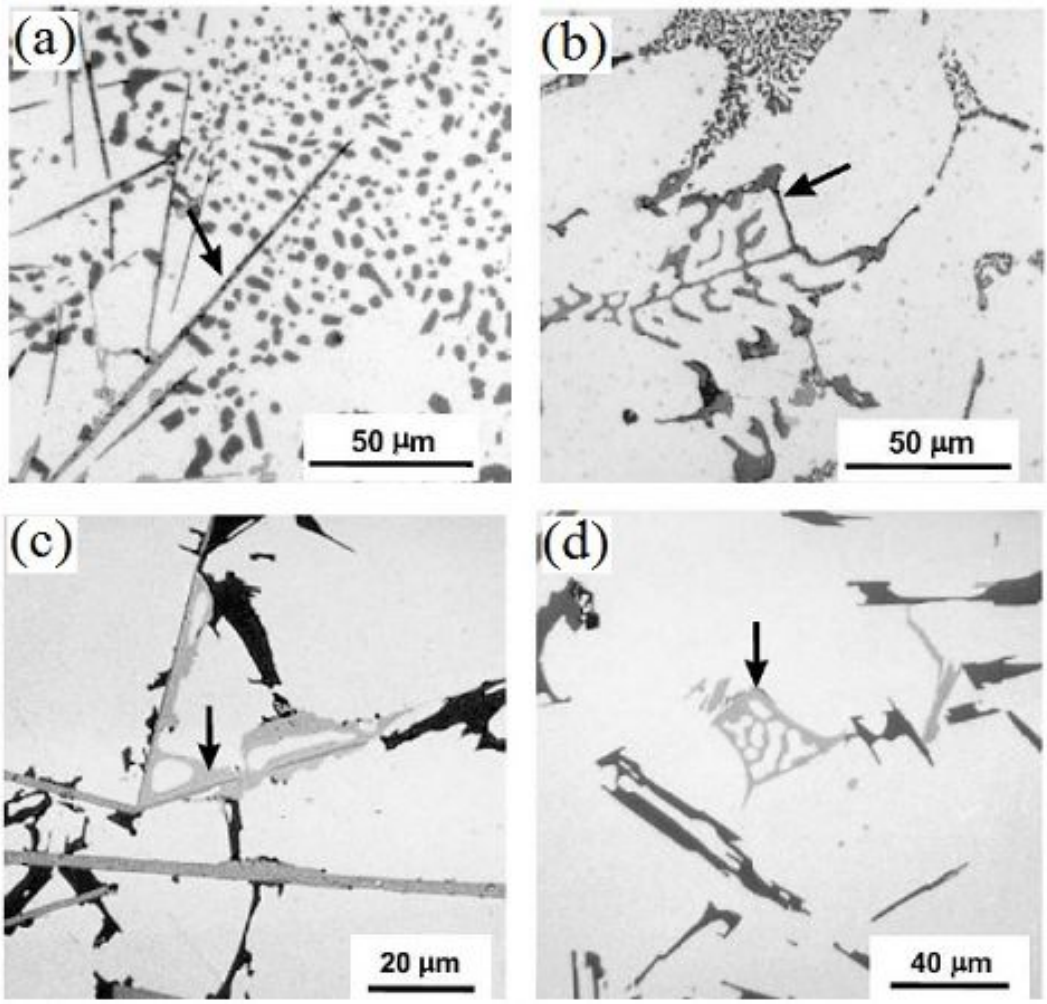

Figure 2.2: Micrographs of Common Iron-Containing Intermetallics Shown by Arrows: (a) β-Fe; (b) α-Fe (c) Π-Fe Growing from β-Fe (d) Π-Fe(Taylor, 2004).

380 alloy has been found to decrease fluidity(Ravi, Pillai, Amaranathan, Pai, & Chakraborty, 2008); and in another instance increased the size and amount of shrinkage porosity(Ammar, Samuel, & Samuel, 2008; Wang et al., 2003), since the intermetallics formed interfere with interdendritic feeding. Porosity is detrimental to both impact and fatigue properties.

A number of approaches to mitigate the deleterious effect of iron has been suggested(Lakshmanan, Shabestari, & Gruzleski, 1995; Taghaddos et al., 2009; Taylor, 2004; Wen, Hu, & Gottstein, 2003). The approaches point at either discouraging formation of β-Fe and/or promoting formation of α-Fe in molten metal. Two strategies favoring development of α-Fe include: temperature manipulation and iron correction. Temperature manipulation involves superheating of melt to high temperatures before pouring, and accelerating the cooling rate. Super heating followed by high cooling rate suppresses the formation of the β-Fe and some of it reacts with the remaining melt to form the π-Fe.

Addition of iron correcting elements including manganese, chromium and cobalt to aluminiun alloys neutralize the harmful effects of iron. When trace additions of manganese are added to aluminium-silicon alloys, the more detrimental β-Fe intermetallics are modified to α-Fe. Optimum results are obtained when the ratio of manganese to iron is maintained at 2:1. The resultant phase is visible in the microstructure either usually as Chinese script or occasionally as polyhedrons when solidified as a primary phase that is less harmful compared to β-Fe. Additionally, manganese refines Al-Si eutectic grains in the solidifying metal and thus boosting feeding; and consequently reducing micro-porosity(Taylor, 2004). Manganese above the recommended level should be avoided at all costs because it forms a sludge that has a potential of destroying furnace walls and forming hard spots in castings(Taghaddos et al., 2009). The spots are difficulty to machine.

However, presence of iron has been found to have 3 benefits(Kaufman & Rooy,

2004; Kraisat & Jadyil, 2010; Taghaddos et al., 2009). First, adding about 0.5 % iron to aluminum (Al-99.84 %) used for electrical cables lead to grain refinement that resulted to superior mechanical properties. Their strength was increased while maintaining suitable ductility at ambient temperature. Secondly, iron is intentionally added (up to 1 %) in die casting to prevent die soldering or sticking. Finally, iron improves hot tear resistance.

2.3 Applications of Aluminum Alloys

Applications of aluminum alloys to a number of the major markets has been reviewed(EAA, 2011; Kaufman, 2006). The various markets include: marine, rail automobile and air transport as shown in Table 2.5. Non transport markets include electrical, packaging, chemical industry, building and construction and others, as shown in Table 2.6. An understanding of the markets and their associated products can be beneficial while identifying the potential alloys in the scrap.

Table 2.5: Transport Markets for Aluminium Alloys.

Market	**Products**	**Aluminum alloys**
	structural beams	5083, 5383, 6061 and 6063
Marine transportation	hull material	5083, 5383, 6061 and 6063
	beams	2014, 6061 and 6070
	exterior panels	5456 and 6111
Rail transportation	tank cars	5083 and 5454
	coal cars	5083, 5454 and 5456
	cars for hot cargo	5454
	wheels	2014 T_6 and A356.0
	Housings and gear boxes	A357.0
Automobile	Truck trailer bodies	5083, 5454 and 5456
	Truck beams	2014 and 6070
	Racks and rails	6061 and 6063
	Engine components	2618
Aircraft	wing and fuselage skin	2024 and 7050
	wing structures	2024, 2124, 2314 and 7050
	propellers	2025

Table 2.6: Non Transport Markets for Aluminium Alloys.

Market	Products	Aluminum alloys
	electrical cable	1350 and 6201
Electrical	bus conductor	6101
	electrical cable tower	6063 and 6061
	bridges and highway structures	5083, 5454, 6061 and 6063
Building and	building sheet and siding	3005, 3105 and 5005
construction	composite wall panel	6063
	bridge rail mount	357.0 T_6
	aluminum foil	1175
Packaging	can bodies	3004
	can ends	5182
	piping	1060, 5254 and 6063
2-3Chemicals	pressure vessels	5083, 5086, 6061 and 6063
	cryogenic tankage	5052, 5083, 5454, 6061 and 6063
	containers for hydrogen peroxide	5254 and 5652
	screw machine products	2011 and 6262
	door handles and roofing sheets	5005 and 5052
Others	tread plate	6061
	wire	4043, 5183, 5356 and 5556

2.3.1 Applications of Cast Alloys

Common cast alloys used fall in 3xx.x series. This comprises of cylinder heads 319 (AlSi6Cu3.5), 354 (AlSi9Cu1.8Mg0.5), 356 (AlSi7Mg0.32) and 380 (AlSi8Cu3.5); alloy wheels 356 and 357 (AlSi7Mg0.52); and gear housing 319 and 357. Al-Si alloys with Cu, Mg and Ni have been used to cast pistons (Z. Li et al., 2004; Ng'ang'a et al., 2010). Engine blocks are made of A380.2 and A319 cast alloys. Copper allows the casting to maintain strength at high temperatures. Silicon improves fluidity and in presence of magnesium strength is improved. Scrap from these components have been used to produce secondary alloys. Most studies (Mbuya et al., 2010; Ng'ang'a et al., 2010; Wangombe, 2014; Zeru, 2014) have used scrap from one automotive component for example piston, cylinder head or alloy wheels to ensure that the resulting secondary alloy has a composition similar to the source.

Alloy 380 has high amount of silicon and copper compared to 319, 356, 357. This

means that scrap from these three later alloys can be used directly to cast the former alloy with minor alloy modification.

2.3.2 Structural Wrought Aluminium Alloys

Common structural wrought aluminium alloys fall in 5xxx and 6xxx alloy series. The alloys are mostly applied in transport, building and construction industries (EAA, 2011). Automotive structural components from aluminium magnesium wrought alloys include: body frames (5754), inner panels (5754), truck trailer bodies (5454, 5083 and 5456) and auto trim (5257, 5657 and 5757). Aluminium magnesium and silicon wrought alloys are used to fabricate motor vehicle parts include: bonnet and trunk lids (6016 and 6111), truck beams (6070), automotive frames (6063 or 6061) and exterior panels (6111).

Construction industry uses aluminium alloys that meet the set architectural and/or structural criteria. The alloys are used in the construction of buildings including residential houses, commercial godowns; conference centers and arenas; infrustructures including: bridges, roadside guard rails; and fluid holding tanks and chemical structures. The choices include: siding sheet (5005), housing structures (6063), arena roofs (6061), architectural trim (5257, 5657 and 6463). Bridges and guard rails utilize extrusions of 6063 and 6061 together with plates of 5083 and 5454.

Alloy 6061 is widely used since it has a fair strength of 310 MPa while subjected to T6 temper (Vargel, 2004). The alloy has a high resistance to corrosion and can be processed through extrusion, drawing, rolling and forging. The alloy has been used in automotive parts, pipelines, boiler work, small planes and furniture work.

2.4 Material Flow Analysis of Aluminum

Material flow analysis (MFA) examines how materials and energy flow into, through, and out of a system (Brunner & Rechberger, 2016; OECD, 2008). The system may be

a county, town or a continent. Material flow analysis for melting of aluminum scrap in European Union was done with year 2002 as the base year (Boin & Bertram, 2005). The study provided a comprehensive view of the interconnections within aluminum industry. Quantities of secondary aluminum and salt recovered from dross were identified.

MFA uses the principle of material balance that is based on the law of conservation of matter (Dahlström, Ekins, He, Davis, & Clift, 2004; OECD, 2008). The law upholds that physical processes cannot create or destroy matter. Therefore, processes only transform matter. Material flow during a given process can be analyzed using this principle; whereby inputs and outputs in a processes are evaluated (Agamuthu, Mahendra, & Mohd, 2011). The difference between the inputs and outputs yields the net stock. The net stock (S) for the period in question can be determined using Equation 2.1 (Dahlström et al., 2004). The time period in the MFA, is from the end preceding year (t_1) to the end of the following year (t_2) and the flows (F) are thus given as flow rates per year. The flows are associated to production (F_p), consumption (F_c), import (F_i), export (F_e), recycling (F_r) and disposal (F_d).

$$\int_{t_1}^{t_2} S = \int_{t_1}^{t_2} (F_p - F_c + F_i - F_e - F_r - F_d)dt \tag{2.1}$$

The availability of the scrap for development of the recycled alloys needs to be established through a mass balance (Das, 2006). A mass balance involves the study of the aluminum loop within the locality in which the scrap is being generated. A study was done for structural aluminum used in the manufacture of window and door frames in France (Billy, 2012). Flow of aluminum in the whole life cycle of the products was established. In the study it was possible to establish the amount of the available structural scrap as well as forecast the future supply.

Kenyan aluminum material flow analysis has been done with an aim of establishing a local industry (Weramwanja, 2010). The data used was captured from the industries

that handled only wrought alloys; and left out micro foundries and scrap dealers that handle both the cast and wrought alloys. Consequently, the internal flow of cast alloys and aluminum scrap was not considered exhaustively in the study. The two groups handle a lot of structural scrap that required for the development of the needed structural alloys. There is a need to collect the missing data about the flow of this scrap through a survey. This will establish the availability of the scrap for developing the alloy. Additionally; the aluminium contained in imported automobiles that flows into the county was not taken into account. The study generalized wrought alloys, without identifying the alloys that are used to manufacture structural components. Therefore; the study was general and hence did not pay particular attention to scrap suitable for structural applications. Other studies have developed alloys from a specific scrap like alloy wheels, cylinder heads or pistons (Mose, 2009; Ng'ang'a et al., 2010; Njuguna, 2007; Wangombe, 2014). Therefore, these latter studies too did not apply the principle of mass balance while evaluating the local aluminium flows. Thus there is a need to apply MFA analysis in the determination of suitable aluminium scrap for the structural applications. The main focus of current study was to investigate Kenyan flows of aluminium so as to single out the scrap appropriate for structural applications which include 6xxx alloys.

2.5 Challenges Associated with Recycling Aluminium Alloys

Demand for structural alloys, particularly 6xxx series in the rapidly expanding construction and transport industry has been on the rise. The structural alloys are produced by either melting well-defined wrought scrap of a similar composition or in case of mixed scrap, primary aluminium is used to dilute the scrap melt followed by addition of the alloying elements. Dilution lowers the level of impurities to acceptable levels but also increases the production cost of the alloys.

Production of wrought alloys has been found to be demanding, since they have a very limited ability to tolerate elements not normally present in their composition (Kevorkijan, 2010). The alloys have tight compositions on the alloying elements as opposed to cast alloys. These alloys therefore require careful selection of the scrap. It has been recommended to sort wrought scrap into same alloy or alloy group (Kevorkijan, 2013). However lack of affordable scrap sorting equipment leaves this technique to rely only on the experience of the personnel performing hand sorting which is never accurate.

Aluminum scrap is generally sorted as wrought or cast. Other general sorting criterion is by products. The methods require skilled experts. These two techniques are limited in the sense that they cannot identify with precision the alloy series or an individual alloy. The challenge has been overcome by development of superior techniques that are capable of sorting scrap into individual alloys (Bell, Davis, Javaid, & Essadiqi, 2003; Gaustada et al., 2012). The techniques include colour sorting, laser and X-ray induced breakdown spectroscopy, and hot-crush technique. The methods are promising except that they are limited by presence of coatings on the surface of scrap and cost of their implementation.

The main challenge encountered while melting scrap to produce wrought alloys is the increase or reduction of alloying elements and addition of impurities in the molten scap. This affects the composition of the alloy and hence, its properties. Lack of a cheaper technology other than diluting the molten scrap to reduce the alloying elements when they exceed the specified limit and addition of alloying elements to increase elements that fall below the recommended level have made the alloys to be costly. Other methods for reducing the alloying elements include fluxing, electrolysis, fractional crystallization and distillation (Gilstad & Hammervold, 2014). At the moment only fluxing is applicable at a commercial scale in reducing impurities during aluminum scrap melting. Fluxing involves bubbling chlorine gas through the molten aluminum to form $MgCl_2$ which floats on molten metal and forms part of dross.

Alternatively, incorporation of chloride salts in the cover flux has the same effect. Consequently, the level of Mg can be reduced. $Na_2B_4O_7$ and Ca have been used to remove Fe and Si respectively. However, Gilstad (Gilstad & Hammervold, 2014) cautions against use of multiple fluxing agents as they complicate refining. Therefore, reducing alloying elements in the scrap melting remains a major challenge.

Wrought alloys are produced based on documented empirical compositions which the customers are aware of. As a result, a producer is obligated to adhere to the stipulated standards. Consequently, the producer has no choice other than using primary aluminum to dilute the melt and add alloying elements. On the other hand, it is evident that wrought alloys have a practical compositional tolerance limit. It is suggested that an in depth study of the limits for all alloying element is required (Kevorkijan, 2013). The influences of the tolerance limits on alloy properties have not been fully investigated. At times the customer may request narrower compositional tolerances than necessary. This adds unnecessary costs to producers and customers. Consequently, minimizing their profit. To overcome this challenge there is a need to develop structural wrought aluminium alloys that will readily accept recycled wrought aluminium. The developed alloys will be able to compete with standard alloys; and thus, produce high quality structural products.

The secondary wrought aluminum alloys will have relatively broad composition specification limits on major and minor alloying elements while being more tolerant on impurity limits, without significant restriction on performance characteristics for wide uses (Das, 2006). The alloys are capable of increasing the opportunity to recycle aluminum scrap directly or with only minimal adjustments. However, the scrap batch must be carefully pre-sorted so as to predict accurately the target alloy.

2.6 Predicting Secondary Wrought Alloy Compositions

Aluminum scrap once identified through material flow analysis requires to be sorted so as to give raw compositions that are ready to utilize. It is reported (Das, 2006) that Huron Valley Steel Corporation (HVSC) sorted aluminium scrap and came up with the compositions shown in Table 2.7. Wrought A with minor modifications matched standard wrought alloys like 3005, 3104, 3105 and 6061. However, wrought B had relatively varying compositions of copper and zinc; and was suspected to contain 2xxx and 7xxx alloys. Through investigations on the properties of the alloys it is possible to determine whether similar secondary alloys can accept relatively broad specification limits.

Table 2.7: Sample Composition (%) of Carefully Sorted Recycled Aluminum (Das, 2006).

LOT	Al	Cu	Fe	Mg	Mn	Si	Zn	Others
Wrought A	97.1	0.11	0.590	0.82	0.21	0.51	0.45	0.19
Wrought B	93.1	0.95	1.01	0.89	0.12	2.41	1.25	0.27
Cast A	83.5	4.40	1.10	0.4	0.30	8.0	1.905	0.40
Cast B	88.4	2.50	0.75	0.58	0.26	5.18	1.27	1.09
Mixed W and C	90.1	2.3	0.80	0.50	0.20	4.50	1.20	0.30

In a recent study, an attempt was made to predict a target alloy by grouping the source scrap (Zeru, 2014). The following alloys A356, EN AC-4200, ZL101A, JIS AC4C and LM 25 were grouped together based on the argument that they had close compositions. However; this was alloy, Al-7Si-0.4Mg that was referenced by different standards including: ASTM, European, Germany, Japanese and British standards respectively. In another study cast scrap was carefully sorted into groups of similar components and cast into alloys whose composition was found to match that of commercial alloys used to cast the components (Ng'ang'a et al., 2010). This was

possible since cast alloys have wider compositional tolerances as opposed to wrought alloys.

Table 2.8: Composition (%) of Recycled Aluminium Structural Alloys (Das, 2006).

Alloy	Si	Fe	Cu	Mn	Mg	Zn	Others
2xxx	0.7	0.6	5.5 - 7.0	0.2 - 0.4	0.7	0.5	0.3
5xxx	0.7	0.6	0.3	0.05 - 0.35	2.0 - 3.0	0.5	0.3
6xxx	0.3 - 1.0	0.6	0.3	0.3	0.4 - 1.0	0.5	0.3
7xxx	0.5	0.6	0.5 - 1.2	0.3	2.0 - 2.8	4.0 - 6.0	0.3

It has been suggested that the concentration of major alloying elements be broadened to levels of ± 0.5 % and the limits of increased to levels of those elements typically found in recycled metal (Das, 2006). Based on this rationale the candidate structural wrought alloys shown in Table 2.8 were suggested (Das, 2006). The alloys were designed to fall as much as possible within the existing alloy families, to ensure optimum forming and mechanical properties. In addition to that the alloys should have the desired performance characteristics for reuse in a variety of applications (Das, Green, & Kaufman, 2007). This focus on product properties, in addition to alloy chemistry helps to avoid limitations caused by very tight chemical compositions of standard alloys. Automotive cast alloys require characteristics like castability, strength and high temperature resistance among others. Structural alloys also require strength, corrosion resistance and fatigue resistance.

Further, performance of candidate alloys must be evaluated to assess their abilities to meet the requirements of representative structural applications as compared to existing alloys (Das et al., 2007). The assessment will cover microstructure analysis and mechanical properties evaluation. Performance requirements of the resulting recycled friendly alloys will be based on existing alloys, customer requirements and the need to make them cost effective.

It has been suggested that target applications of the candidate recycle friendly alloys should be the same as those of the existing counter parts with tighter limits (Das, 2006). Further results of composition and mass balance studies may suggest focusing upon candidate alloys from the series that have the best fit with the available scrap. High level Si and Fe may make applications of these alloys in fracture critical components in aerospace untenable. The difficulties associated with formability and joining of 2xxx and 7xxx series makes it attractive to focus on 6xxx series which responds well to extrusion and has broad structural applications.

2.7 Post Cast Processing of Wrought Aluminium Alloys

Formability and mechanical properties of structural aluminum alloys are determined by the quality of its microstructure which is depicted by the fineness of the structure and the morphologies of the micro constituents present therein. Normally, the microstructure is controlled through the processes of grain refinement, Si modification and Fe neutralization. The microstructure can be improved further by subjecting the cast material to forming processes like extrusion and severe plastic deformation (SPD). Examples of SPD processes include high pressure torsion (HPT), friction stir welding (FSW) and friction stir processing (FSP).

2.7.1 Extrusion of Structural Wrought Alloys

Extrusion is the process by which a block/billet of metal is reduced in cross section by forcing it to flow through a die orifice under high pressure. The billet is forced through a die opening in a shape of desirable cross-section as shown in Figure 2.3. A sample laboratory die that was used for forward extrusion of aluminium alloy 2014 and 2024 is as shown in Figure 2.4.

Extrusion force (F) depends on: process variables (temperature and velocity),

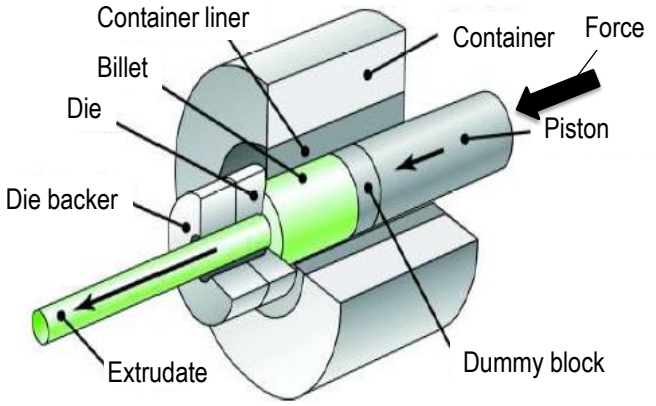

Figure 2.3: Schematic Illustration of the Direct-Extrusion Process (Kalpakjian & Schmid, 2010).

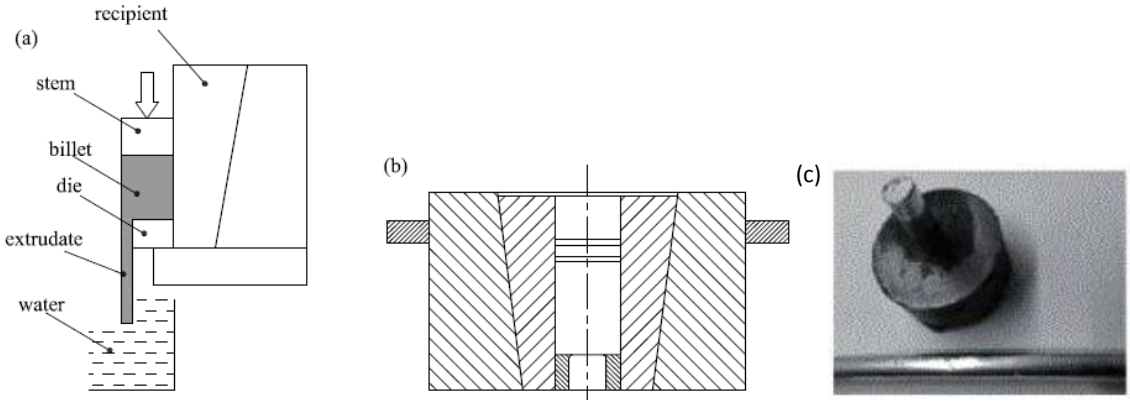

Figure 2.4: Extrusion Process: (a) Schematic Diagram of Extrusion (b) Extrusion Assembly (c) Extruded Material (Lesniak & Woznicki, 2012).

friction between the billet and either chamber or die surfaces, strength of billet material, extrusion ratio (R) and extrusion pressure (P) (Kalpakjian & Schmid, 2010).

Hot extrusion compared to cold extrusion requires less force. Extrusion temperature of a metal ranges between 50 - 75 % of its melting point, and at this temperature the metal has low flow stress. Hot extrusion of Aluminium is performed at temperature and pressure ranges between 375 ^{0}C - 475 ^{0}C; and 700 - 500 MPa respectively. Steel dies are adequate at low temperature of up to 500 ^{0}C. Lubricants are applied to reduce friction. Low temperature lubricants include graphite and oils; however, at high temperatures glass powder is used.

Extrusion ratio or reduction (R) is the ratio of billet cross sectional area to that of the extrudate. The ratio of aluminium can reach 400:1; and is given by Equation 2.2. Extrusion force is directly proportional to the extrusion ratio. However, normal extrusion ratio range for hard and soft alloys is from 10:1 to 35:1.

$$extrusion \quad ratio \quad (R) = \frac{billet \quad crosssectional \quad area \quad (A_0)}{extrudate \quad crosssectional \quad area \quad (A_f)} \tag{2.2}$$

Velocity of the extruded product (V) is the product of the ram velocity (v) and the extrusion ratio (R) and is given by Equation 2.3. Aluminum 6060 and 6063 alloys can be extruded up to a speed of 100 m/min.

$$V = v \times R \tag{2.3}$$

Extrusion pressure (P) can be hydraulic or pneumatic and is given by Equation 2.4,

$$pressure \quad (P) = \frac{extrusion \quad force \quad (F)}{billet \quad cross \quad sectional \quad area \quad (A_0)} \tag{2.4}$$

Extrusion force (F) is given by Equation 3.1 (Kalpakjian & Schmid, 2010),

$$F = KA_0 \ln \frac{A_0}{A_f} \tag{2.5}$$

where K is the extrusion constant that is determined experimentally. The constant is a measure of the strength of a material being extruded and the frictional conditions. For aluminium 1100 alloy it has been approximated to be 75 MPa at a temperature of 400 ^{o}C (Kalpakjian & Schmid, 2010)

A laboratory extrusion tool is required to investigate the effect of extrusion on the properties of recycled wrought aluminium alloys. The extruded material can be subjected to severe plastic deformation.

2.7.2 Severe Plastic Deformation (SPD)

2.7.2.1 Introduction of SPD

Severe plastic deformation (SPD) processes may be defined as metal forming processes in which an ultra-large plastic strain is introduced into a bulk metal without the introduction of any significant change in the overall dimensions of the solid, in order to create ultra-fine grained (UFG) metals (Azushima et al., 2008; Sakai et al., 2005). The exceptionally high strain introduces a high density of dislocations that subsequently re-arrange to form an array of grain boundaries of mostly high angle misorientation (Azushima et al., 2008). UFG materials are defined as polycrystals having very small grains with average grain sizes less than $\sim$1 μm. For bulk UFG materials, there are additional requirements of fairly homogeneous and reasonably equiaxed microstructures and with a majority of grain boundaries having high angles of misorientation. The presence of a high fraction of high-angle grain boundaries is important in order to achieve advanced and unique properties.

The UFG materials created by the SPD processes exhibit high strength, increased

hardness, superior fatigue properties and a potential superplastic forming capability at elevated temperatures (Azushima et al., 2008; Saito, 1998). The yield stress, σ_y of a polycrystalline metal is related to the grain size diameter, d by the Hall-Petch Equation 2.6 (H. Jiang et al., 2000).

$$\sigma_y = \sigma_0 + Ad^{-\frac{1}{2}} \tag{2.6}$$

Where σ_0 is the friction stress and A is a constant of yielding. From Equation 2.6 it can be seen that the yield stress increases with decreasing square root of the grain size. The decrease of grain size leads to a higher tensile strength without reducing the toughness, which differs from other strengthening methods such as heat treatment.

Consequently, SPD has attracted the interest of many researchers and experts in materials engineering as a means of processing materials. Common SPD techniques include high-pressure torsion (HPT) (Sakai et al., 2005), friction stir welding (FSW) and friction stir processing (FSP), equal channel angular pressing (ECAP) (Y. T. Zhu & Lowe, 2000), accumulative roll bonding (ARB) (Vorhauer & Pippan, 2004) and multiple forging.

Metals processed by SPD exhibit high strength, ductility and fatigue characteristics. Due to these properties UFG metals are used as structural materials. Bolts are manufactured with titanium alloys and carbon steel processed by ECAP, and they are widely used in the automobile and aircraft industries (Azushima et al., 2008). Other potential markets include medical implants, defence applications, aerospace components, sport equipment and construction industries. Medical implants include hip, knee and dental implants; various screws; plates and meshes used in orthopaedic applications. Popular materials usually used in these applications are cobalt-chrome alloys, stainless steel and titanium alloys. Due to the small sizes of the HPT processed samples, most of these materials can find applications in micro-mechanical systems and biomedical mini components (such as screws, springs and staples).

HPT-processed ring specimens can find application in producing washers.

This study will be limited to HPT and FSW severe plastic deformation techniques.

2.7.2.2 High Pressure Torsion (HPT)

The principle of processing by HPT is based on the classic work of Bridgman where a bar was subjected to compression and torsion to produce large strains (Zhilyaev & Langdon, 2008). The principle of the early work was as shown in Figure 2.5 (Zhilyaev & Langdon, 2008). The two ends of the bar were held rigidly and subjected to longitudinal compression, while the central portion was rotated with respect to the ends. The two sections with reduced radii experienced a torsional strain.

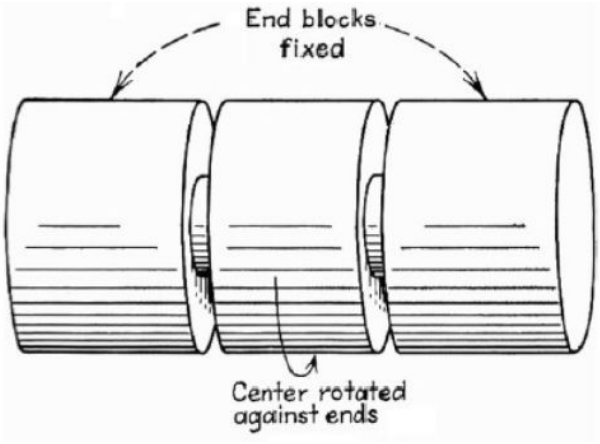

Figure 2.5: Schematic Illustration of the HPT Principle Showing the Apparatus Used by Bridgman (Zhilyaev & Langdon, 2008).

There are three types of HPT processing; namely unconstrained, constrained and quasi- constrained as shown in Figure 2.6 (Zhilyaev & Langdon, 2008). In unconstrained HPT, the specimen is free to flow outwards when subjected to an applied pressure and torsional straining. An introduction of a cavity in the lower anvil during constrained condition restricts the outward flow of the material during the torsional straining. However, it is generally difficult to achieve an idealized constrained condition and experiments are often conducted under a quasi-constrained condition where there is at least some limited outward flow between the upper and

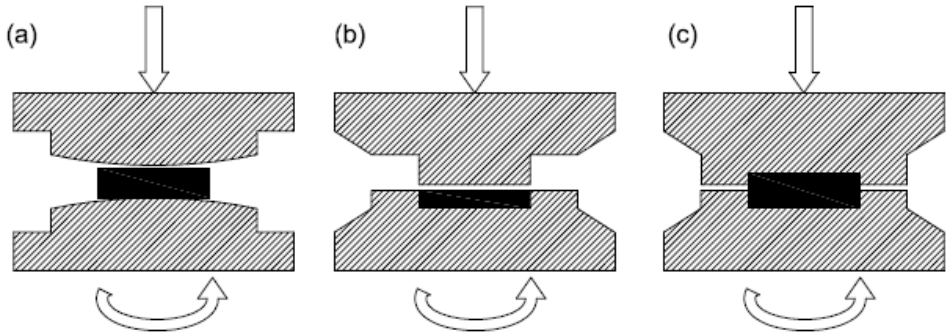

Figure 2.6: Schematic Illustration of HPT for (a) Unconstrained; (b) Constrained; and (c) Quasi-Constrained Conditions (Zhilyaev & Langdon, 2008).

lower anvils.

The principles of modern quasi-constrained HPT processing are illustrated schematically as shown in Figure 2.7 (Sakai et al., 2005). The facility consists of an upper and lower anvil made from high-strength tool steel with the surfaces nitrified and with spherical depressions carefully machined at the centres of each anvil having diameter of 10mm and depth of 0.25 mm. Specimens of 10mm diameter and ∼0.8mm thickness are placed in these depressions, and a lubricant of MoS_2 is applied around the depressions. The disks are subjected to concurrently high pressure, P and torsional straining, ϵ; the strain is expressed simply in terms of the number of revolutions, N imposed on the sample. Processing is conducted at room temperature by rotating the lower anvil with respect to the upper anvil at a speed of 1 rpm. A small reduction in the specimen thickness to ∼0.74 mm upon the application of the load has been observed (Kawasaki et al., 2010).

The shear strain γ can be calculated according to Equation 2.7 (H. Jiang et al., 2000),

$$\gamma = \frac{2\pi n}{t} r \tag{2.7}$$

where the values r, n and t are the distance from the centre of the sample (axis of rotation), the number of revolutions and the thickness of the sample, respectively.

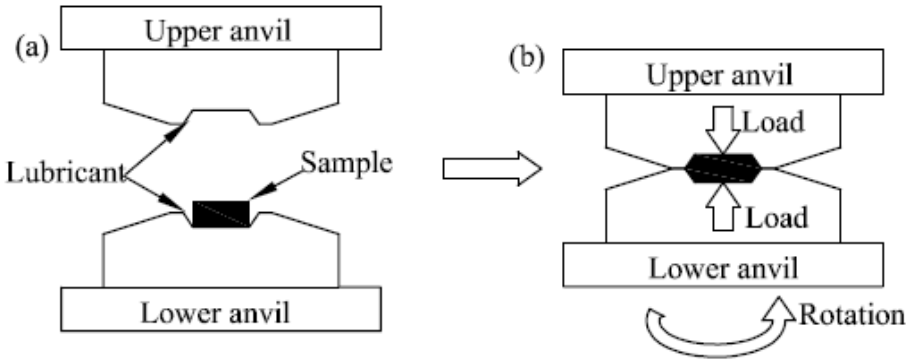

Figure 2.7: Schematic Illustration of Quasi- Constrained HPT Principle; (a) Loading and (b) Processing of the Sample. (Kawasaki et al., 2010).

The shear strain in the centre should be zero and should increase linearly with the radius, provided that the height of the billet remains constant during the torsional deformation of the material. This means that the centre of the sample should be un deformed. However; misalignment of anvil axis and high compressive force can lead to the deformation of the centre of the specimen (Zhilyaev & Langdon, 2008).

The equivalent Von Mises strain is calculated using the Equation 2.8 (Zhilyaev & Langdon, 2008),

$$\varepsilon = \frac{\gamma}{\sqrt{3}} \tag{2.8}$$

The use of Equation 2.8 is correct for small imposed shear strains but for large strains, where $\gamma \geq 0.8$, the equivalent strain is given by Equation 2.9 (Zhilyaev & Langdon, 2008),

$$\varepsilon = \frac{2}{\sqrt{3}} ln[(1 + \frac{\gamma^2}{4})^{\frac{1}{2}} + \frac{\gamma}{2}] \tag{2.9}$$

Benefits of HPT over other SPD methods include the following:

1. Compared to ECAP, HPT achieves higher grain refinement since higher strains are involved as shown in Table 2.9. This is because there is application of both torsion and compression on the sample during HPT.

Table 2.9: Comparison of Grain Refinement by ECAP and HPT (Sakai et al., 2005).

Material	Approximate grain size (nm)	
	ECAP	HPT
Al - 3 % Mg alloy	270	90
Al - 5 % Fe alloy	300	100
High - purity Ni	350	150
Pure Ti	300	200
Al - 3 % Mg - 0.2 % Sc	200	150

2. HPT processed materials have minimal change in overall dimensions.

3. HPT-processed materials exhibit high strength and ductility at room temperatures; since deformation in UFG materials occurs through grain boundary sliding and enhanced grain rotation rather than dislocation motion, thereby enhancing both ductility and strength.

4. They exhibit super plastic properties at 50 % absolute melting temperature ($0.5T_m$)

5. They also have high fracture toughness.

Studies have been conducted on the properties of HPT processed pure metals such as high purity nickel, austenitic steel, copper and aluminium (Edalati & Horita, 2011; Xu, Horita, & Langdon, 2010; Zhilyaev, McNelley, & Langdon, 2007). Microstructure and mechanical properties of bulk nanostructured tantalum and tungsten materials have been studied. Recently, microstructural and microhardness characterization of HPT processed high purity aluminium, commercial purity aluminium and aluminium alloys has been reported; some of these alloys include Al-Mg-Sc alloy, cast Al-7%Si alloy, Al-7075, Al-2024, Al-2%Si-0.25%Sc and many others.

HPT specimens have been processed inform of disks, and subjected to varying pressure and torsional strain. Rods of Al-Mg-Sc were sliced into disks of diameter 10

mm and thickness ∼0.8 mm (Sakai et al., 2005). The disks were subjected to loads of 5, 10, 20 and 48 tons equivalent to imposed pressures, P, of 0.62, 1.25, 2.5 and 6.0 GPa, respectively, and rotated at a speed of 1 rpm. The tests were terminated after 1, 3, 5 or 7 turns. Abrasive papers have been used to polish Zn - 22Al alloy disks ∼1.5 - 2.0 mm thick to thickness close to ∼0.80 mm (Kawasaki et al., 2010). Use of wire electric discharge machine (EDM) produced HPT samples ∼0.8 - 0.9 mm thick (Xu et al., 2008). Therefore; use of high precision cutting tools has been found to eliminate grinding and polishing of disks. Pure aluminium specimen was subjected to a load of 8 kN equivalent to an applied pressure of 1 GPa, and rotated at a speed of 1 rpm. The rotation was terminated after 1/8, 1/4, 1/2 and 1 revolution (Ito & Horita, 2009).

After HPT straining, pure aluminium specimens were polished to a mirror-like surface, and the Vickers microhardness was measured at a load of 0.25N applied for 15 s (Horita & Langdon, 2008). The Vickers microhardness, HV, was recorded at selected points across the disks by imposing a load of 10 g for 15 s for pure Cu or 25 g for 20 s for the Al-Mg-Sc alloy (Horita & Langdon, 2005). Compared to the initial solution treated condition, the hardness increased from the centre towards the edge of the disk by a factor of 2 and 3 respectively.

The microhardness measurements of HPT Al 6061 were recorded across the diameter of each disk in incremental steps of 0.3 mm (Xu et al., 2008). At each selected point, the average hardness was obtained by taking individual measurements of Hv at four separate points uniformly positioned around the selected point at equal distances from the point of 0.15 mm. By taking four separate values at each point it was possible to estimate the associated error bars at the 95% confidence level. After a single turn of HPT, the average hardness increased with respect to the unprocessed material and the measured hardness values were low in the central regions of the disks but high near the peripheries as shown in Figure 2.8.

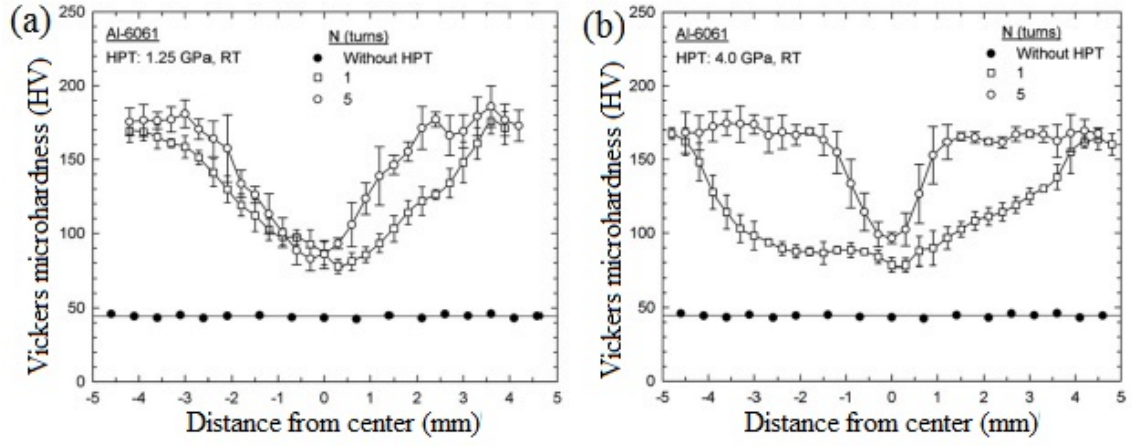

Figure 2.8: Microhardness Distribution Across Diameter of Al- 6061 Specimen at a Pressure of (a) 1.25 GPa; and (b) 4.00 GPa (Xu et al., 2008).

The experiments show that the extent of the inhomogeneity in the central region decreases with increasing numbers of turns and/or with increasing applied pressure. The profiles shown in Figure 2.8 demonstrate there is a visible difference in the values of Hv at the centres and at the edges of the disks. However, this difference tends to become relatively small after larger numbers of turns because of the overall increase in the microhardness level as shown in Figure 2.9. By increasing the numbers of rotations there is a clear increase in the average values of Hv both at the centre and at the edges of the sample. It is apparent that the values of Hv in the central region increase with increasing numbers of whole revolutions and thus they increased with the total imposed strain.

Hardness has been found to be directly proportional to the distance from the core, applied pressure and the number of turns (Sakai et al., 2005). Hardness increased with increasing distance from the centre of the disk and ultimately stabilized at distances beyond ∼2 - 3 mm. Higher hardness values were attained with increasing applied pressure and/or increasing numbers of turns but ultimately the hardness stabilized in the outer regions of the disks at a value of ∼3× the value of the initial hardness in the solution-treated condition. It was suggested that saturation occurred

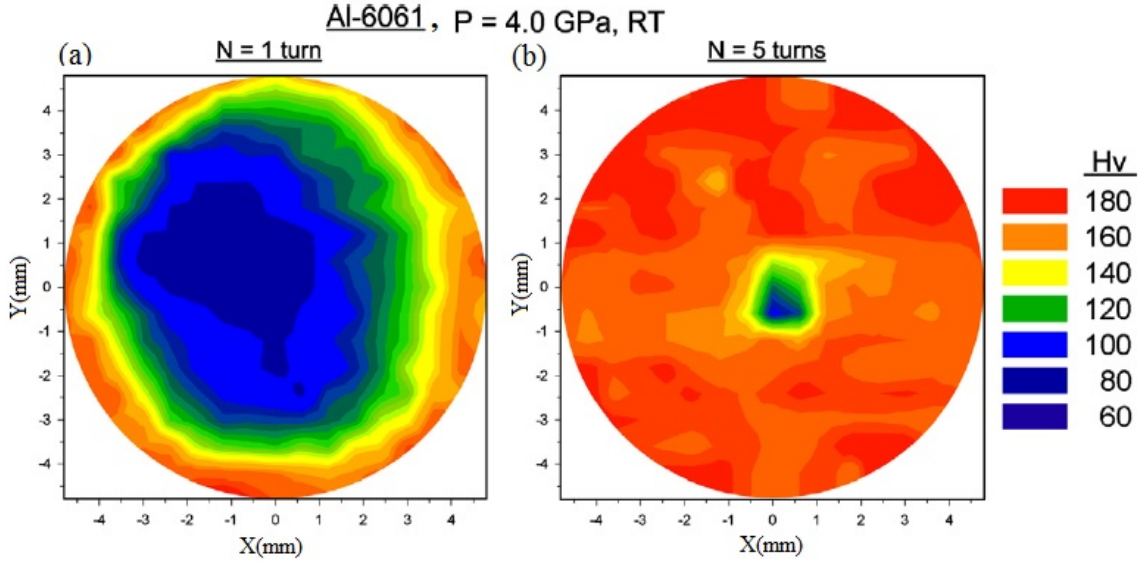

Figure 2.9: Colour-Coded Contour Maps Showing Vicker's Microhardness Across the Surfaces of Disks Processed by HPT at (a) 1 Turn and (b) 5 Turns (Xu et al., 2008).

when there was a balance between the rates of dislocation nucleation and dislocation recovery.

The effect of stacking fault energy (SFE) on hardness of HPT processed materials has been reported (Zhilyaev & Langdon, 2008). High purity aluminium has high SFE so that the partial dislocations are not widely separated and there is easy cross-slip. By contrast, materials such as nickel and aluminium-based alloys have lower SFE and the rates of recovery are significantly slower. This suggests that microstructural evolution will occur at a slower rate in the latter materials and higher imposed strains will be needed to achieve a reasonable level of microstructural homogeneity. For materials having low stacking fault energies and slow recovery rates, it is anticipated that higher levels of hardness will be reached in the peripheral region in the early stages of HPT as shown in Figure 2.10(a). By contrast, materials such as high purity aluminium have high SFE so that the measured hardness initially will be high in the central region because of the advent of dynamic recovery in the peripheral region. The centres of the disks for pure Copper exhibit micro hardness values which are

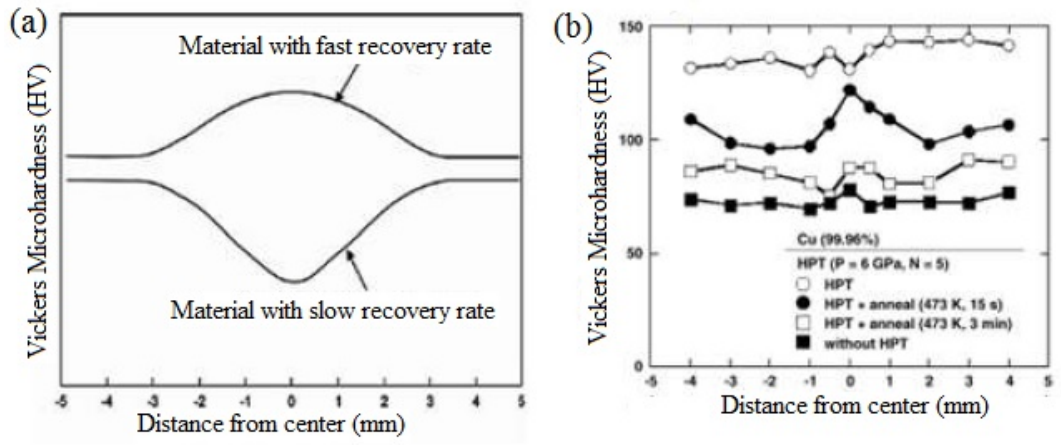

Figure 2.10: Effect of Recovery Rate on Vicker's Microhardness of a HPT Processed Material (a) Schematic Diagram for Materials Having Either Slow or Fast Rates of Recovery (Zhilyaev & Langdon, 2008); (b) Cu Has a High Rate of Recovery (Ito & Horita, 2009).

higher than the edges at lower values of strain (Zhilyaev & Langdon, 2008) as shown in Figure 2.10(b). With increasing strain, the inhomogenity was minimised. For both types of material, there is a gradual evolution towards an equilibrated and homogeneous microstructure as the torsional straining continues to higher numbers of revolutions.

Table 2.10: The Effect of SFE on Cu and Cu-Al Alloys (An et al., 2011).

	Cu and Cu - Al alloys				
	Cu	Cu - 2Al	Cu - 5Al	Cu - 8Al	Cu - 16Al
SFE (mJm^{-2})	78	48	28	17	6
Average grain size (nm)	120	100	65	45	30
Presence of twins and stacking faults	Increased significantly $\longrightarrow$				
Yield strength and UTS	Increased significantly $\longrightarrow$				
Ductility	Uniform elongation increased significantly to an optimum and then reduced slightly				

The effect of SFE on mechanical properties of copper and its alloys was investigated as shown in Table 2.10 (An et al., 2011). Reductions in the SFE lead to a significant grain refinement of the materials. Consequently, yield strength (YS) and ultimate tensile strength (UTS) were significantly increased as shown in Figure 2.11. However,

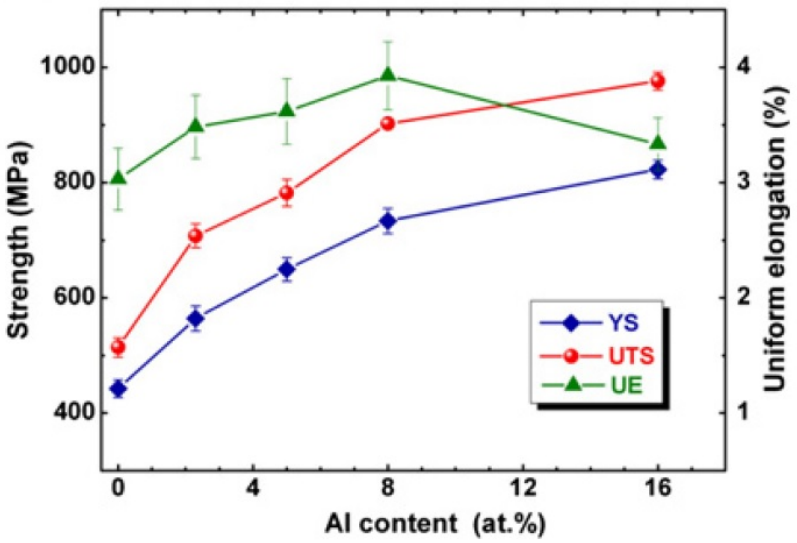

Figure 2.11: The Effects of Stacking Fault Energy on Yield Strength, Ultimate Tensile Strength and Internal Energy (UE) of Cu and Cu-Al Alloys (An et al., 2011)

increase in uniform elongation reached an optimum and decreased when grains were reduced excessively.

HPT processed pure copper when subjected to very short-term anneals at 473K (for example, for times of 15 s to 3 min) lost the hardness (Saito, 1998). Therefore, rise in temperature can affect the hardness. However, an investigation on the onset of this effect on HPT processed materials is needed.

Tensile tests have shown that HPT processed materials exhibit superplasticity. An Al-3% Mg-0.2% Sc alloy had an elongation of 500% when subjected to a temperature, pressure and number of turns of 673K, 6.0 GPa and 5 respectively (Sakai et al., 2005). HPT experiments have been conducted on larger bulk samples of AL-Mg-Sc of 10 mm diameter and 8.57 mm length (Horita & Langdon, 2005). The size of the grains was extremely small around the edges, as opposed to the larger ones, ∼130 nm in the centre. Tensile results demonstrate excellent superplastic characteristics after HPT including a maximum tensile elongation of 1600 % at a testing temperature of 573 K. Maximum elongation was observed in specimens cut from sections near the

edges.

HPT processed materials have been found to possess low temperature thermal stability. Hardness achieved in pure Cu by HPT processing, could not be retained when samples were subjected even to very short-term anneals at 473K (for example, for times of 15 s to 3 min) (Kawasaki et al., 2010). Annealing of the HPT processed Cu samples at temperatures as low as 50 ^{0}C decreased the microhardness, indicating a very low thermal stability of the deformation induced microstructures (H. Jiang et al., 2000). Presence of Cu, Mn and Fe in the HPT processed Al-2024 alloy led to the formation of second phase particles that inhibited grain growth and contributing to the stability of the fine-grained structure at elevated temperatures (Alhamidi & Horita, 2015). Zirconium and scandium also inhibit grain growth at higher temperatures. Annealed and solution treated specimens of Al 2024 gave grains of average size 160 and 300 nm respectively after HPT processing (Dobatkin et al., 2005). Therefore, annealing of Al 2024 improved its grain refinement and super plastic properties.

Attempts were made to relate hardness, tensile strength and ductility of pure copper with the equivalent strain (Edalati, Fujioka, & Horita, 2008). When hardness values across the diameter of HPT processed pure copper were plotted against equivalent strain, it was found that the values fell on a single unique curve regardless of the pressure or the number of turns. The hardness increased with an increase in the equivalent strain at an early stage of straining; thereafter levelled off; and finally entered into a steady-state where the hardness remained unchanged with further straining. Additionally, the tensile strength of the copper also followed a similar single function of the equivalent strain as the hardness. This is true because microhardness, Hv is related to tensile strength, σ by Equation 2.10 (Edalati et al., 2008).

$$\sigma = 3.4H_V \tag{2.10}$$

However, the elongation to failure initially decreased with increase in equivalent strain; with the lowest point coinciding with the onset of a steady state, where recrystallized grains were formed, and the grains were free from dislocations. Compared to Pure aluminium, pure copper has no maximum hardness in a plot of hardness versus equivalent strain because aluminium has a higher SFE and homologous temperature. Consequently, dislocations are able to move faster in aluminium than in copper. Therefore, the dislocation mobility is affected by the presence of impurity elements, the difference in stacking fault energy (SFE) and difference in the homologous temperature.

The procedure of conducting transmission electron microscopy (TEM) on HPT specimens has been explained by a number of authors (Horita & Langdon, 2005; Ito & Horita, 2009; Vorhauer & Pippan, 2004). Disks 3mm diameters were punched at the central and the peripheral regions of the HPT processed specimens. The disks were then ground mechanically to a thickness of 150 - 100 μm, and further thinned to perforation using a twinjet electro-chemical polishing facility with a solution of 20% $HClO_4$, 10% $C_3H_8O_3$, and 70% C_2H_5OH at room temperature. TEM microscope like Hitachi H-8100 operated at 200 kV has been used to capture bright field and dark field images. Selected area electron diffraction (SAED) patterns were taken using an aperture size of 2.5 - 6.3 μm.

Al-3% Mg-0.2% Sc alloy disks of 0.5mm grain size were processed by HPT (Sakai et al., 2005). The observations showed that the microstructure was inhomogeneous within the disks after HPT. Outer region microstructure was highly deformed and consisted of an array of homogeneous ultrafine grains with boundaries having high angles of misorientation and an average size of $\sim$0.15 μm. By contrast, the central region of the disk had a coarse and ill-defined microstructure. Careful examination within this region revealed irregular grains and poorly defined grain boundaries to the extent that it proved impractical to obtain a meaningful measure of the effective grain size. Based on the presence of diffraction spots in the SAED pattern, it was

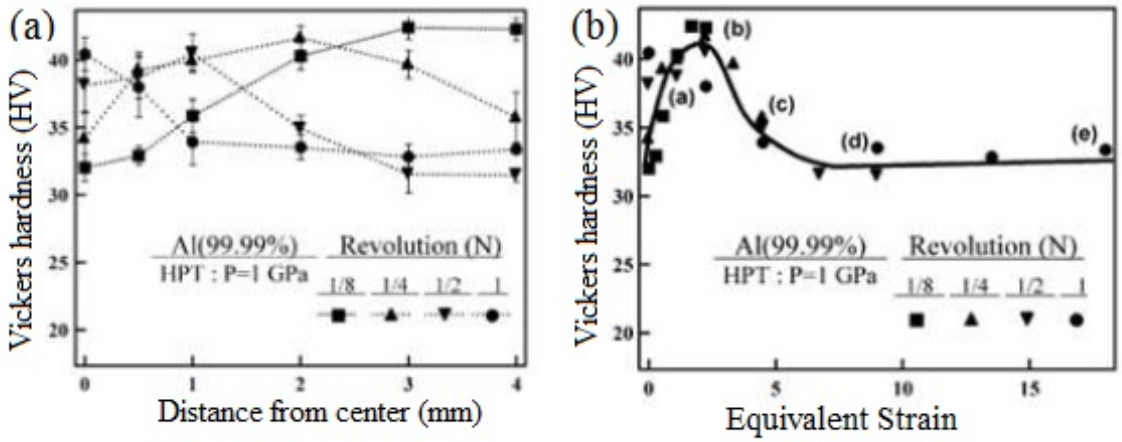

Figure 2.12: Vickers Microhardness Plotted Against (a) Distance from Centres of Disk Samples After Processing with HPT Under Pressure of 1 GPa for Revolutions of 1/8, 1/4, 1/2 and 1; (b) Equivalent Strain for All Data Points Shown in (a) (Ito & Horita, 2009)

apparent that their grain boundaries had low angles of misorientation.

Experiments were conducted on an Al- 3Mg- 0.2Sc alloy and pure Cu to evaluate the effect of high-pressure torsion (HPT) (Saito, 1998). The outer region of the HPT processed Aluminium alloy contained ultrafine and reasonably equiaxed grains with an average size of ∼150 nm after 5 turns at a pressure of 6.0 GPa. In addition, the presence of rings in the SAED pattern indicated that many of the grain boundaries had high angles of misorientation.

During the investigation of microstructure evolution in pure aluminium processed by HPT an attempt was made to relate the hardness, strain and the microstructure (Ito & Horita, 2009). All the hardness data presented in Figure 2.12(a) was plotted as a function of equivalent strain obtained using Equation 2.7 as shown in Figure 2.12(b). All the data points were found to lie on a single unique curve which exhibited a maximum at an equivalent strain of ∼2 and a steady state level beyond an equivalent strain of ∼6 where the hardness remained constant with straining.

Crystal orientation image analysis using electron backscatter diffraction (EBSD) was

conducted for the pure aluminium samples at five representative strained conditions indicated by (a) - (e) in Figure 2.12(b). Electron backscatter diffraction (EBSD) analysis was conducted using a Hitachi S-4300SE scanning electron microscope equipped with a field-emission gun at an accelerating voltage of 20 kV. Grain sizes and misorientation angles were determined along with the EBSD analysis. Analysis over an area of 25 μm $\times$25 μm revealed that a single crystal orientation prevailed throughout the analyzed area at strained condition corresponding to (a), and grains with a different orientation appeared at (b). Many grains in these two areas were surrounded by low angle boundaries. Area (c) compared to (b) had a fairly reduced grain size, increased misorientation angle and many well defined grain boundaries. The orientation image at (d), corresponding to the onset of the steady state, had many equiaxed grains having different orientations, well defined grain boundaries and increased fraction of misorientations. The orientation image at (e) was essentially the same as (d), indicating that the microstructural features were well maintained in the steady state.

TEM bright-field image and dark field image with SAED pattern taken at a point of maximum hardness had many dislocations within grains, and many tangled dislocation near grain boundaries. Whereas the images taken with equivalent strain at steady state of hardness had few dislocations within the grains, and the grain boundaries were smooth and straight.

A mechanism for the formation of fine grains surrounded by high angle boundaries was proposed as shown in Figure 2.13:

(i) dislocation accumulation occurs,

(ii) sub-grain boundaries form,

(iii) some dislocations are annihilated at sub-grain boundaries to increase the misorientation angels and finally balance is established between generation of

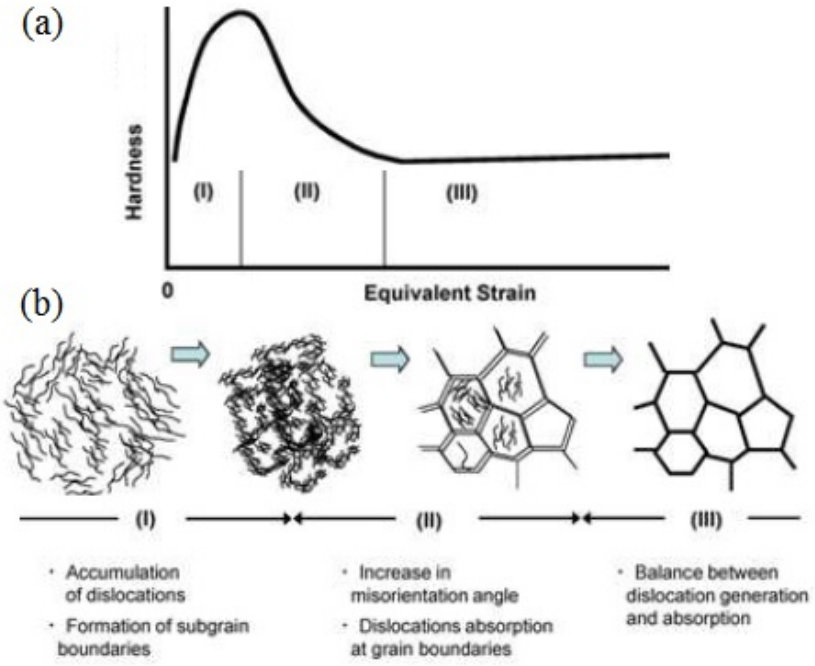

Figure 2.13: Formation of Fine Grains Surrounded by High Angle Boundaries (a) Hardness Equivalent Strain Curve (b) Mechanism (Ito & Horita, 2009)

dislocations by SPD and absorption of dislocations at grain boundaries.

Coarse-grained copper was subject to high-pressure torsion (HPT) and thermal treatment to study the effects of increasing amounts of deformation and subsequent annealing on the evolution of microstructure and microhardness (H. Jiang et al., 2000). Cellular sub-grains with low-angle grain boundaries were first formed at low strain. Some of the low-angle sub-grain boundaries transformed to high-angle grain boundaries at higher strains, refining the average grain size from 200 μm to 150 nm.

The HPT-processed material had a small grain size, high dislocation density and high internal stress that made their microstructures thermally unstable. Presence of bend contours (see the arrows) as shown in Figure 2.14(a) implied the presence of a high level of internal stress in the sample. The SAD pattern showed elongated and clustered diffraction spots, which suggested a sub-grain microstructure with

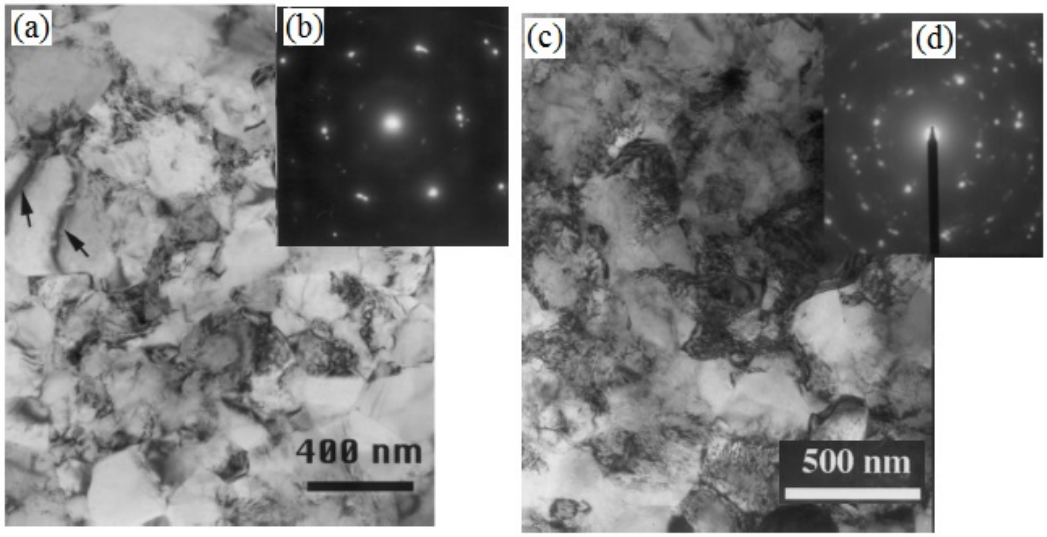

Figure 2.14: TEM Images and SAD Patterns of the Cu Samples Processed by HPT for (a) and (b) 1/2 Turn; and (c) and (d) 1 Turn Respectively (H. Jiang et al., 2000)

low-angle grain boundaries. A finer grain size was reflected in a SAD pattern shown in Figure. 2.14(b) which had many more diffraction spots that almost formed continuous diffraction rings, which suggested the existence of a large quantity of high-angle grain boundaries. Annealing of the HPT processed samples at temperatures as low as 50 ^{0}C decreased the microhardness, indicating a very low thermal stability of the deformation induced microstructures.

The initial small size of HPT processed materials had limited their full industrial use. Over time the size has evolved from discs 10mm to rings 20mm inside diameter and 30mm outside diameter (Edalati et al., 2008). The rings increased the size and homogenized the properties of the processed materials. Larger diameters of 40mm discs and 100mm rings have been reported (Edalati & Horita, 2009). The recent improvement of HPT to continous high pressure torsion has made room for processing of long sheets and rods (Edalati et al., 2012). The CHPT specimens are large and have homogenized material properties. Long nanostructured materials of 14mm diameter have been processed through high presure torsion extrusion (HPTE)

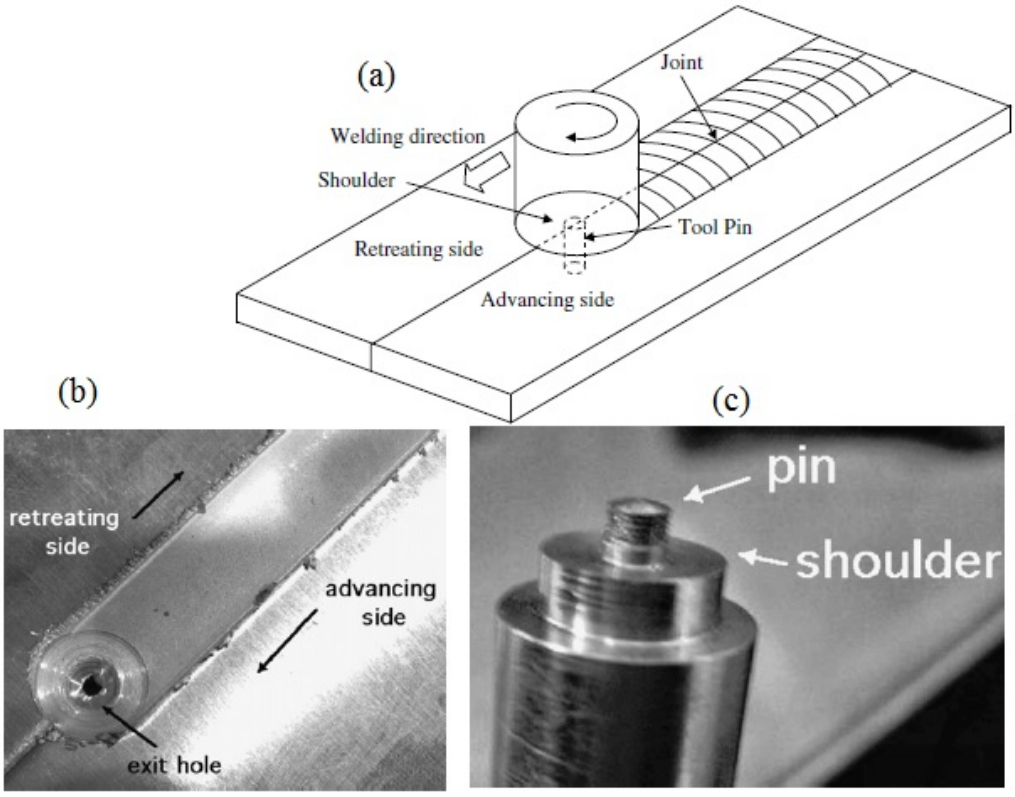

Figure 2.15: (a) Schematic Illustration of (FSW) Process; (d) FSW Welded Aluminium Sheets; (C) FSW Cylindrical Tool with a Threaded Pin (Nandan et al., 2008).

(Omranpour et al., 2021).

2.7.2.3 Friction Stir Welding (FSW)/ Friction-Stir Processing (FSP) of Aluminium Alloys

FSW was invented in 1991 by Wayne Thomas at The Welding Institute (TWI) in Cambridge Kwon et al. (2002); Sen and Sharma (2016). It is a solid-state, joining process in which a rotating tool with a shoulder and terminating in a pin, moves along the butting or lapping surfaces of two rigidly clamped plates placed on a backing plate as shown in Figure 2.15 (Nandan et al., 2008; Su J, Nelson, Mishra, & Mahoney, 2003; Thomas & Nicholas, 1997).

The shoulder makes firm contact with the top surface of the work-piece. Heat

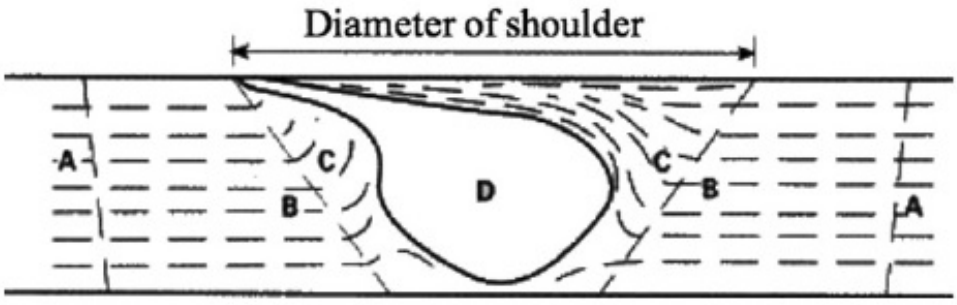

Figure 2.16: Schematic Cross-Section of a FSW Joint Showing Four Distinct Zones: A, B, C and D (Nandan et al., 2008).

generated by friction at the shoulder and to a lesser extent at the pin surface, softens the material being welded. Severe plastic deformation and flow of this plasticised metal occurs as the tool is translated along the welding direction. The material is transported from the front of the tool to the trailing edge where it is forged into a joint. The half-plate where the direction of rotation is the same as that of welding is called the advancing side, with the other side designated as being the retreating side. This difference can lead to asymmetry in heat transfer, material flow and the properties of the two sides of the weld. For example, the hardness of particular age-hardened aluminium alloys tends to be lower in the heat-affected zone on the retreating side (Nandan et al., 2008).

The thermally softened region below the tool shoulder takes up a frustum shape as shown in Figure 2.16; and corresponds to the overall tool geometry (Thomas & Nicholas, 1997). The region appears much wider at the top surface in contact with the shoulder, tapering down to the pin diameter. A typical cross-section of the joint consists of four zones marked A, B, C and D; namely: base metal (BM), heat-affected zone (HAZ), thermomechanically affected zone (TMAZ), and stirred zone (SZ) respectively. The HAZ is similar to that in conventional welds although the maximum peak temperature is significantly less than the solidus temperature, the heat source is rather diffuse, and can lead to somewhat different microstructures when compared with fusion welding processes. The SZ or nugget region containing the

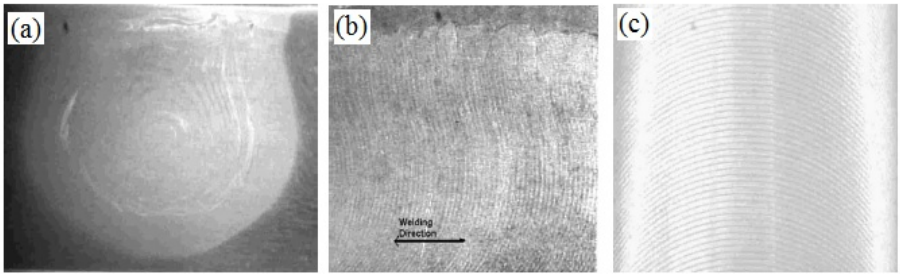

Figure 2.17: Section Views of FSW Joint Showing the Marks at a Plane: (a) Perpendicular, (b) Parallel and (c) Traverse to the Plane of Tool Rotation (Nandan et al., 2008).

"onion-ring" appearance is the one which experiences the most severe deformation, and is a consequence of the way in which the tool deposits material from the front to the back of the weld. The TMAZ lies between the HAZ and SZ; the grains of the original microstructure are retained in this region, but often in a deformed state. FSW results in microstructural changes which influences the weld mechanical properties (Su J et al., 2003).

Onion rings were observed in the FSW joint of 2024 and 6061 Al alloys (Y. Li, Murr, & McClure, 1999). They consisted of intercalated (Swirl and vortex-like) flow patterns in the SZ as shown in Figure 2.17. The rings were formed in a plane perpendicular to that of tool rotation. Krishnan (Krishnan, 2002) explained that the formation of the rings was a geometric effect due to the fact that cylindrical sheets of material were extruded during each rotation of the tool, and cutting through the section of the material produced apparent "onion rings". It was postulated that the tool appeared to wait for a very short time to produce frictional heat and extrude a cylindrical shaped material around to the retreating side of the joint. The spacing of the markings was found to be equal to the forward motion of the tool in one rotation. At a constant feed rate, the spacing of the rings was found to be inversely proportional to the rotation speed.

A recent study on the role of FSW tool on material flow and weld formation

in 7020-T6 alloy, found that there were two different modes of material flow regimes involved in the friction stir weld formation; namely "pin-driven flow" and "shoulder-driven flow" (Kumar & Kailas, 2008). Material transfer in the pin-driven region took place in successive layers that had crescent cross-section with wide top and narrow bottom, and had an upward flow. The shoulder deflected the pin-driven material from the retreating side to advancing side. The layer thickness in the centre of the weld was comparable with distance traveled per rotation of the tool. These material flow regimes merged, and resulted in formation of a defect-free weld. The etching contrast in the regimes gave rise to onion ring pattern in the FSW joint.

FSW joints are known to be free from defects like porosity, slag inclusion and solidification cracks; which deteriorate the weld quality and joint properties (Olabode et al., 2013). The defects are minimised due to absence of melting during welding, since the metals are joined in the solid state itself due to the heat generated by the friction and flow of metal by the stirring action. However; FSW joints are prone to other defects like pin holes, tunnel defect, piping defect, kissing bond and cracks (Elangovan & Balasubramanian, 2008a). The defects result from improper plastic flow and insufficient consolidation of metal in the joint. Defects have been observed when the optimal temperature and hydrostatic pressures are not maintained during FSW (Krishnan, 2002).

Presently, FSW is commercially used in industries, such as ship-building, high-speed train manufacturing, and aviation industry (Cam & Mistikoglu, 2014).

Friction stir processing (FSP) was developed as a generic tool for microstructure modification based on the basic principles of Friction Stir welding (FSW) (Sen & Sharma, 2016). The concept of FSP technique is similar to that of FSW, as illustrated in Figure 2.18. A high strength tool with a shoulder and a pin attached underneath is used for friction stirring. Heat, generated by the friction between the rotating tool and the material surface and the high-strain-rate plastic deformation, softens the

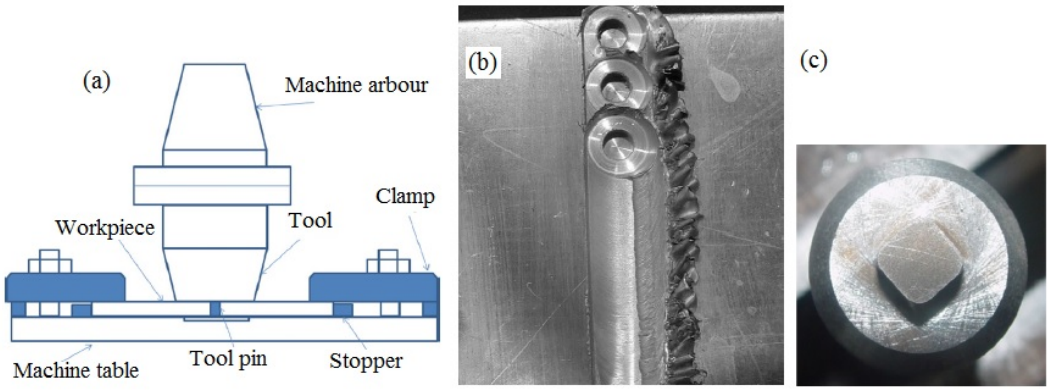

Figure 2.18: (a) Experimental Set-Up of FSP on a Milling Machine; (b) FSP'ed Sample Using 3 Overlapping Passes (c) FSP Tool Photograph Showing the Tool Shoulder and the Square Pin (El-Rayesa & El-Danafa, 2012).

material (without melting). The tool traverses through the material, which is then brought from the front to the back of the tool and forged down under the action of the tool shoulder.

The tool is normally made of high-speed steel, high carbon steel (the tool steel for hot work), polycrystalline cubic boron nitride, and wolfram alloys (Charit & MishraLow, 2005; Elangovan & Balasubramanian, 2008a; El-Rayesa & El-Danafa, 2012; Kwon et al., 2002; Nandan et al., 2008; Thomas & Nicholas, 1997). The tool pin shapes include cylindrical (straight, tapered and threaded), triangular and square. There is evidence that the tools have been manufactured from end mills that were ground to size on a circular grinder and it was ensured that they conformed to standard sized collets (Hofmann & Vecchio, 2005). The ratio of tool shoulder to pin diameter is 2.5; and the pin diameter is always equal to the plate thickness. However, the length of the pin is slightly less than the plate thickness.

Friction-stir processing is used to enhance metal properties through grain refinement, homogenization of second phase particles, elimination of defects like porosity, and surface modification. Although predominantly applied to aluminium alloys, the reach of FSP has now extended to a variety of materials including steels and polymers.

This review deals with the fundamental understanding of FSW and its metallurgical consequences. The focus is on parameters required for control of microstructure and mechanical properties of welded joints.

Methods for refining grains in metals include inoculation, control of cooling rate during solidification and severe plastic deformation (SPD). However; inoculation and control of cooling rate produce grain of about 150 μm average size. On the other hand; SPD has been used to develop ultrafine grained (UFG) microstructures (grain size <1 μm) in aluminium alloys; resulting in improved mechanical properties, such as, strength, ductility, fatigue strength, fracture toughness and superplasticity (Charit & MishraLow, 2005; Elangovan & Balasubramanian, 2008a). Superplasticity is the ability of a material to sustain tensile elongation >200% prior to failure. UFG material with a submicrocrystalline structure can be produced with only a "single pass" of FSP; As compared with ECAP which generally requires several passes (Elangovan & Balasubramanian, 2008a).

Attempts to modify the structure of materials with the FSP method have been carried out on aluminium, copper, magnesium, steels, and also composites with a metallic matrix (Kemal, Kulekci, & Buldum, 2015a). There are six areas of research interest using FSP on rolled or milled aluminium plates. Mainly, FSP has been established as a potential grain refinement technique for Al alloys including 6061 (Elangovan & Balasubramanian, 2008a), 319 (Santella, Engstrom, Storjohann, & Pan, 2005), 356 (Ma, Sharma, & Mishra, 2006), and 6082 (El-Rayesa & El-Danafa, 2012). Further; FSP has homogenized second phase particles and minimized porosity (Ma et al., 2006). It has been suggested that the FSP technique may be applicable to homogenization of MMC materials with inhomogeneous microstructure (Kwon et al., 2002). Additionally; local modification of material properties, such as: strength, ductility, hardness, fatigue life, fracture toughness and corrosion resistance have been enhanced (Ma et al., 2006). Finally; FSP has been used for the creation of composite structures in the surface layer of the material by the introduction of a

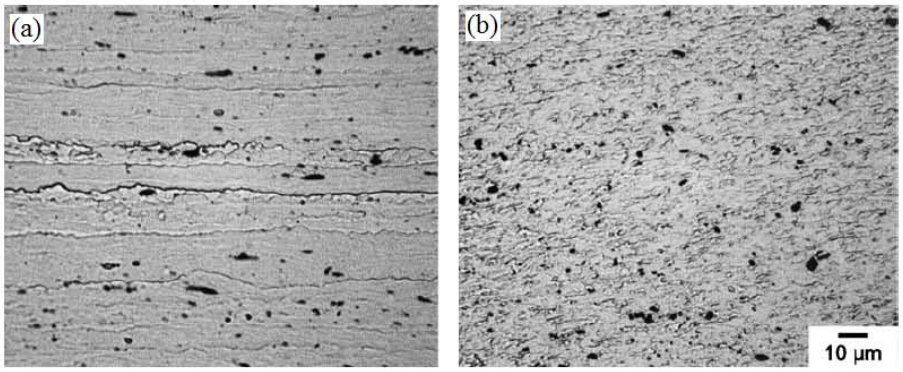

Figure 2.19: Comparison of Second-Phase Particles (a) in BM and (b) in SZ of Aluminum 1050 Alloy Specimen Processed at a Speed of 560 rev/min and Feed of 155 mm/min (Kwon et al., 2002).

strange phase, e.g. carbon nanotubes, SiC, Al_2O_3 and SiO_2 particles, and others (Bahrami, Dehghani, & Givi, 2014; Kemal, Kulekci, & Buldum, 2015b).

Studies on the microstructure of stirred zone, demonstrated that it consisted of fine recrystallized grains resulting from a severe plastic deformation of the magnitude experienced in equal-channel angular pressing (ECAP) and high-pressure torsion (HPT) (Kwon et al., 2002). Additionally, the recrystallized grain sizes in 1050 (Elangovan & Balasubramanian, 2008a), 1100, 6061 (Y. Li et al., 1999) and 7050 (Su J et al., 2003) aluminium alloys ranged from 2 to 10 μm. These sizes were approximately10 to 100 times smaller than in the original work piece materialsKwon et al. (2002). FSP was used to create a microstructure with grain size 0.68 μm in as-cast Al-8.9Zn-2.6Mg-0.09Sc (wt.%) alloy (Charit & MishraLow, 2005). Microstructure of the FSP zones in 1050 aluminium alloy had recrystallized equiaxed grains of size 0.5 - 4 μm (Kwon et al., 2002). The results suggest that the stirred zone is composed of refined grains.

Grain size measured within the SZ zone ranged between 2.0 and 6.0μm, depending on the processing temperature (Charit & MishraLow, 2005). Second-phase particles in 1050 aluminium alloy were broken down and homogenized in the SZ as compared with the unprocessed zone as shown in Figure 2.19. Combined effect of deformation

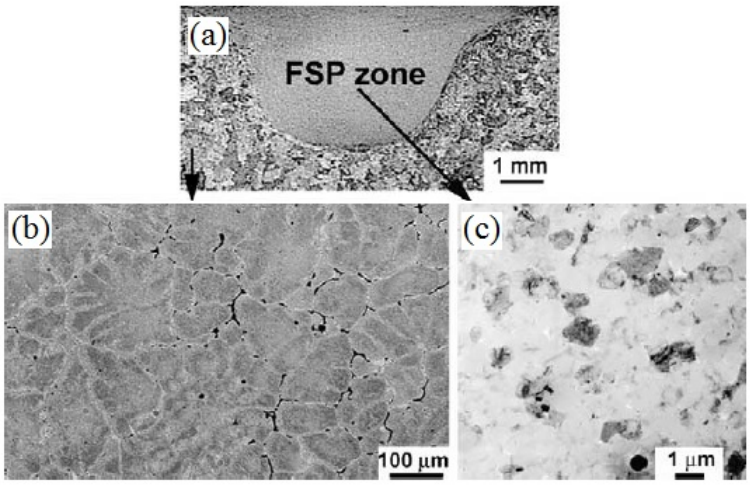

Figure 2.20: Optical Macrographs of the FSP Al-Zn-Mg-Sc Alloy, (a) Processed Zone (b) Unprocessed Material Showing Typical Dendritic Microstructure, and (c) a Bright Field TEM Image of the FSP Zone, Showing Ultra Fine Grains (Charit & MishraLow, 2005).

and temperature lead to very fine grain sizes through the dynamic recrystallization (DRX) process and break-up of constituent particles as shown in Figure 2.20 (Charit & MishraLow, 2005; Elangovan & Balasubramanian, 2008a; Y. Li et al., 1999). Low peak processing temperature and a fast cooling rate kept the post-DRX growth of grains limited. This, in turn, helped in the generation of the UFG microstructure.

Rolled plates of high strength Al 7050 and Al-Li-Cu alloys have been found to have highly elongated and pancake shaped BM grains (Jata & Semiatin, 2000; Su J et al., 2003). These grains were several hundred micrometers long, approximately 75 μm thick and had average grain diameter of 87 μm. The microstructure of FSW 7050 alloy showed that the BM grains had low angle boundaries, and low dislocation density, and deformation in the TMAZ resulted in severe bending of the grain structure. In contrast, the microstructure within the SZ contained equiaxed grains formed through continuous dynamic recrystallization (CDRX). During CDRX the BM grain low-angle boundaries are replaced by high-angle boundaries in the DXZ by a continuous rotation of the original low-angle boundaries during FSP; under conditions of frictional heating and plastic strain. Consequently; the TMAZ and SZ

grains achieves high-misorientation, high dislocation density and high angle grain boundaries. Within the TMAZ, the grain structure of Al 2024 alloy has been reported to be highly elongated and with a considerable grain distortion due to mechanical effect of the tool, and the grain structure of HAZ was observed to be similar that of the BM (Bussu & Irving, 2003).

Use of a coolant has been found to produce ultrafine grains. Al 6061-T6 plates, with an initial grain size of $\sim$50μm were subjected to FSP in air and also under water at speed of 1000 rpm and feed of 1.27 mm/s. The final average grain size for air and submerged process were $\sim$5 μm and $\sim$200 nm respectively (Hofmann & Vecchio, 2005). FSP 7075 Al was quenched by pouring methanol and ice on the joint immediately after the withdrawal of the tool (Ouyang, Yarrapareddy, & Kovacevic, 2006). Microstructural characteristics of five samples from the processed material $\sim$0, 0.3, 1 and 3mm away from the pin, and the fifth sample was prepared from the joint area outside the tool shoulder were investigated. The average grain sizes starting from specimen 1 - 5 were 0.1 - 0.4, 0.8, 1.2, 1.5 and 1 - 4 μm. Initial sizes of newly recrystallized grains of 7050 alloy were 25 - 100 nm, and grew to 2 - 5 μm after 1 - 4 min due to frictional heating at 350 - 450 ^{0}C (Rhodes, Mahoney, H., & Calabrese, 2003). Consequently; attempts to minimize the heat generated have prevented the grain growth.

It has been demonstrated that FSW and FSP eliminates casting defects like porosity and microsegregation in a single step, and modify the coarser dendritic microstructure into a relatively homogenized one with ultrafine grains (0.68 μm) (Charit & MishraLow, 2005). The second phase particles have been broken down and distributed homogenously in the SZ (Kwon et al., 2002). Within the SZ, and due to the intensified stirring action, the second phase particles were homogeneously dispersed and had almost regular size, whereas, on the TMAZ side the particles size is heterogeneous ranging between coarse to fine particles.

In addition, density of particles within TMAZ has been found to be less than that of SZ (El-Rayesa & El-Danafa, 2012). Therefore, microstructural development in each region is usually a strong function of the local thermo-mechanical cycle experienced.

Preparation of UFG Al alloys via FSW or FSP has been limited to variation of main processing parameters including: tool rotational speed, transverse speed (feed rate), vertical pressure on the tool, tilt angle of tool and tool geometry.

TEM microstructure of FSP zones in 1050 aluminium alloy at tool rotation speed of 560, 960 and 1840 rpm were composed of recrystallized equiaxed grains 0.5 μm, 1 - 2 μm and 3 - 4 μm, respectively (Kwon et al., 2002). Therefore, recrystallized grain size increased with increase in maximum temperature from 190 to 310 ^{0}C, which resulted from the increase in the tool rotation speed. FSW of 2024 to 6061 Al alloys produced a temperature rise that was directly proportional to increase in tool rotation speeds in the range 400 - 1200 rpm (Y. Li et al., 1999). Consequently; the grains were observed to grow by 10 to 102 times the original recrystallized grain. Further peak temperature has been found to increase significantly with increasing rotational speed and vertical pressure on the tool, and to decrease slightly with transverse speed (Kwon et al., 2002). Therefore, rise in peak temperature has been found to have a marked increase in the grain size. Increase in feed rate has been inversely proportional to grain size (Commin, Dumont, Masse, & Barrallier, 2009); however, it has not shown a significant effect on the grain size (Charit & MishraLow, 2005; Kwon et al., 2002; Sen & Sharma, 2016). Consequently; grain growth is observed with an increase in the processing parameters that promote heat generation.

Tool geometry include pin diameter, pin length, pin profile and shoulder diameter. Pin profile has been found to play a crucial role in material flow and in turn regulate the transverse speed of FSP. During the investigation of the Influence of tool pin profile and tool shoulder diameter on the formation of friction stir processing zone of 6061 and 2219 alloys (Elangovan & Balasubramanian, 2008a, 2008b), five different

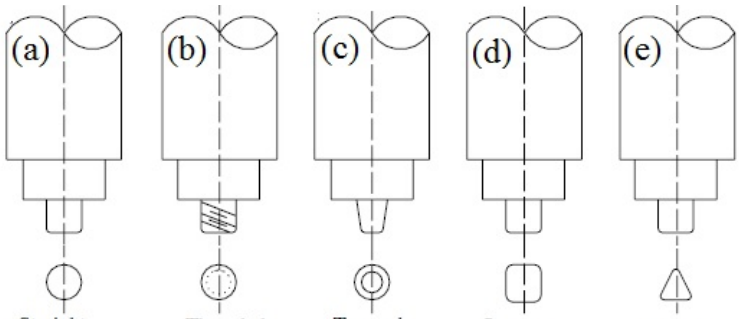

Figure 2.21: Tool Pin Profiles Used in FSP (a) Straight Cylindrical, (b) Threaded Cylindrical, (c) Tapered Cylindrical, (d) Square and (e) Triangular (Elangovan & Balasubramanian, 2008a).

tool pin profiles (straight cylindrical, tapered cylindrical, threaded cylindrical, triangular and square) as shown in Figure 2.21 were used, and each profile had three different shoulder diameters.

Eccentricity of the pin allows the hydromechanically incompressible plasticised material to flow more easily from the leading edge to the trailing edge of the rotating tool (Thomas & Nicholas, 1997). Off-centre or non-circular pin allows plasticised material to pass around the pin. The square pin had the highest eccentricity with dynamic volume and static volume in the ratio of 1 to 1.56, and produced the highest stirring pulsating action of 4 pulses per revolution of the tool in the flowing material due to flat surfaces. Consequently, the square profile produced the finest equiaxed grained microstructure, highest tensile strength, greatest microhardness, and least defects. Three shoulder diameters (15, 18 and 21mm) of the square pinned tool were considered. The combined effect of higher eccentricity, higher number of pulsating stirring action during metal flow and an optimum tool shoulder diameter may be the reason for superior tensile properties of the joint fabricated using square pin profiled tool with 18 mm shoulder diameter. Increasing the shoulder diameter has been reported to produce an increase in the heat generated during the FSP, and promoting grain growth (Commin et al., 2009). During the investigation of the influence of multi-pass friction stir processing on the properties of alloy 6082, it was

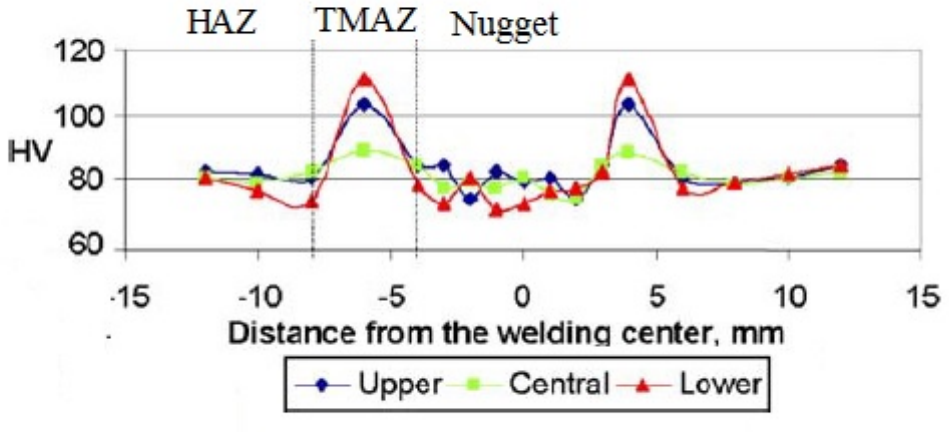

Figure 2.22: Hardness Profiles on the Cross-Section of the FSW 7005 10% Al_2O_3 Composite (Ceschini et al., 2007).

found that the accumulated heat accompanying multiple passes resulted in increase in the grain size, dissolution of precipitates and fragmentation of second phase particles (El-Rayesa & El-Danafa, 2012). The number of passes had bigger effect than that of the processing parameters.

Vickers microhardness measurements have been conducted across the section of FSW and FSP specimens. Hardness profiles across the SZ, TMAZ, HAZ and BM were found to vary. The microhardness profile of 7005 10% composite shown in Figure2.22 had a minimum hardness in the SZ (nugget), accompanied by an increase in the TMAZ to a peak, there after another minimum hardness was attained in the interface between TMAZ and HAZ, in the HAZ the hardness increased (Ceschini et al., 2007). However; in another study (El-Rayesa & El-Danafa, 2012) on FSP of alloy 6082, the lowest microhardness was found in the TMAZ on the advancing side and hardness was found to rise in the BM as shown in Figure 2.23. The study failed to distinguish the HAZ from the BM. Additionally from the two studies, it is not clear whether the hardness profile in the TMAZ is increasing or decreasing. Unlike in the hardness of 6082 alloy where the lowest hardness was noted on the advancing side, no significant difference in hardness between the advancing and retreating sides were found in the study of alloy 6061 (Hwang, Kang, Chiou, & Hsu, 2008). The microhardness

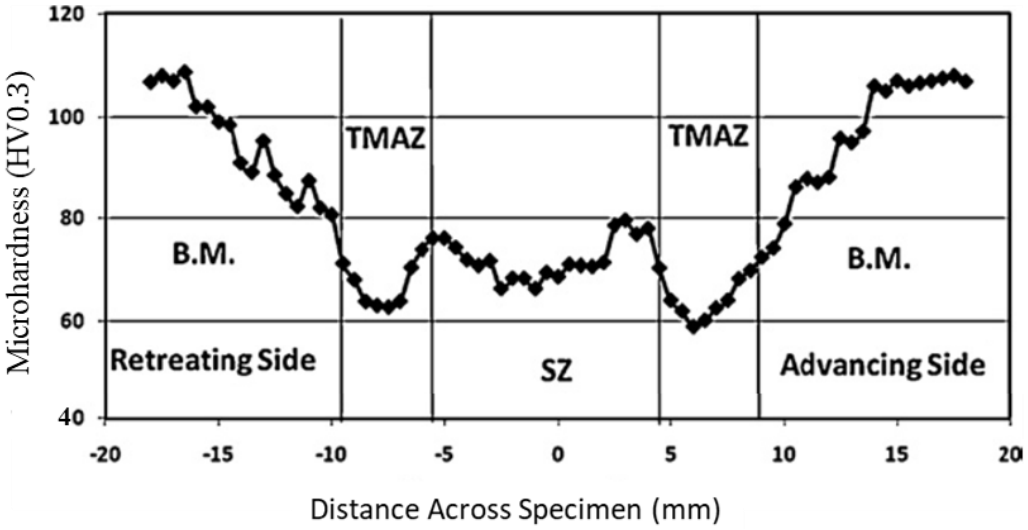

Figure 2.23: Hardness Distribution Across FSP-ed 6082 Al Alloy at 850 rev/min and 160 mm/min Using Two Passes (El-Rayesa & El-Danafa, 2012) .

of the 6061 and 6082 alloys was found to be lowest on the retreating side at the transition between the TMAZ and HAZ, and the point was within the limits of shoulder diameter (Moreira et al., 2009). In the study of FSW 2024-T351 alloy the SZ was found to be significantly harder than the region of TMAZ immediately outside the SZ boundary (Bussu & Irving, 2003). The point of minimal hardness in 5083 alloy has been found to possess high residue stress (Peel, Steuwer, Preuss, & Withers, 2003); and tensile fracture occurred at the same point in both the 6082 and 6061 alloys (Moreira et al., 2009).

In general, it can be seen that the SZ became much softer than the unaffected BM. The relatively high hardness of the base material was due to heat treatment. Softening of SZ with respect to the BM was due to the decomposition of β'' precipitates, over ageing of the precipitates and fragmentation of second phase particles. In addition, the TMAZ experienced more softening than the SZ due to the dissolution and growth of precipitates.

The microhardness measurements across friction stir welded 2024-T351 joint gave the

hardness of each zone (Bussu & Irving, 2003). The centre of the SZ was significantly harder than the TMAZ immediately outside the SZ, and hardness was lowest in the middle of the TMAZ. There after hardness increased steadily towards the boundary with HAZ, and into the HAZ until the BM hardness was realised. The lengths of the three zones were: the SZ from plate joint line (PJL) extending 5 - 6 mm out, the TMAZ from 5 - 6 mm to 10 - 12 mm, and the HAZ from 10 - 12 mm to 30 - 45 mm. The distance from the PJL to the end of the HAZ was approximately 48 mm. The residual hardness of FSW 6061 - T6 alloy varied from 55 VH near the top of the weld to 65 VH near the bottom; in contrast to a workpiece hardness which varied between about 85 and 100 VH (Peel et al., 2003). Microhardness variation across FSW plates of two dissimilar metals shown in Fig. 12 showed a clear distinction between the three zones and the BM (Liu, Murr, Niou, McClure, & Vega, 1997). A zone lying in the transition between TMAZ and HAZ on the retreating side had the lowest hardness value (Y. Li et al., 1999), and in the case of the mixed joint it was located in the AA6082-T6 alloy plate side (Moreira et al., 2009).

FSP has been applied to aluminium silicon alloys. FSP was applied to cast 356 Al alloy to modify the as-cast microstructure (Ma et al., 2006). FSP eliminated porosity, homogenized and refined the cast microstructure. The resultant microstructure contained fine Si particles (0.25 - 0.42 μm) that were distributed in a fine equiaxed grain aluminium matrix of size 3 - 4 μm. A post-FSP T6 heat treatment did not alter the Si particle distribution, but did significantly coarsen the Si particles. In another study (Santella et al., 2005) A319 and A356 castings were treated by friction stir processing to reduce porosity and to create more uniform distributions of second-phase particles. The dendritic microstructures were eliminated in stirred zones. Ultimate tensile strengths, ductility, and fatigue lives of both alloys were increased by FSP.

SZ in 6061 - T6 and 6082 - T6 alloy was characterized by a dynamic continuous recrystallization microstructure, and second-phase particles in the workpiece were

essentially "stirred" into the weld zone; resulting in a homogeneous structure containing equiaxed grains and a reduced dislocation density (El-Rayesa & El-Danafa, 2012; Liu et al., 1997). The SZ grain size averaged 10 μm in contrast to 100 μm for the workpiece. Although TMAZ underwent plastic deformation, recrystallization did not fully occur in this zone due to insufficient deformation strain and lower pick temperatures compared to the SZ. As a result, it was characterized by a less deformed structure, in which the parent metal-elongated grains were markedly bent due to plastic deformation into the direction inclined to the TMAZ/SZ boundary. The heat affected zone (HAZ) experienced a thermal cycle, without plastic deformation and thus retaining a grain structure similar to the parent material. Residual hardness of the zone varied from 55 VH near the top of the weld to 65 VH near the bottom; in contrast to a workpiece hardness which varied between about 85 and 100 VH. For the 6061 - T6 and 6082 - T6 alloys it was observed that the minimum microhardness occurred in the transition between TMAZ and HAZ, and on the retreating side (Liu et al., 1997). Further tensile failure occurred at the point. An increase of tool rotational speed from 400 to 1200 rpm during the FSW of 2024 to 6061 resulted to rise in temperature to 0.6 - 0.8 Tm within the processed zone (Y. Li et al., 1999). Introduction of multi FSP passes on 6082 - T6 alloy was found to raise the temperature too (El-Rayesa & El-Danafa, 2012). The heat generated dissolved the β'' precipitates, and upon cooling a softer β' precipitate was formed; hence decrease in hardness. Consequently, the microhardness was reduced by about 45%, and the grains were observed to grow by 10 to 10^2 times the original recrystallized grain size (El-Rayesa & El-Danafa, 2012; Hwang et al., 2008).

FSW of 6061 aluminum alloy to copper was difficult due to the brittle nature of intermetallic compounds formed in the SZ (Moreira et al., 2009). Joining of the dissimilar metals, Al 6061 alloy and copper weld consisted mainly of several intermetallic compounds such as $CuAl_2$, CuAl, and Cu_9Al_4 together with small amounts of α-Al and the saturated solid solution of Al in Cu. The measured peak

temperature in the weld zone of the 6061 aluminum side reaches 580 ^{0}C, which was distinctly higher than the melting points of the Al-Cu eutectic.

2.8 Summary

There is a need to understand aluminum together with its alloys, and their applications. Aluminum and its alloys have definite applications. Therefore, products manufactured from the materials can be categorized into families based on their applications. Scrap from aluminum products is recyclable. Sorting it according to families of parent products will most likely yield a secondary alloy similar to the primary alloy during recycling.

An aluminum MFA study is instrumental for establishing the likely classes, sources and quantities of local aluminum scrap. Results of the study will be useful during determination of suitable scrap for production of secondary wrought aluminium alloys for automotive and structural applications. The properties, quantity and availability of the selected sorted scrap must guarantee sustainability of production of the alloys.

Meticulous sorting of the scrap, melting of the scrap and post cast processing are instrumental in enhancing the microstructure, mechanical properties and weldability of the alloys. Impurities, inclusions and casting defects need to be avoided during melting since they have deleterious effects on the mechanical properties of the alloys. Extrusion has been found to homogenize the second phase particles and minimize porosity in structural wrought aluminum alloys. Lately HPT has been found to improve the mechanical properties of aluminum alloys (An et al., 2011; Ito & Horita, 2009). FSW has been found to produce superior joints than fusion weld (Kwon et al., 2002; Olabode et al., 2013; Sen & Sharma, 2016). Evaluation of the performance of the developed alloys will ascertain the beneficial effects of post cast processing operations on the wrought alloys.

From literature, the following gaps were identified;

1. Data on the quantity and type of available structural wrought aluminium scrap in Kenya is missing.
2. Production of recycled structural standard wrought aluminium alloys depend on addition of costly primary aluminium for dilution and alloying element adjustment during melting.
3. The mechanical properties of the recycled structural aluminum alloys are low, thus limiting their applications.
4. Joining of wrought aluminium alloys relies on fusion welding which has defects including wide heat affected zone, porosity, cracking and inclusions.

This research will address all the four identified gaps.

CHAPTER THREE

METHODOLOGY

3.1 Introduction

This chapter presents methodology for Kenyan aluminium material flow analysis, hand sorting and melting wrought aluminium scrap. Further, procedure for post cast processing of aluminium wrought alloy through extrusion, HPT and FSW are outlined. Finally, procedure for evaluation of the effects of post cast processes on microstructure and mechanical properties of the secondary wrought aluminium alloy are reported.

3.2 Aluminium Material Flow Analysis

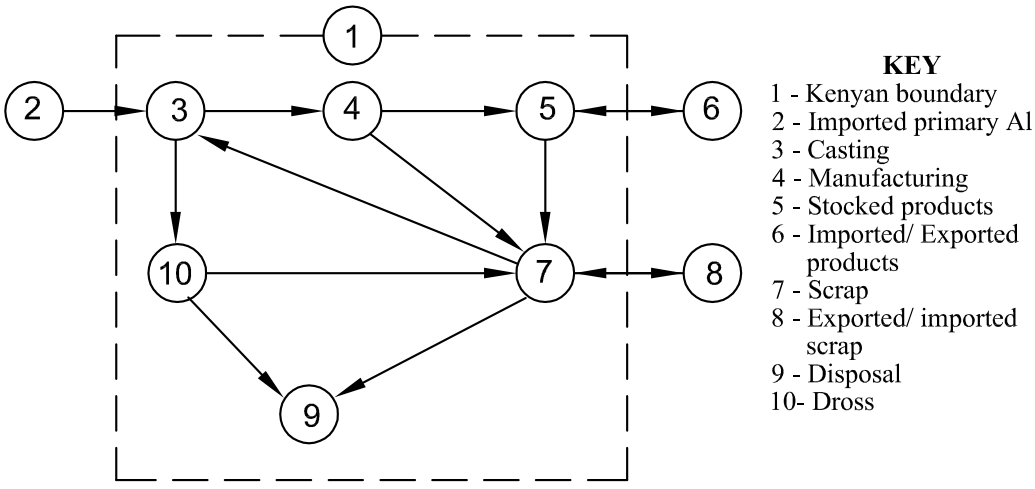

Figure 3.1: A Model of Local Aluminum Flow.

A survey was conducted to determine Kenyan aluminium mass flow. The flow was modelled as shown in Figure 3.1. The model represented the aluminium flows in, out

and within Kenya. Selection of participating institutions and data acquisition tools was guided by the availability of aluminium data in nodes 2 - 10. This was guided by the results of a preliminary survey and report of previous studies Mose (2009); Wangombe (2014). The studies had reported that the institutions which collected or consumed aluminium scrap were located in Nairobi, Mombasa and Nakuru as shown in Figure 3.2. Aluminium scrap is collected from the rest of the country and transported to these three towns where it is sold to dealers or foundries.

Figure 3.2: Map of Kenya Indicating Cities of Nairobi, Mombasa and Nakuru where Surveyed Institutions are Found.

The institutions include:

1. Kenya Association of Manufacturers (KAM), which provided data on industrial players.

2. Kenya National Bureau of Statistics (KNBS), that provided data on aluminium exports, imports and volume of local scrap generated.

3. Kenya Ports Authority (KPA), which provided data on imports and exports.

4. 25 Scrap dealers listed in Appendix A, were selected for the study. Nairobi, Mombasa and Nakuru had 15, 5 and 5 dealers respectively. They provided data related to sources, types and volume of scrap aluminium alloys. They also helped to identify local and overseas consumers of the scrap.

5. 29 Foundries listed in Appendix B, were studied. Nairobi, Mombasa and Nakuru had 18, 6 and 5 foundries respectively. They provided data related to consumption of different types of aluminium scrap, and products generated.

Data acquisition tools used included a questionnaire, Site visits, interviews and Literature review. A summary of application of the tools to different target groups is as shown in Table 3.1.

Table 3.1: The Participating Firms and Their Relevant Data Acquisition Tools.

Target group	**Tools used**
KAM, KNBS, KRA and KPA	Site visit, interviews and literature review
Scrap dealers	Questionnaire (section 1 - 3 and 8),site visit and interviews
Foundries	Questionnaire (section 1 - 8),site visit and interviews

A questionnaire was designed as shown in Appendix C. A summary of its general structure was as shown in Table 3.2. The questionnaire was sent to scrap dealers and foundries in order to collect data for the year 2017.

Visits were made to KAM, KNBS, scrap dealers and foundries. Observations regarding the handling of aluminium were made. Interviews were made, to give more information that was not covered by the questionnaire. During such visits

Table 3.2: The Questionnaire Structure.

S No.	**Issue**	**Question focus**
1	Cover letter	Introduction from JKUAT
2	Preamble	Introduction, Benefits of the study, confidentiality, contact person
3	General company information	Respondent's identification data (name, address, telephone and contact person)
4	End of life scrap (EOL)	Type, source (local and imports), quantity, value, purpose, destination (local and export) and reuse
5	New (in house and process) scrap	source, quantity and Value
6	Primary Al	Source, quantity, value and purpose
7	Melting	Primary Al, EoL scrap, new scrap, quantity generated, dross, destination and value
8	Fabrication and manufacturing	Products (semis or new products) - quantity, value, destination and quantity of new scrap
9	New goods	local, imports, exports, quantity and value
10	disposal (land fill)	Any amount thas is not recycled
11	Research interest	To report outcome of the survey to the participating groups

references were made to other firms which were not identified initially or were hard to reach.

3.3 Wrought Structural Aluminium Scrap Sorting and Melting

Wrought aluminium scrap from Nairobi scrap yards was hand sorted. Hand sorting was based on colour, density, method of processing and applications. The colour of aluminium was silvery white. Aluminium has a density of about 2.7 g/cm^3. Structural aluminum wrought alloys are mainly processed through extrusion and

Figure 3.3: Extruded Aluminum Scrap Batches: (a) A; (b) B; (c) C; and (d) D.

rolling. Dilute hydrochloric acid (HCl) was used to distinguish aluminium from magnesium which has a gray white appearance and a density of 1.8 g/cm^3. When 1M HCl solution was applied to the surface of aluminium scrap there was no reaction. When the same was repeated on the surface of magnesium scrap, there was a reaction. Bubbles of hydrogen gas were evolved. The reaction was as shown in Equation 3.1.

$$Mg_{(g)} + 2HCl_{(aq)} \rightarrow MgCl_{2(aq)} + H_{2(g)} \tag{3.1}$$

A solution of 0.3 % HCl and 1% $CUSO_4$ was used to differentiate 5xxx scrap from 6xxx scrap. The solution did not affect the 6xxx alloys. However, the surface 5xxx alloys which have a higher concentration of maganesium were expected became dull when the solution was swabbed on its surface.

The scrap from extruded wrought aluminium structural products was sorted into four batches, each of 50 kg. The batches were labelled as A, B, C, and D as shown in Figure 3.3. All the four batches were etrusions which had silvery white colour on thier freshly scratched surface, and did not react with 1M HCl or a solution of 0.3% HCl and 1% $CUSO_4$. Their former applications, sectional thickness, colour and response while sawing were summarized as shown in Table 3.3.

Batch A was composed of light extruded sections of scrap from construction site

Table 3.3: A Summary of the characteristics of the four Scrap Batches

Batch	Former Application	Thickness (mm)	Colour	Response while sawing
A	construction	1.5	Silvery white	soft
B	window frame	3	anodized and dyed	soft
C	Automotive frame	5	Silvery white	soft
D	Building	5	dull white	hard

that were used for partitioning. Batch B constituted of light extruded sections for house window frames which were anodized and dyed using different colours. Batch C consisted of extruded wrought aluminium sections derived from automotive body structure. Batch D comprised of heavy sections from buildings. They were used to support heavy structures. All the scrap was cut into sections 600 mm long. Batch D was relatively hard to cut compared to the others.

Each batch was heated to a temperature of 740 ^{0}C in an oil fired crucible furnace as shown in Figure 3.4 (a). Before pouring, specimens for chemical analysis were poured in a copper mould and chilled. The specimens were subjected to optical emission spectroscopy using SPECTRO equipment model MAXxLMF06. The results were an average of tests taken at three different points of the specimen. The remaining molten metal was cast into ingots as shown in Figure 3.4 (b).

Further, optical microstructure analysis, tensile, and microhardness tests were performed on specimens from batch C. Finally ingots of batch C were cast into billets of 50mm diameter and 60mm height for extrusion as shown in Figure 3.4 (c).

Figure 3.4: Melting of wrought Aluminium scrap: (a) Melting Batch A Scrap Using Oil Fired Furnace; (b) cast Ingots From Batch A; and (c) Billets Cast From Batch C.

3.4 Extrusion of the Identified Cast Wrought Alloy

The JKUAT general purpose pneumatic press was modified to act as an extrusion press by incorporation of an extrusion assembly as shown in Figure 3.5. Detailed drawings of the extrusion assembly were as shown in Appendices D and E. Primary characteristics of the press that were considered during design and fabrication of the extrusion assembly include: maximum ram extension, maximum pressure and distance between ram rest point and table top. Their quantities were 100 mm, 34.3 MN/m^2 (350 kgf/cm^2) and 340 mm respectively. The ram had a recess of 40 mm diameter and 60 mm height for supporting piston. The table had a stepped central hole of 98 mm and 70 mm diameter, and its top was raised 550 mm above the ground level. The other considerations made during the design of the extrusion assembly included the billet size, material for the different parts, extrusion force and extrusion ratio. The billet had a diameter of 60 mm and a height of 50 mm.

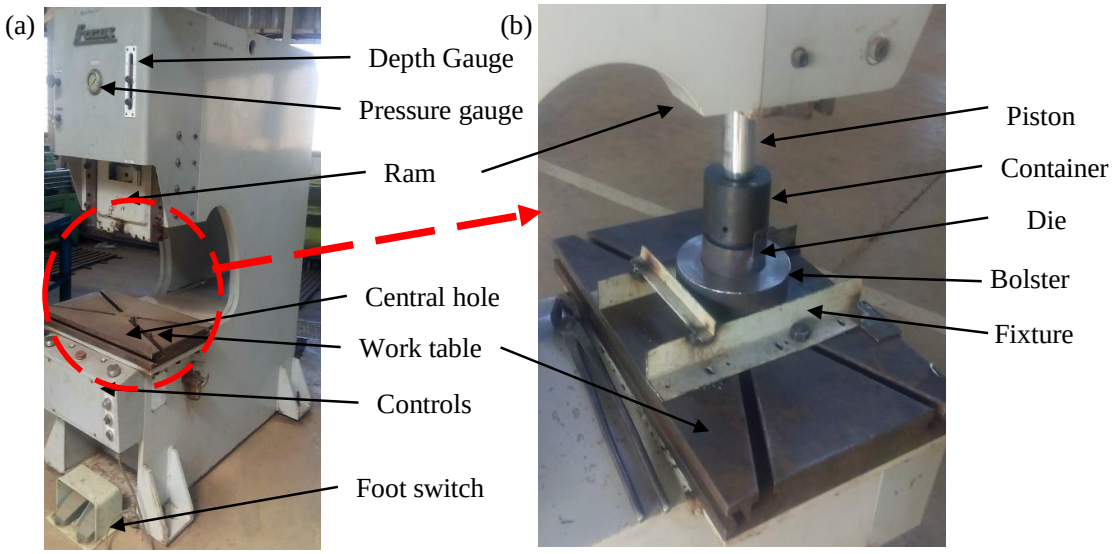

Figure 3.5: (a) General Purpose Pneumatic Press; and (b) Fabricated Extrusion Assembly Fixed Between Ram and Work Table of the Press

Extrusion billets of diameter 50 mm and length 110 mm were cast by melting the ingots of wrought Aluminium alloy 6061 in a muffle furnace as shown in Figure 3.4 (c). The billets were sliced into cylindrical pieces of diameter 50 mm and length 50mm. The slice, container and die were heated in a muffle furnace that was placed along side the press, to a temperature of 500 ^{0}C for about 1 hour. The hot components were quickly assembled on the bolster. Immediately graphite lubricant was applied around the slice, a dummy was placed on the slice and the piston was lowered in order to extrude the slice in one pass. Maximum working extrusion pressure was 0.0196 MPa.

The extrudate was subjected to tensile test, microhardness test, metallograpy (optical microscopy (OM) and scanning eletron microscopy (SEM)) and high pressure torsion.

3.5 High Pressure Torsion of the Extruded Material

The extruded rods of 14 mm diameter were turned to a diameter of 10 mm using a lathe machine while applying a coolant. Disks of 10 mm diameter and 1 mm thick were sliced from the turned rods using a low speed cutter shown in Figure 3.6 (a). The disks were ground to 10 mm diameter and 0.8 mm thickness using silicon carbide papers mounted on the table shown in Figure 3.6 (b).

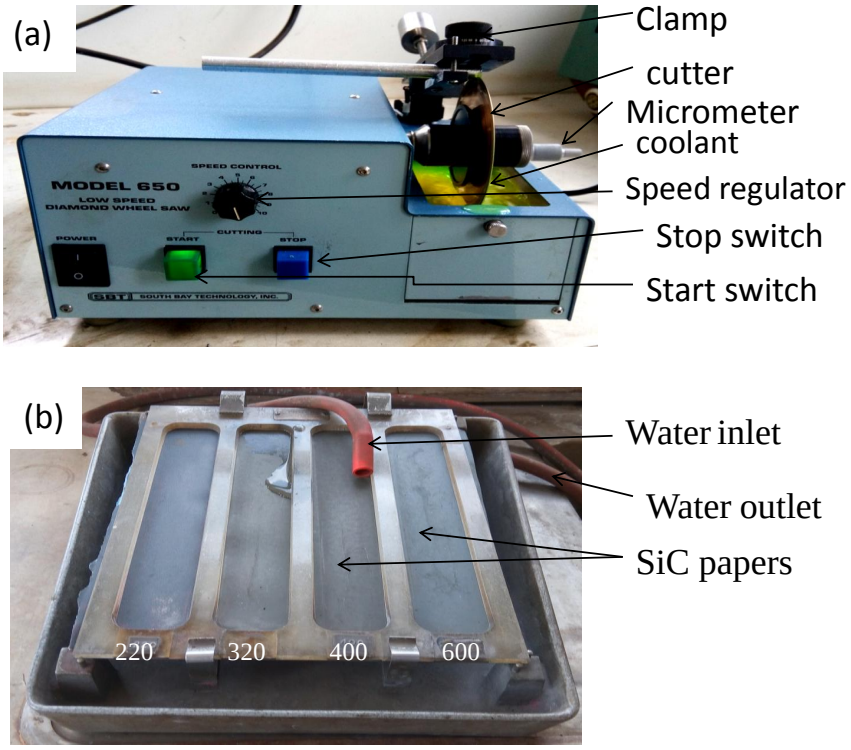

Figure 3.6: (a) Low Speed Wheel Cutter for Slicing Specimens (b) Hand Grinding Equipment

HPT equipment used for this study was as shown in Figure 3.7. The disks were gripped in recesses in the anvils of 10 mm diameter and 0.25 mm depth. Edges of the anvils were lubricated using MoS_2 to reduce friction between them and specimens;

since very high friction results in sticking of the sample onto the anvil. A pressure of 6 GPa was applied at a room temperature and a speed of 1 rpm.

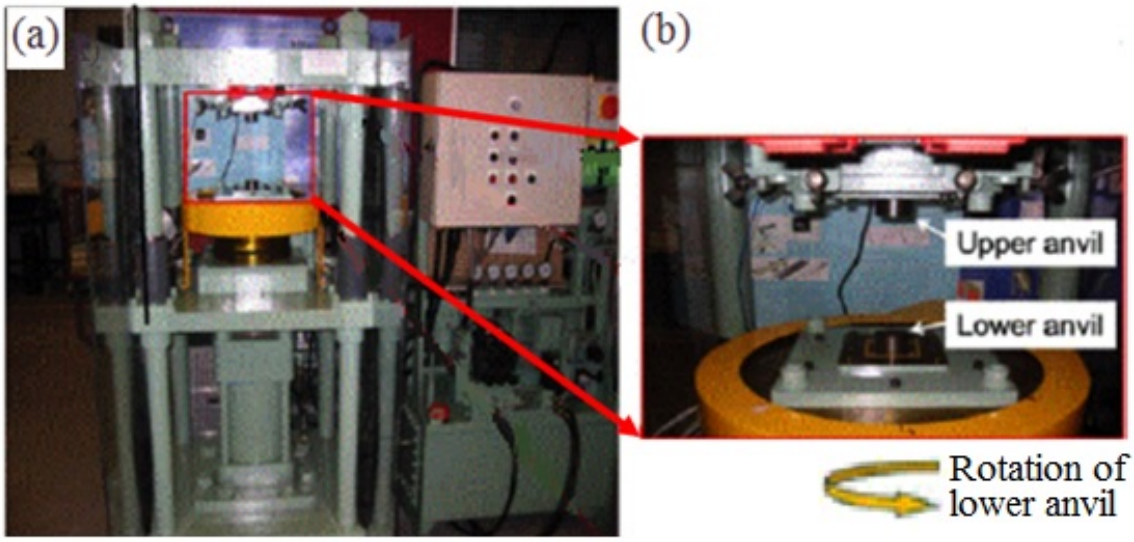

Figure 3.7: HPT Processing (a) The Rig Used for This Study; (b) Expanded Anvils for Gripping the Specimens.

The disks were subjected to HPT under constant pressure, (P) and varying number of revolutions (N), as shown in Table 3.4. Selection of pressure and the level of straining was based on previous studies on 6061 standard alloy (Intan, Lee, & Horita, 2013; Kawasaki et al., 2010). Five specimens were processed at a pressure of 6 GPa for $\frac{1}{4}$, $\frac{1}{2}$, 1, 5, and 10 turns; and consequently they were coded as $\frac{1}{4}$T, $\frac{1}{2}$T, 1T, 5T, and 10T respectively.

Table 3.4: HPT of secondary Al 6061 alloy Specimens at a Pressure of 6.0 MPa and Varying Number of Revolutions.

Pressure, P(GPa)	**Number of revolutions, N (per Min)**				
6	0.25	0.5	1	5	10

Later the processed specimens were subjected to Vickers microhardness, tensile test and metallurgical analysis (OM and SEM). The analysis was carried out along

the diameter of the specimen to determine the grain size and the extent of grain refinement effect on second phase particles.

3.6 Friction Stir Welding of Wrought Alloy

Setup of FSW process in a milling machine was as shown in Figure 3.8. Enshu universal milling machine in JKUAT machine shop was used in vertical position during the FSW. The machine spindle speed range was 68 - 1760 RPM. Table could move automatically along X (transverse), Y (longitudinal) and Z (vertical) axis using a feed motor. Three automatic coarse table feeds were available, in fast, faster and fastest modes; and each mode could be fine tuned. Therefore the machine was able to vary rotation and feed speeds during the FSW. A fixture for holding work pieces was designed and fabricated as shown in Appendix F and Figure 3.8 (b).

FSW tools had three basic parts: shank, shoulder and pin; and were machined from high speed steel (broken end mills) and heat resistant alloy. The tool materials were ground using either cylindrical or surface grinder to provide cylindrical and square tool profiles respectively as shown in Figure 3.9. Pin diameter (d) and height were equal to thickness (t) of workpieces. Ratio of shoulder diameter (D) to pin diameter was 2.5.

A 6061 extruded Al-alloy J - section, 400 mm long and 6 mm thick shown in Figure 3.10 was studied. The extruded alloy was sawn into 3 plates: 400 x 75 x 6 mm, 400 x 100 x 6, 400 x 110 x 6 mm.. Specimens 100 x 50 x 6 mm were cut from the plates.

Fixture, workpiece and tool were setup in the milling machine as shown in Figure 3.11. Processing direction was normal to the plate extrusion direction. Single pass processing procedure was followed to process the specimens. Variations of rotation speed and feed rate was made during processing in order to determine their effect on the microstructure and mechanical properties of the alloy. Specimens were processed

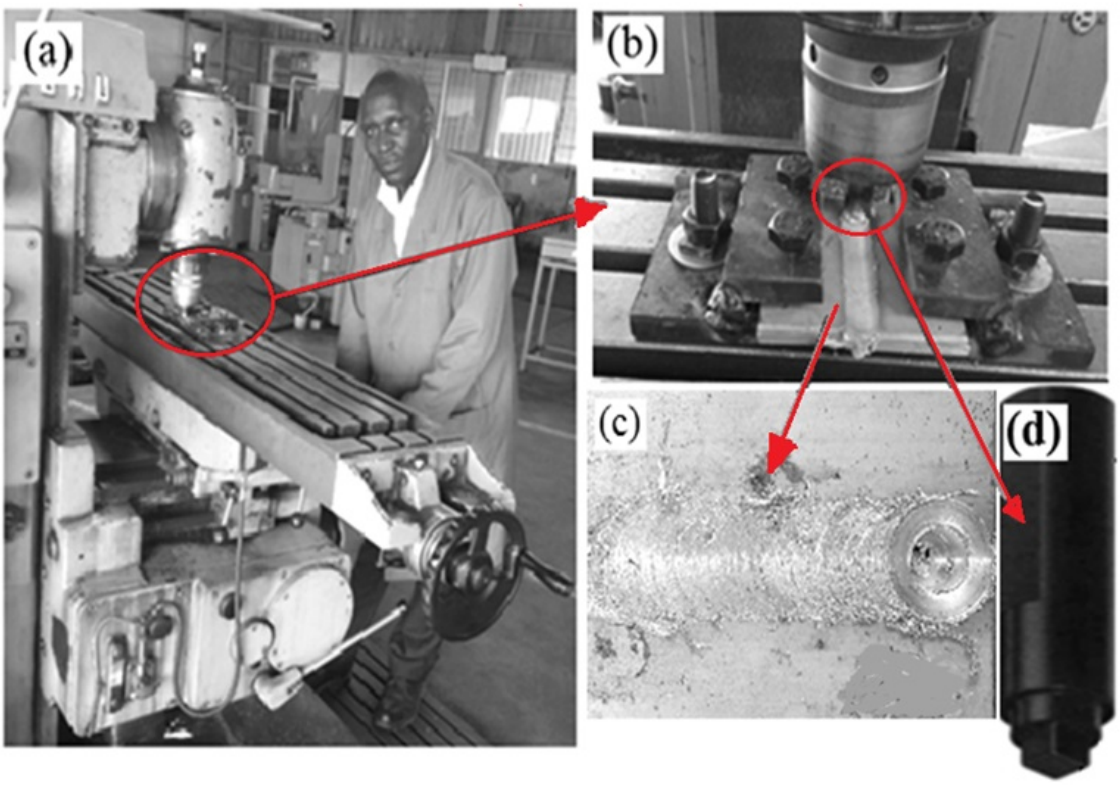

Figure 3.8: The FSW Setup: (a) Enshu Universal Milling Machine; (b) Detailed Spindle, Fixture and Workpiece; (c) Workpiece Processed at 1320 RPM and 100 mm Feed Rate and (d) Square Tool

at 370, 530, 715, 915 and 1320 RPM. Selection of the speed was based on the available speeds on the milling machine. While feed rate was either 40 or100 mm/Min. The aceptability of the universal milling machine and selection of speeds and feeds were based on the parameters used by other researchers who studied structural standard wrought alloys including Al 6061, Al 6082 and Al 7050 (Commin et al., 2009; Elangovan & Balasubramanian, 2008a; El-Rayesa & El-Danafa, 2012; Hofmann & Vecchio, 2005; Y. Li et al., 1999). Therefore, the selected speeds and feeds were enough to show the effects of heat generated on the properties of the material that was welded. The tool was rotating in a clockwise direction and the feed was as shown in Figure 3.11. Consequently, advancing and retreating sides were on the right and left hand side of the specimen respectively.

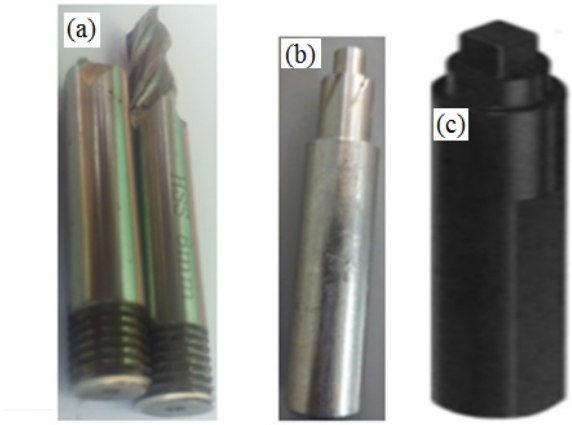

Figure 3.9: (a) End Mills for Preparation of FSW Tools; and Fabricated FSW Tools From (b) High Speed Steel (End Mills), (c) Heat Resistance Alloy

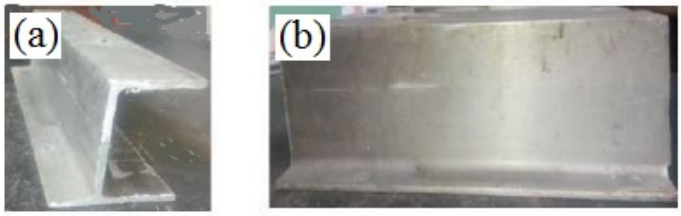

Figure 3.10: Views of the Extruded Al 6061 Alloy; (a) Section and (b) Side View

The FSW material was subjected to spectroscopic analysis, optical microscopy, tensile test and Vickers microhardness test.

3.7 Microhardness Test

Microhardness test was performed using a Leco Vickers hardness tester (Model LV800AT) set on a HV scale, 300g test load and 10s dwell time as shown in Figure 3.12 (a). Specimens were prepared from extruded, HPT and FSW material. Surface of the specimens was ground and polished. Diamond shaped indentations with a spacing of 0.15mm were made along a length of a specimen in three parallel lines spaced at 0.15mm as shown in Figure 3.12 (b). The hardness tester measured the diagonal of each indentation in μm and used it to calculate the hardness.

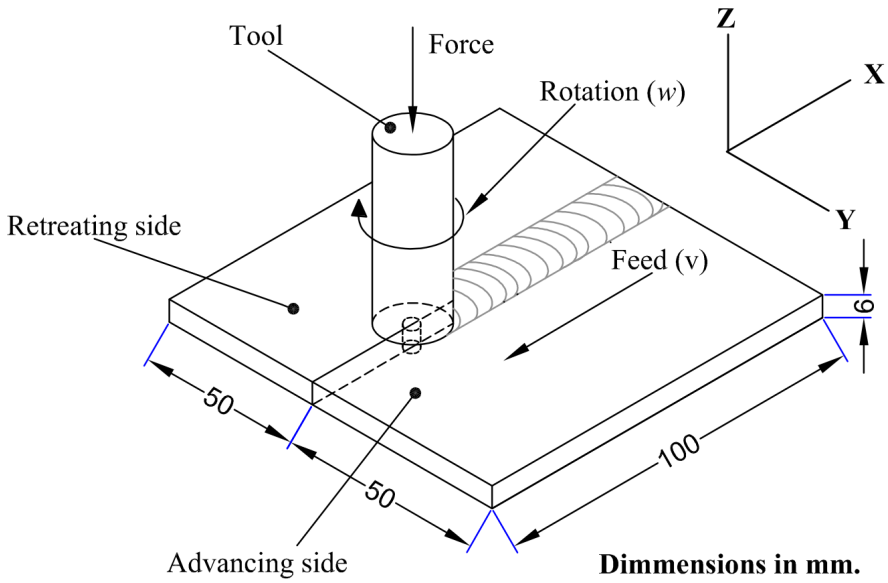

Figure 3.11: A Schematic Representation of FSW Setup in a Vertical Milling Machine.

Microhardness of a given point X was a result of the average hardness of the five highlighted points. Hardness of the extruded and HPT specimen was measured along the diameter of the disc; while that of the FSW specimens was determined across the different zones of the processed specimen.

3.8 Tensile Test

Tensile test was performed on standard and miniature specimens. Standard tensile test was performed in accordance with ASTM E8 standard using equipment and specimens which were as shown in Figure 3.13 and 3.14. A computerized Enkay universal tensile testing machine; model UT-10 of 100 kN capacity was used to pull the specimen at an average load rate of 0.1 kN/Sec at a room temperature. Data was captured by use of Mat Bench 5.0 software. Round and flat tensile specimens were machined from wrought aluminium alloy. Three round specimens of 50 mm gauge length 10 mm diameter were turned from the as cast and extruded materials. Five flat specimen of 50 mm gauge length and 4 mm thick were milled from the friction

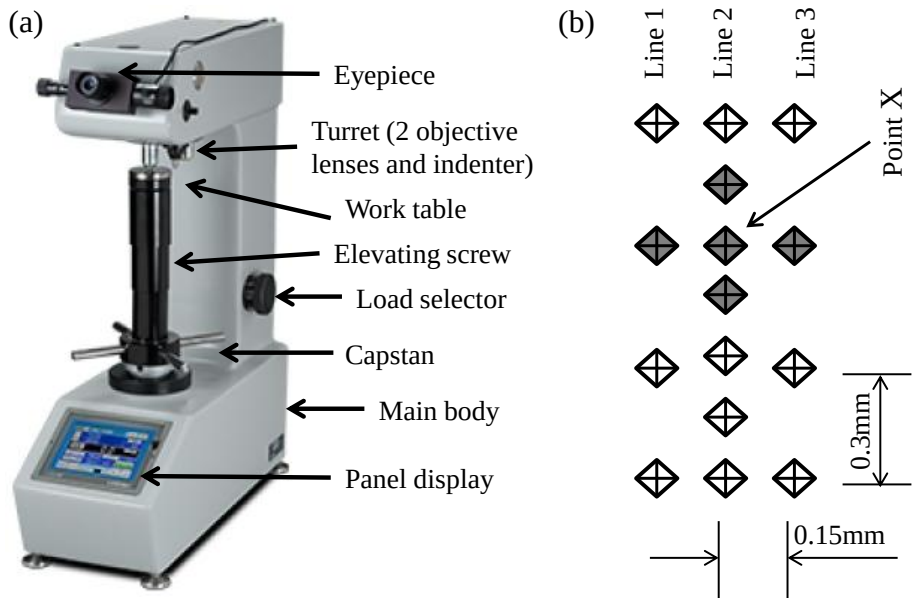

Figure 3.12: (a)Leco Vickers Hardness Tester (Model LV800AT); (b) Microhardness Measurement Along a Specimen Surface.

stir welded material. A lot of coolant was applied during turning and milling of the specimens.

Miniature tensile specimens were cut from HPT processed disc samples with $\frac{1}{2}$ and 10 turns. Two miniature tensile specimens were cut from each processed disc using a wire electrical discharge machine (EDM) as shown in Figure 3.15. The centre of each tensile specimen was 2 mm from the centre of the disc, to avoid the non-uniform microstructure in the central region. The gauge length was 1.0 mm with cross-sections of 1.0 x 0.7 mm^2. Tensile tests were conducted at room temperature using a Zwick tensile testing machine, and the specimens were pulled to failure for initial strain rates of 1.0 x 10^{-3} s^{-1}.

3.9 Metallography

Specimens for optical microscopy were prepared from the as cast, extruded, HPT and FSW materials. The number of specimens analysed were 2, 2, 5 and 10 respectively.

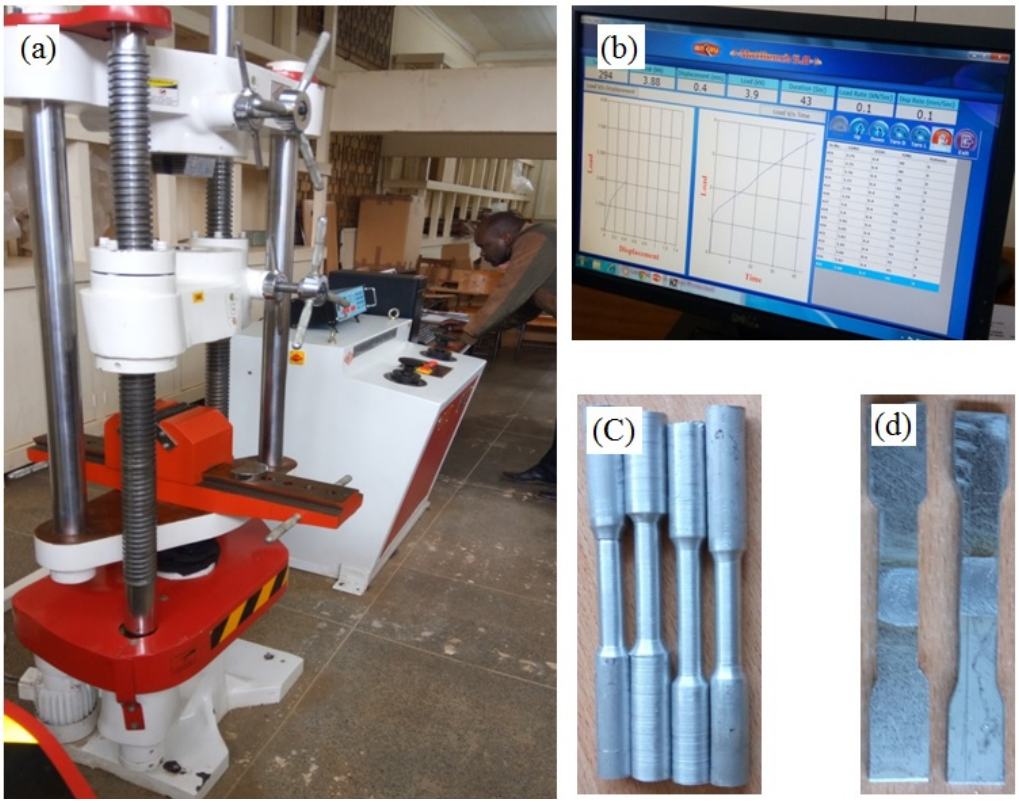

Figure 3.13: Tensile Test Apparatus: (a) Enkay Universal Tensile Testing Machine; (b) Mat Bench 5.0 Software; (c) Round Specimens and (d) Flat Specimens.

All specimens were cut using low speed wheel cutter shown in Figure 3.6(a). The specimen were mounted, followed by grinding and polishing. Grinding and polishing was performed using Leco equipment as shown in Figure 3.16. Silicon carbide papers sizes 240, 400 and 600 were used. Grinding speed, force and time were set to 300 RPM, 100 N and 10 minutes. Water was applied during grinding. Polishing was done at four stages using diamond paste 6, 3, 1 and $\frac{1}{4}$ μm, and finally oxide polishing.

Macro- examination of FSW 6061 alloy was performed by use of an enchant composed of 5 ml HF(48%), 10 ml H_2SO_4 and 85 ml H_2O.

Microstructure analysis was carried out using a light optical microscope (Make: Olympus; Model: BX41M-LED) incorporated with an image analyzing software

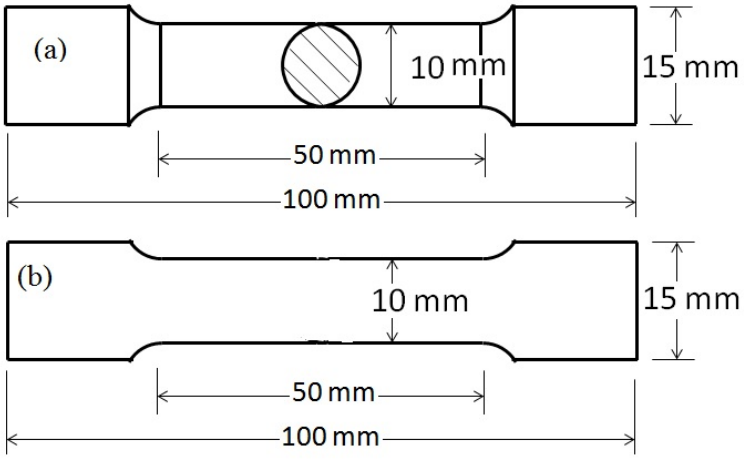

Figure 3.14: Tensile Specimens: (a) Round; and (b) Flat.

(stream essentials) as shown in Figure 3.17. Polished specimens were observed using the microscope in both etched and un etched condition.

Flick's reagent (10 ml HF, 5 ml HCl and 90 ml H_2O) was used for grain boundary etching of the specimens for 30 s. Etching was stopped when the surface changed from brightly polished to dull appearance. Thereafter specimens were dipped in hot water to remove the etchant, dipped in HNO_3 to clean the smut, rinsed in distilled water, rinsed with ethanol and finally drying in hot air.

Scanning electron microscopy was carried out using a microscope model: JEOL JSM 6500F in conjunction with Energy-dispersive X-Ray spectroscopy (EDS). Two specimens from the extruded material were analyzed in order to determine the elemental composition of the specimens.

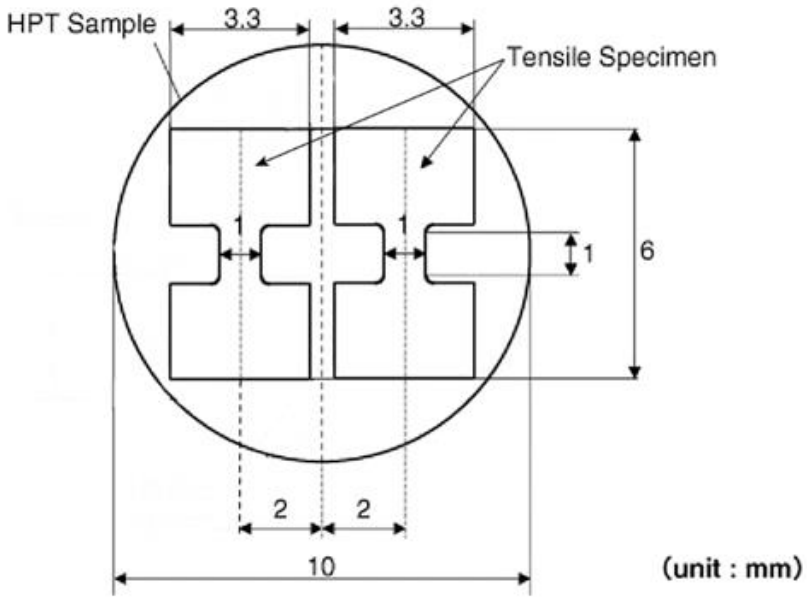

Figure 3.15: Miniature Tensile Specimen Cut From HPT Disc.

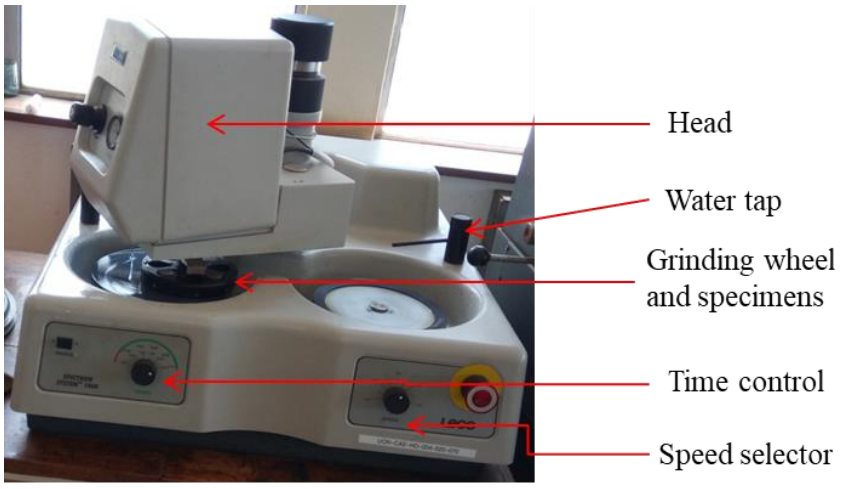

Figure 3.16: The Leco Grinding and Polishing Equipment

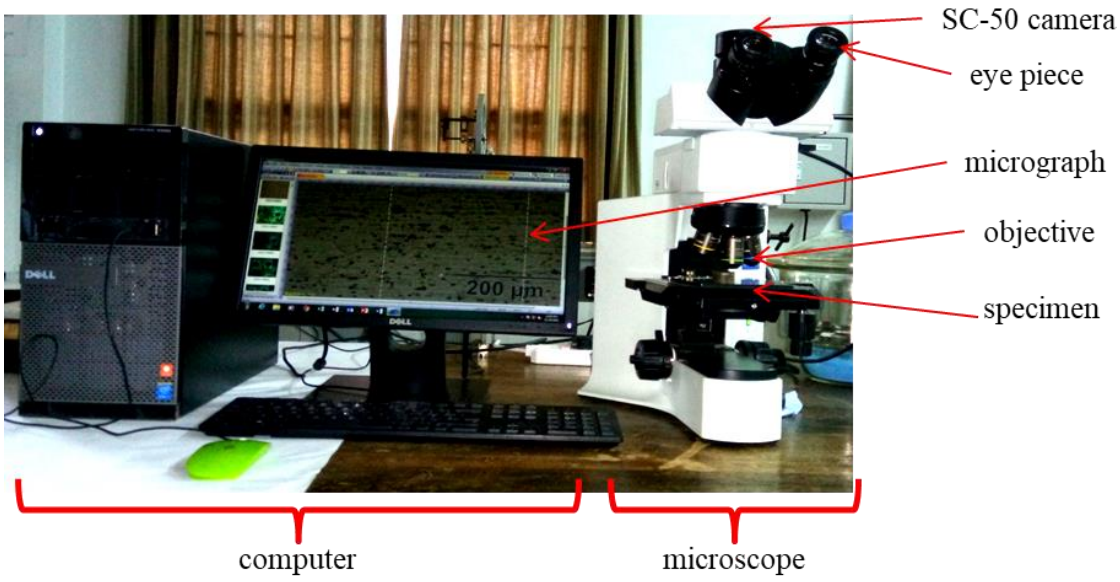

Figure 3.17: The BX41M - LED Olympus Optical Microscope Equipped With SC-50 Camera; and Attached to a Computer Output

CHAPTER FOUR

RESULTS AND DISCUSSION

4.1 Introduction

Results and discussions for industry survey, identified recycled friendly structural alloy, extrusion and severe plastic deformation (HPT and FSW) are presented in this chapter.

4.2 Industry Survey

4.2.1 Results

The firms that participated in the survey were identified from KAM data bank, literature from the previous surveys, preliminary survey and referrals from those already contacted. The full list of the dealers and Foundries, with their names and location was as shown in appendices A and B. The number of scrap dealers and foundries that participated in the survey was as shown in Figure 4.1. These firms were located in Nairobi, Mombasa and Nakuru. Firms located in Thika were considered as a part of Nairobi.

A summary of responses to the questionnaire by scrap dealers and foundries are as shown in Appendices A and B respectively. Each firm was given a code consisting of two digits and two letters, in place of their names for quick identification. The two digits represented serial number, while first and second letters represented locality and and type of firm respectively. Where M, N and n represented Mombasa, Nairobi and Nakuru respectively; s and f represented a scrap dealer and foundry respectively.

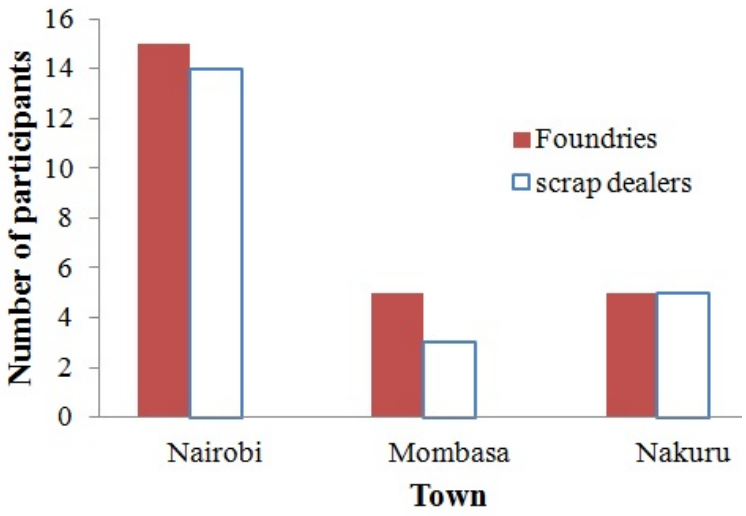

Figure 4.1: A Summary of Scrap Dealers and Foundries That Participated in Survey.

For example, a code **02Ms** represented **Makupa Steel**. This was a scrap dealer serial number 2 (02), that was based in Mombasa (M). A summary of aluminium handled by the dealers and foundries in year 2017 was as shown in Tables 4.1 and 4.2 respectively.

Table 4.1: A Summary of Aluminium Scrap Handled by Dealers (tonnes/yr).

Town	Automotive		Construction		Household	Electrical	Total	Export	
	cast	wrought	sheet	structural				cast	wrought
Mombasa	54	9.6	4.8	42	27.6	-	138	-	-
Nairobi	2255	392.4	241.2	1708.8	1232.4	180	6010	1800	-
Nakuru	115	18	10.8	48	67.2	2.4	262	-	-
Total	2424	420	257	1798.8	1327	182.4	6409	1800	-

Scrap quantities by the major alloying series 3xx.x, 1xxx, 3xxx and 6xxx used for casting, extrusion, rolling and extrusion respectively were as shown in Figure 4.2. The figures indicated that about 92 % of the scrap was collected in Nairobi. This is because 64 % of dealers and 60 % of foundries were based in the town. Further, the dealers had a national network for collecting scrap. They had rights to purchase industrial scrap; and won tenders to buy scrap in government institutions

Table 4.2: A Summary of Aluminium Scrap Handled by Foundries (tonnes/yr).

Town	cast	wrought			New scrap	Recovery	Total	Exports	Imports
		casting	Rolling	Extrusion				(products)	(Pure AL)
Mombasa	48	-	4080	-	78	66	4272	1734	1800
Nairobi	419	26	960	1920	355	32	3712	480	1080
Nakuru	114	48	-	-	2	-	164	-	-
Total	581	74	5040	1920	435	98	8148	2214	2880

and other corporate bodies. Major foundries had contracted them to supply scrap and the government allowed them to export the surplus. Nakuru and Mombasa towns collected about 8 % of the remaining scrap. Mostly this scrap was collected in the towns unlike Nairobi which is big and had a wider national supply network. The local demand for wrought scrap aluminium was high and as a result there were no exports. Export of cast scrap was 74.3 %; the rest was consumed locally. Small scale foundries operating in all the towns were the major consumers of cast scrap.

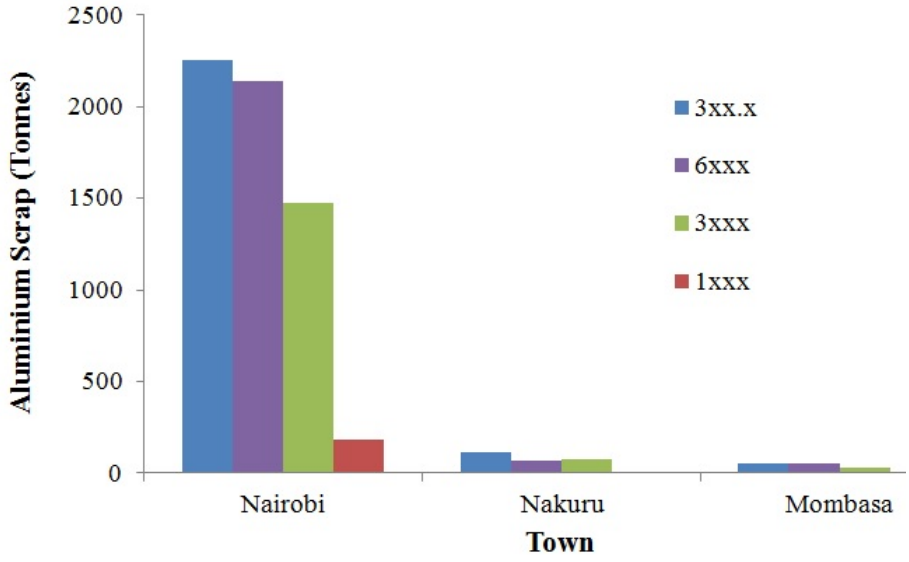

Figure 4.2: Scrap Generated in the Surveyed Towns.

The scrap collected was distributed by the dealers amongst foundries in the towns as shown in Figure 4.3. The 3xxx, 6xxx and 3xx.x scrap was used for rolling, extrusion

and casting respectively. Nairobi was leading in extrusion and casting, Mombasa was best in rolling while Nakuru performed only casting in a small scale. Nairobi is the home of major aluminium extrusion companies including Booth Extrusions and General Aluminium fabricators. This industries consumed most of aluminium scrap that was used for extrusion. Most local aluminum casting foundries are located in Nairobi where cast scrap is readily available. From Nairobi the cast components can be distributed to other locations in the country. Basically, it was convinient for the foundries to distribute their products from Nairobi to their Kenyan markets. Mombasa was the home of major aluminium rolling mills including Kaluworks KARM, Narcol and Kitchen King. Mombasa is close to the port where it is cheap for the foundries to recieve imported primary aluminium and simultaneous export their finished products. Nakuru had only micro foundries that were casting products for use in the agricultural based industries and house wares for their customers in the sorround towns. Nakuru foundries had a challege of sourcing scrap in the towm. Consequently, some scrap was sourced from Nairobi and the sorrounding towns. Rolling, extrusion and casting consumed 61.9, 23.6 and 8 % of the scrap. Cast scrap was used mostly by small scale foundries. The total exported scrap and imported pure aluminium were 1800 and 2880 tonnes. The imported pure aluminium was used by the foundries that were undertaking rolling and extrusion to dilute the wrought scrap. Products from foundries were either consumed locally or exported. Internal scrap generated in the foundries was 6.5 % of the consumed scrap; and was recycled internally.

Scrap consumed by foundries was higher than what was collected by dealers by 1206 tonnes (21.3 %). This could have resulted from either some dealers not being covered or others declaring lower values. The former could be true because regions including Kisumu, Kisii, Eldoret, Nyeri, Meru, Garrisa, Mandera and Malindi were not covered. These areas were not covered because preliminary survey showed that scrap from those areas was sold to scrap dealers or foundries either in Nairobi,

Mombasa or Nakuru. To cater for the discrepancy the higher value of 8148 tonnes was taken as the total scrap recycled in the year 2017.

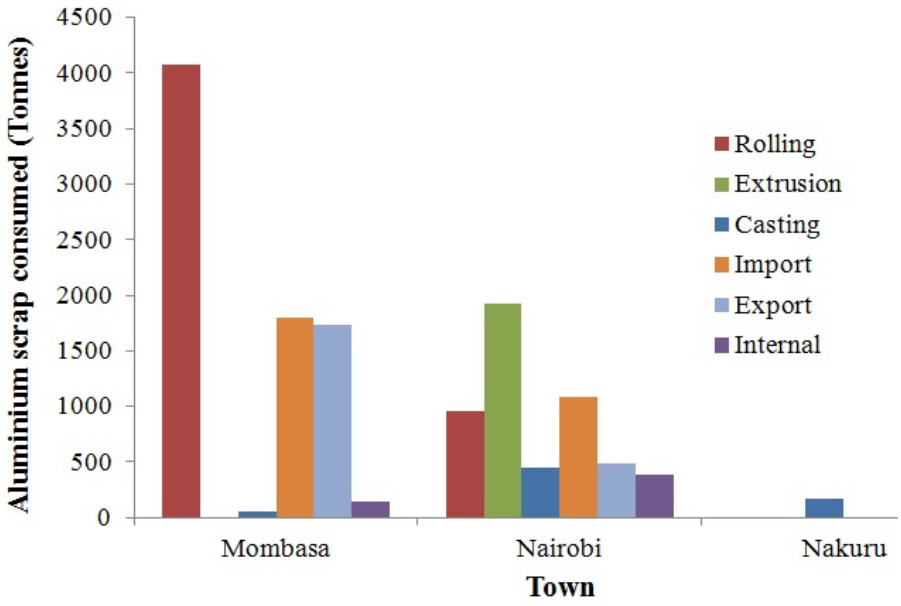

Figure 4.3: Aluminium Handled by the Surveyed Foundries.

KNBS releases yearly reports referred to as Economic Survey and Statistical Abstract. From the reports data about aluminium exports, aluminum imports and motor vehicle imports for the period 2004 - 2015 was extracted (Central Bureau of Statistics, 2001; KNBS, 2012, 2013, 2015a, 2015b, 2016). Data on scrap exports was not considered, since it was not clear. The data had consolidated scrap from non nonferrous metals. Amount of imports of processed aluminium and un-wrought aluminium were given in shillings. From the information gathered from traders, the cost per kilogram was approximated as 300 shillings. The quantity of the wrought and un-wrought aluminum was calculated based on the knowledge of total cost and unit cost. The average weight of aluminium per imported vehicle has been approximated as 140 kg (Lumley, 2011; Schlesinger, 2007). Multiplying the units of motor vehicles imported per year (as per KNBS reports) by 140 gave the approximate quantity of aluminium that entered the county through vehicle importation.

Available data due to import or export of aluminium products between the years 2004 and 2018 was as shown in Figure 4.4. Using the two points linear forecasting method aluminium arising from products export, vehicle imports and total aluminium import for the year 2017 was approximated to be 7.9, 15.4 and 28.0 thousand tonnes respectively.

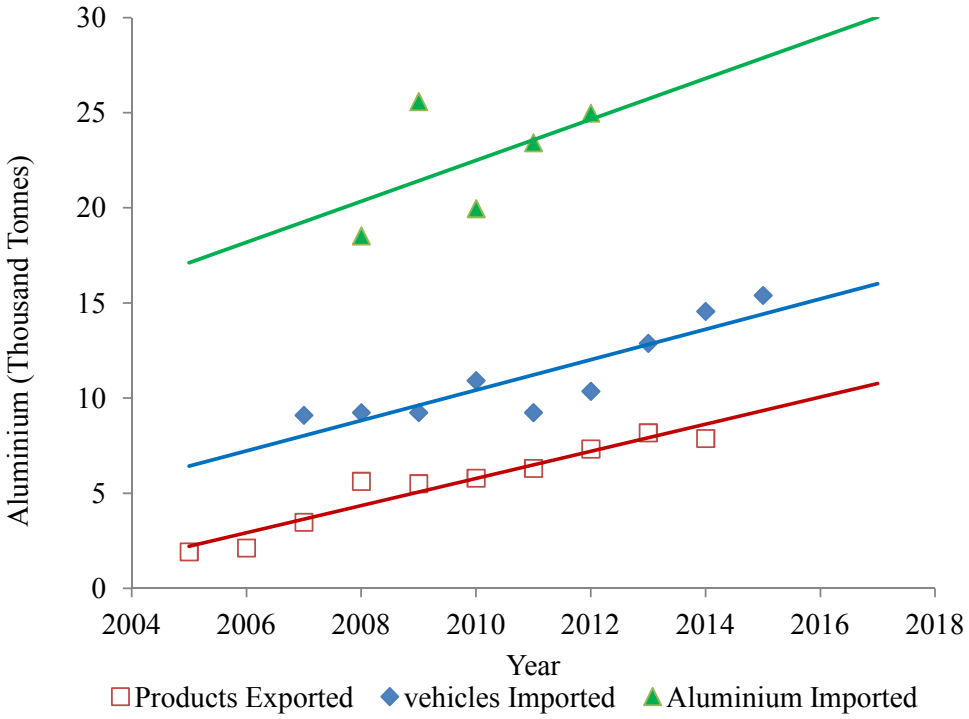

Figure 4.4: Aluminium Export and Import for the Period 2005 - 2017.

About 2,214 tonnes of products were exported by the foundries. This value was lower than the value for exports from the KNBS data. The reason could be due to the fact that there could be some firms which were importing finished goods or semi finished and exporting them after value addition. Consequently, the value of exports was taken as the higher value of 7,900 tonnes.

Based on the scrap dealers, foundries and KNBS data it was possible to apply mass balance analysis to determine the quantities in tonnes (for year 2017) of the aluminium involved in all the stages of the aluminium flow as shown in Figure 4.5.

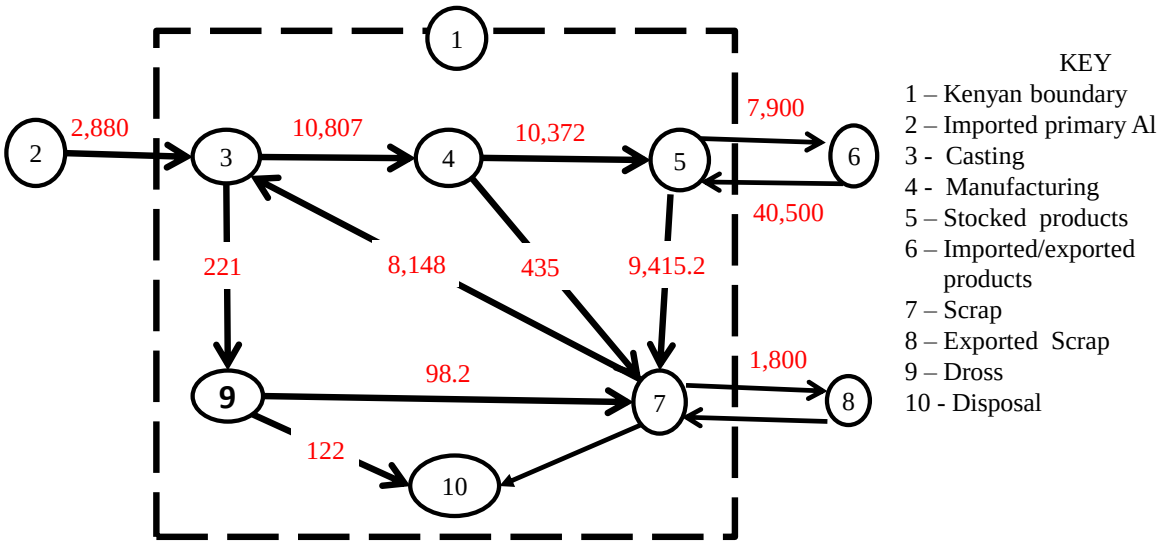

Figure 4.5: Aluminum Mass Flows (tonne/yr) Into, Out of and Within the Kenyan aluminium Recycling Industry for Year 2017.

4.2.2 Discussion

Observations and interviews during visits to dealers and foundries showed that cast scrap mostly originated from automotive components like engine blocks, wheels, cylinder heads, pistons and gear box casing. A small proportion of the scrap arose from industrial machines like motor housings. From the literature review the components are cast from 3xx.x alloys which are silicon based with additions of magnesium and/or copper. Silicon based alloys are popular because of their excellent castability and superior mechanical properties. The scrap was demanded by small scale foundries to cast household goods including pans, pots and ladles; hardware items including cooking stove grill and decorations for steel doors; and machine parts including gears, pulleys and automotive spacers. Some foundries reported that they blended cast scrap with wrought scrap in the ratio of 5:1, so as to increase toughness of their products like pans. The ratio was arrived at from thier practical exprience. Blending mitigated the brittleness of cast products which were susceptible to mechanical shock loads or falling. The foundries used 25 % of the cast scrap; the

surplus was exported to countries including China, India, and Japan.

Wrought scrap originated from a wide range of sources including automotive, building, construction, housewares and electrical items. Automotive based scrap included vehicle body panels, space frames, seat frames, structural beams, window frames, tread plates, hand rails, carriers, tanks and general automotive trim. Building and construction scrap consisted of doors and window frames, office partitions, roofing sheets, green house structural frames, door handles and locks. Housewares including pots, pans, cups, jugs, ladles, cans and plates were found to be source of wrought scrap. Electrical cables were found in only accredited scrap yards, due to rampant cable thefts.

Consumption of the wrought scrap included casting, rolling and extrusion in proportions of 1, 72 and 27 % respectively. The casting industry used a small proportion of the scrap to increase the toughness of their products. The foundries dealing with rolling and extrusion preferred scrap from 3xxx and 6xxx wrought alloys respectively. When alloying elements exceeded the required level, imported logs (billets) and slabs of primary alloys were added while melting scrap for extrusion and rolling respectively. The primary aluminium used amounted to 27 % of the total consumption. Local demand of the extrusions was high due to the rapidly expanding building industry and need for green buildings. Growing transport industry was utilizing the extrusions for body building to reduce weight, ease of fabrication and aesthetic appeal. Importation of motor vehicles, shown in Figure 4.4 was rising steadily. This was an assurance that higher quantities of the scrap was to be available in future.

4.2.3 Conclusion

Aluminum scrap collected in year 2017 was 9948.4 tonnes. Nairobi scrap dealers collected 92 % of the scrap. Proportions of cast and wrought scrap were 24.4 and 75.6

%. Cast scrap was consumed locally and a surplus of 74 % was exported. Cast scrap of 3xx.x series was suitable for direct reuse as automotive components. Therefore cast scrap from alloys 332, 356 and 380 was appropriate for development of secondary alloys for automotive components. Structural wrought alloy scrap accounted for 72 % of the wrought scrap collected and arose from automotive and construction industry. Alloy 6061 in the 6xxx series; was found to be a general purpose structural wrought alloy that was suitable for recycle friendly structural alloys.

4.3 Wrought Aluminium alloy Scrap Sorting and Melting

4.3.1 Results

Four structural wrought aluminium scrap batches were hand sorted from Nairobi scrap dealers based on common and uncommon characteristics. common characteristics include:- colour of scratched surface, reaction with etchants and method of processing. They had a silvery colour on a scratched surface, their former components had been extruded and did not react with either dilute HCL or a solution of 0.3 % HCl and 1% $CUSO_4$. The results of other uncommon characteristics were as shown in Table 3.3. Each of the four scrap batches was cut into pieces 600 mm long as shown Figure 3.3, melt in an oil fired crucible furnace and cast into ingots as shown in Figure 3.4 (a, and b) respectively. Chemical composition analysis of the batches was conducted at Numerical Machining Complex (NMC) on specimens chilled in copper mould. The spectroscopic results were as tabulated in Table 4.3. The batches were Aluminum Alloys with Silicon and Magnesium as major alloying elements.

Optical microscopy results of the batches revealed presence of gas porosity and second phases in aluminum matrix as shown in Figure 4.6. The pores were distributed in

Table 4.3: Chemical Composition (%) of the Four Scrap Batches That Were Melt.

Batch	Al	Si	Fe	Cu	Mn	Mg	Cr	Zn	Ti	Others
A	97.5	0.861	0.740	0.058	0.066	0.582	0.022	0.082	0.017	0.017
B	98.2	0.418	0.685	0.053	0.035	0.238	0.020	0.286	0.021	0.044
C	97.4	0.719	0.203	0.372	0.024	0.863	0.068	0.061	0.022	0.269
D	96.9	1.06	0.716	0.274	0.066	0.645	0.0717	0.126	0.024	0.117

the material. Silicon in the alloy formed phases which appeared as needles or plates during solidification. Presence of iron during melting formed intermetallics which occurred as Chinese scripts or needles.

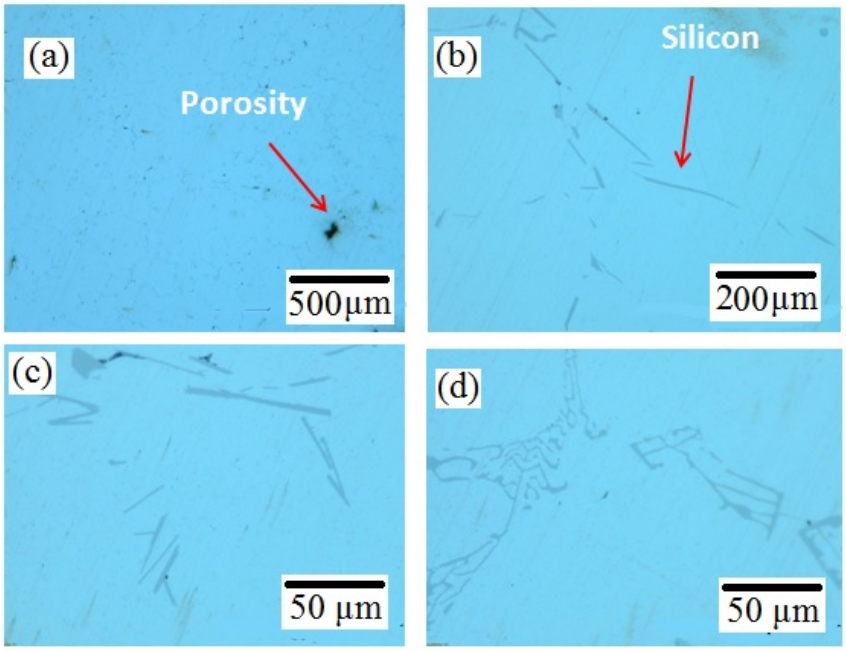

Figure 4.6: Micrographs of Cast Alloy 6061:(a) Gas Porosity; (b) Silicon Needles; (c) Magnified Silicon Needles; and (d) Iron Intermetallics

Micrographs of etched specimens of the as cast secondary aluminum 6061 alloy were as shown in Figue 4.7 and 4.8. The alloy had eqiuaxed grains of 97 μm average size. Its second phase particles were found to be distributed along the grain boundaries.

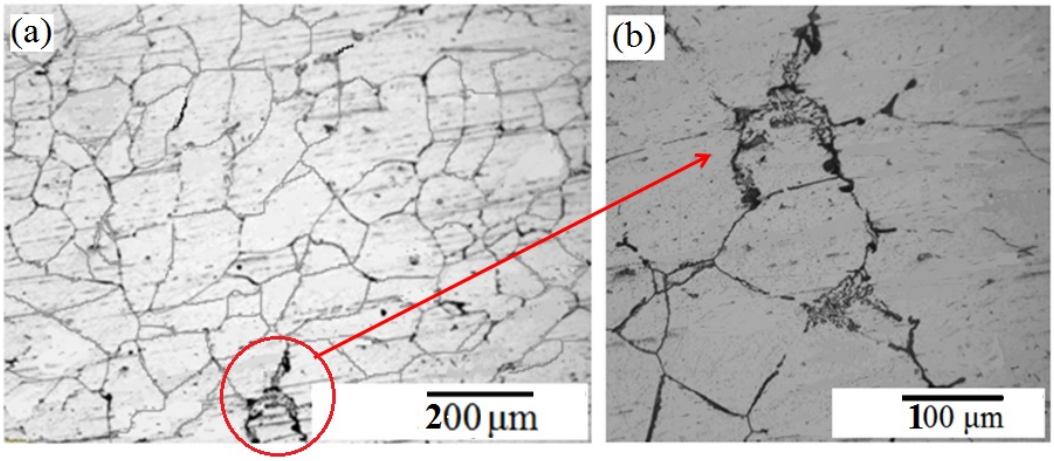

Figure 4.7: Micrographs of Etched as Cast Alloy 6061:(a) Equiaxed Grains; (b) Second Phase Particles Distributed Along the Grain Boundaries

4.3.2 Discussions

Sorting of the four scrap batches was conducted manually using four techniques. First, color sorting was applied while separating aluminum scrap from zinc, copper, brass and stainless steel scrap. Aluminium was identified by its silvery white color. secondly, Density and dilute hydrochloric acid were used to separate magnesium scarp from aluminum scrap. Magnesium alloys were lighter than aluminum alloys by 75 %. Dilute hydrochloric acid was used to distinguish the alloys, because they had a similar silvery white colour. Magnesium alloys reacted with the acid to produce bubbles of hydrogen gas, while aluminum alloys were un affected. Thirdly, aluminum scrap was sorted into wrought and cast aluminum based on their distinctive surface characteristics resulting from their processing technologies including casting, extrusion, rolling and pressing. Finally, the scrap was sorted into series based on the field of application and processing technology. Extruded scrap was selected, since it was made up of structural alloys. The selected structural scrap was sorted into four batches referred to as A, B, C and D. Batch A consisted of sections 1.5 mm thick of scrap from construction site. Batch B constituted of 3.0

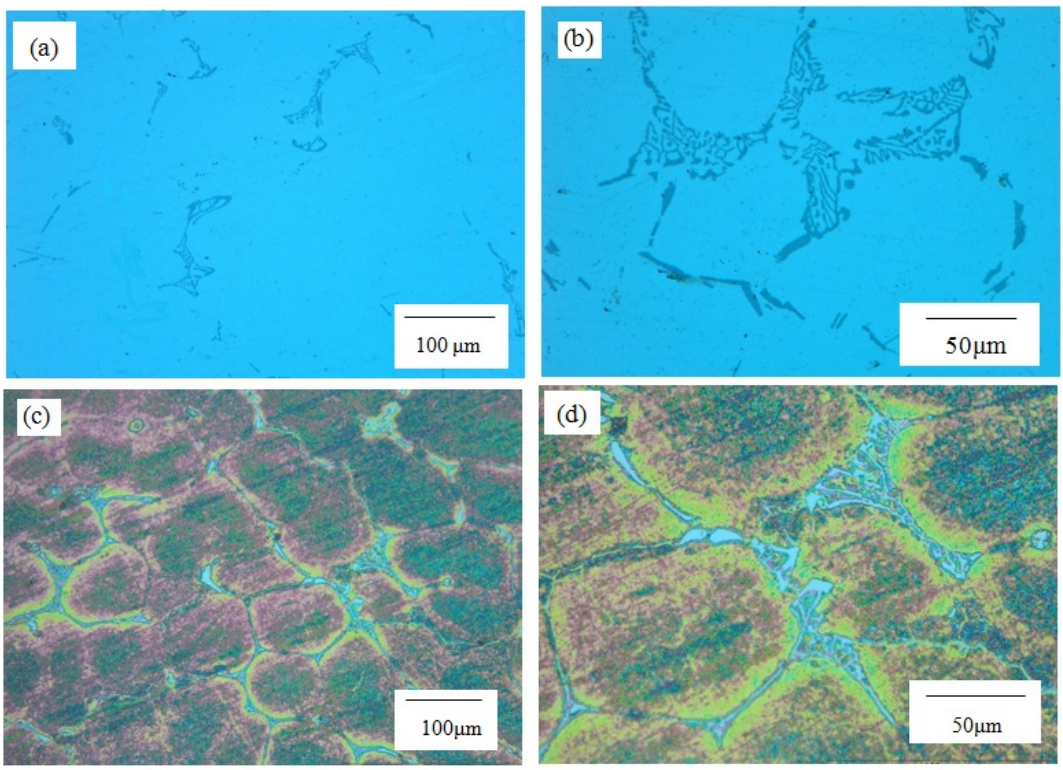

Figure 4.8: Micrographs of as Cast Alloy 6061:(a) and (b) Second Phases in Un Etched Specimen; (c) and (d) Second Phase Particles Distributed Along the Grain Boundaries

mm thick sections for house window frames which were either anadized or anodized and dyed using different colours. Batch C had 5.0 mm thick sections derived from automotive body parts. Batch D comprised of 5.0 mm thick sections used to support building structures. The final step can be improved further by application of chemical etchants as shown in Table 4.4.

Therefore, manual sorting of the scrap was found to use combination of color, surface characteristics, processing technology, knowledge of field of application and use of etchants.

Spectroscopic results indicated that alloys resulting from melting each of the scrap batches belonged to 6000 series; since they contained silicon and magnesium as major alloying elements. Composition of batch A, B, C, and D was found to be close to

Table 4.4: Sorting Aluminum Alloys into Families Using Etchants (Gaustada et al., 2012).

Aluminum series	Etchant	Effect
5xxx and 6xxx	copper sulphate dissolved in hydrochloric acid	reacts with high magnesium containing alloys
3xxx	sulphuric acid	High manganese becomes light gray in color
2xxx	sulphuric acid	high in copper turn a darker color
7xxx	sulphuric acid	high in zinc turn a darker color

alloys 6005, 6063, 6061 and 6070 respectively as shown in Table 4.5.

Table 4.5: The % Composition of 6000 Series Alloys That Were Close to the Cast Batches.

Alloy	**Al**	**Si**	**Fe**	**Cu**	**Mn**	**Mg**	**Cr**	**Zn**	**Ti**	**Others**
6005	Bal	0.6-0.9	0.35	0.10	0.10	0.4-0.6	0.1	0.1	0.1	0.15
6063	Bal	0.2-0.68	0.35	0.1	0.1	0.45-0.35	0.1	0.1	0.1	0.0.15
6061	Bal	0.4-0.8	0.70	0.15-0.4	0.15	0.8-1.2	0.04-0.35	0.25	0.15	0.0.15
6070	Bal	1.0-1.7	0.5	0.15-0.4	0.4-1.0	0.5-1.2	0.1	0.2	0.15	0.15

Batch A compared to alloy 6005, except that it had a higher % of Fe. Batch B compared to alloy 6063; but % of Fe and Zn was higher and % of Mg was lower. Batch C matched alloy 6061. Batch D compared to alloy 6070; however, % of Fe was higher and % of Mn was lower. Problem of Fe concentration rising above recommended levels during melting was noted. Molten aluminum has been found to react with Fe to form intermetallics, that have a deleterious effect on mechanical properties of a material (Kraisat & Jadyil, 2010; Mrówka-Nowotnik et al., 2007; Murali et al., 1997).

Fe contamination of the alloys originated from either presence of iron fasteners and other iron parts in the scrap or handling equipments like ladles. Removal of the Fe in the alloys is impossible. Consequently, care should be taken during scrap sorting, so as to remove all iron components in the scrap. Additionally, iron contamination should be avoided while melting scrap and pouring molten metal. Harmful effects of Fe on contaminated aluminum alloy can be mitigated by either minimizing the

formation of β-phase platelets and/or encouraging the formation of the Chinese script α-phase. This has been achieved through application of high cooling rates and addition of Mn in the ratio Mn:Fe of 2:1 (Taylor, 2004). Alternatively, concentration of Fe can be lowered by addition of primary aluminium to the alloy. Usually, dilution is followed by adjustment of alloying elements. Consequently, the cost of producing the desired alloy tends to increase. Therefore, the best option is to carefully sort scrap, avoid contaminating the molten metal during handling; and incase of contamination, Fe correction is recommended.

Mg tends to fade during melting. During recycling the concentration of Mg can be restored by addition of master alloys. Similarly, all elements that fall below their concentration level can be restored through addition of master alloys.

The chemical analysis results confirmed that the applications of aluminum alloys outlined in the literature were similar to those of the manually sorted scrap. Alloy 6005 is used in construction structural elements; alloy 6063 is applied in automotive body frames, construction structures, bridge frames and electrical cable towers; Alloy 6071 is applied in high strength requirements like truck beams; and alloy 6061 have wide rage of applications. Applications of alloy 6061 range from medium to high strength requirements in the fields of home built aircraft, marine (yachts), auto body sheets and structural members, pipe lines, construction structural elements and electric cable towers. Alloy 6061 compared to 6063 is more tolerant to Fe impurities and has a wide range of applications. Hence, its broad use and high tolerance to iron contamination (upto 0.7 %) guarantees the availability of recyclable scrap for production of extruded structural material with a high demand in automotive, building and construction industries.

Microstructure of the alloys consisted of second phase particles and porosity in aluminum matrix as shown in Figure 4.6. Molten aluminum has a high affinity for hydrogen gas. Upon cooling the dissolved gas is released, thus forming pores in the

material. Presence of pores in a material have detrimental impact on its mechanical properties. Porosity can be minimized by addition of a degasser, ensuring that the scrap is dry and quiescent pouring of the molten metal. The grains of 97 μm average size, were nearly equiaxed as shown in Figure 4.7 and 4.8. The particles were thought to be Silicon particles, Magnesium silicide (Mg_2Si) and Iron intermetallics, since the spectroscopic analysis showed the presence of the elements as tabulated in Table 4.3. The particles were concentrated along the grain boundaries of the etched specimens as shown in Figure 4.7 and 4.8. During solidification, pure Aluminum solidified first, pushing silicon phases and intermetallics to grain boundaries; since they solidified last. Silicon phases solidified as plates and needles as shown in Figure 4.12 and 4.13. Iron intermetallics also solidifies as needles or 'Chinese' script in presence of manganese. Plate or needle shaped particles are usually brittle and thus lowers the mechanical properties of the alloy. At higher temperature molten aluminum has a high affinity for oxygen. The oxygen arises from moisture in the scrap, molten metal handling equipment such as ladles and and trapped air. Upon cooling, Aluminum releases the dissolved air which forms porosity in the cast metal. Porosity deteriorates the metal properties. Use of degassers during melting and quiescent mould filling are used to minimize porosity in castings. Equiaxed grains of smaller size improve the mechanical properties of metals. Presence of such non homogenous particles along the grain boundaries, porosity and big average grain sizes lowers mechanical properties of the cast metal. Mechanical properties of the cast metal can be enhanced through grain refinement, homogenization of second phase particles, heat treatment and iron neutralization. The cast metal is a potential candidate for recycled friendly structural alloy; however it can not be used in this condition.

From the chemical analysis results it was confirmed that the improved hand sorting of the scrap was able to generate secondary wrought structural aluminium alloys that compared with standard alloys. However, care should be observed during scrap melting to avoid Iron contamination and fading of alloying elements. The improved

hand sorting eliminated use of costly pure aluminium and alloy adjustment procedure that follow.

Among the four secondary alloys, alloy C had no impurities and its alloying elements had not faded. It compared well in composition with Aluminium 6061 standard structural alloy. Consequently, it was picked for further analysis. From now onwards batch C will be referred to as secondary Aluminium alloy 6061. The structural products of the alloy are formed through extrusion; hence it was necessary to process its cast ingots through extrusion.

4.4 Extrusion of Secondary Aluminium Alloy 6061

4.4.1 Results

The extruded rods of diameter 14 mm were as shown in Figure 4.9 (b).

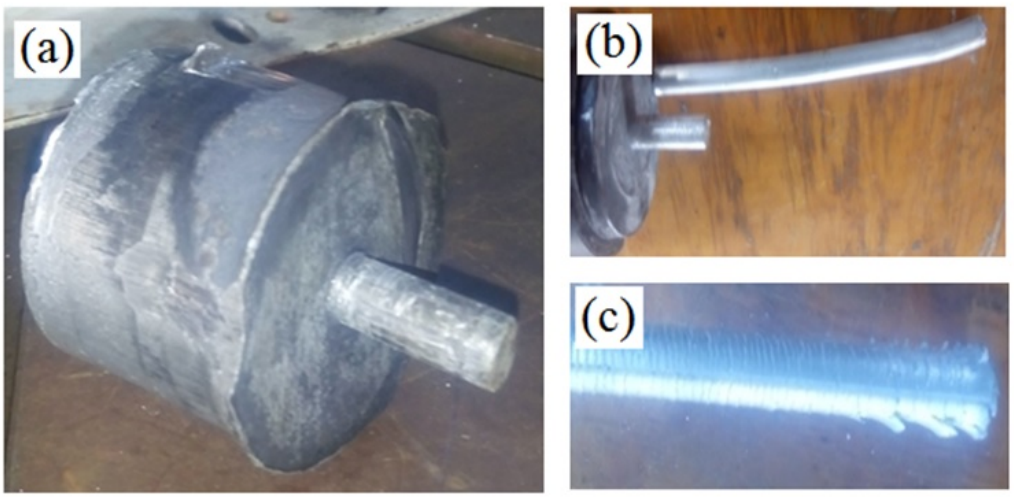

Figure 4.9: Extruded Rod at Different Temperatures:(a) Below 400 ^{0}C; (b) Between 400 ^{0}C and 500 ^{0}C; and (c) Above 500 ^{0}C

Microstructure of extruded specimens in a section perpendicular to direction of

extrusion was as shown in Figure 4.10 and 4.11. Second phase particles in extruded unetched section were needle shaped and shorter compared to those in the non processed material as shown in Figure 4.6. Their distribution compared to that in the material before extrusion was more homogeneous. Chinese scrip particles and gas pores disappeared as a result of extrusion. After, etching grains of average size 30 μm were visible. The grains were equiaxed; and the second phase particles were more homogenous and not necessarily along grain boundaries.

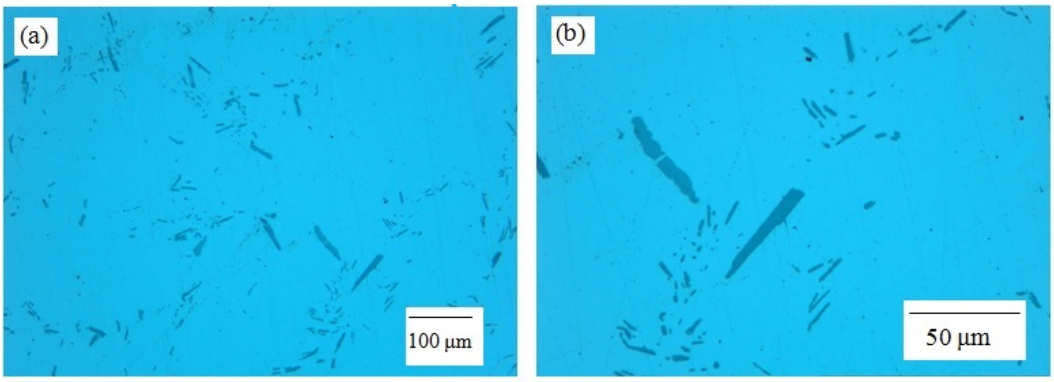

Figure 4.10: Micrographs of Un Etched Extruded Material

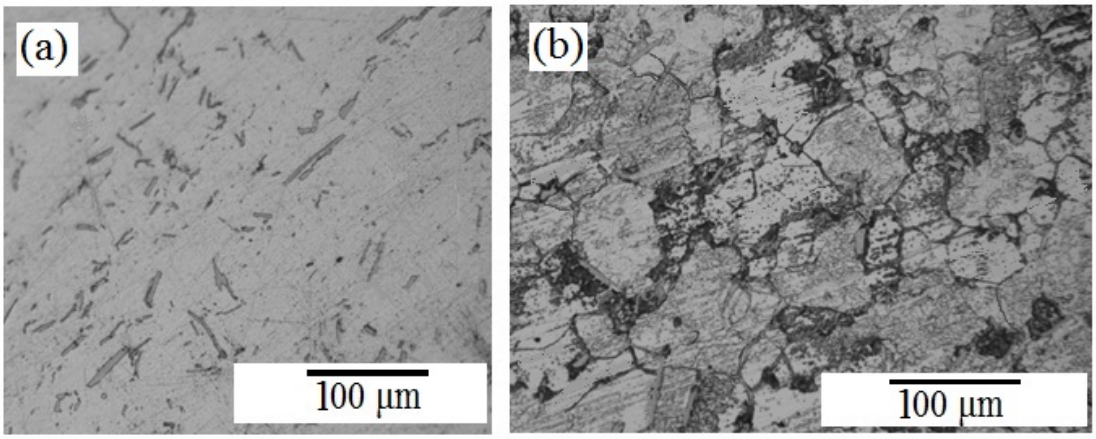

Figure 4.11: Micrographs of Extruded Material: (a) Un Etched; (b) Etched

A SEM EDS analysis of the extruded material confirmed that second phase particles contained Silicon, Magnesium, Calcium and Fe held in Aluminum matrix as shown in

Figure 4.12 and 4.13. Silicon phase and Iron intermetallics had cracked into smaller particles.

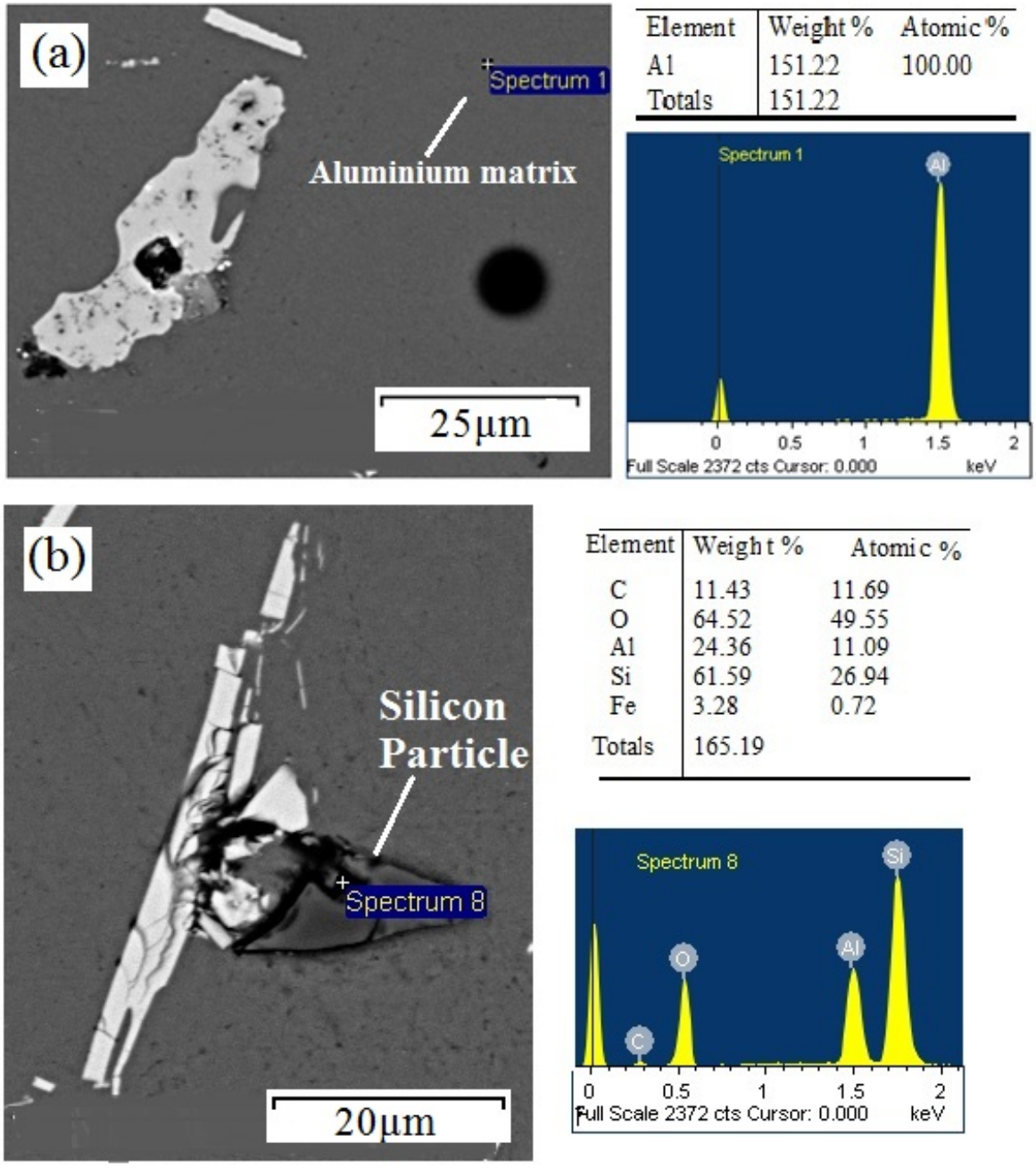

Figure 4.12: Micrographs of Extruded Material: (a) Second Phase Particles in Aluminum Matrix; (b) Fragmentation of Silicon Particle.

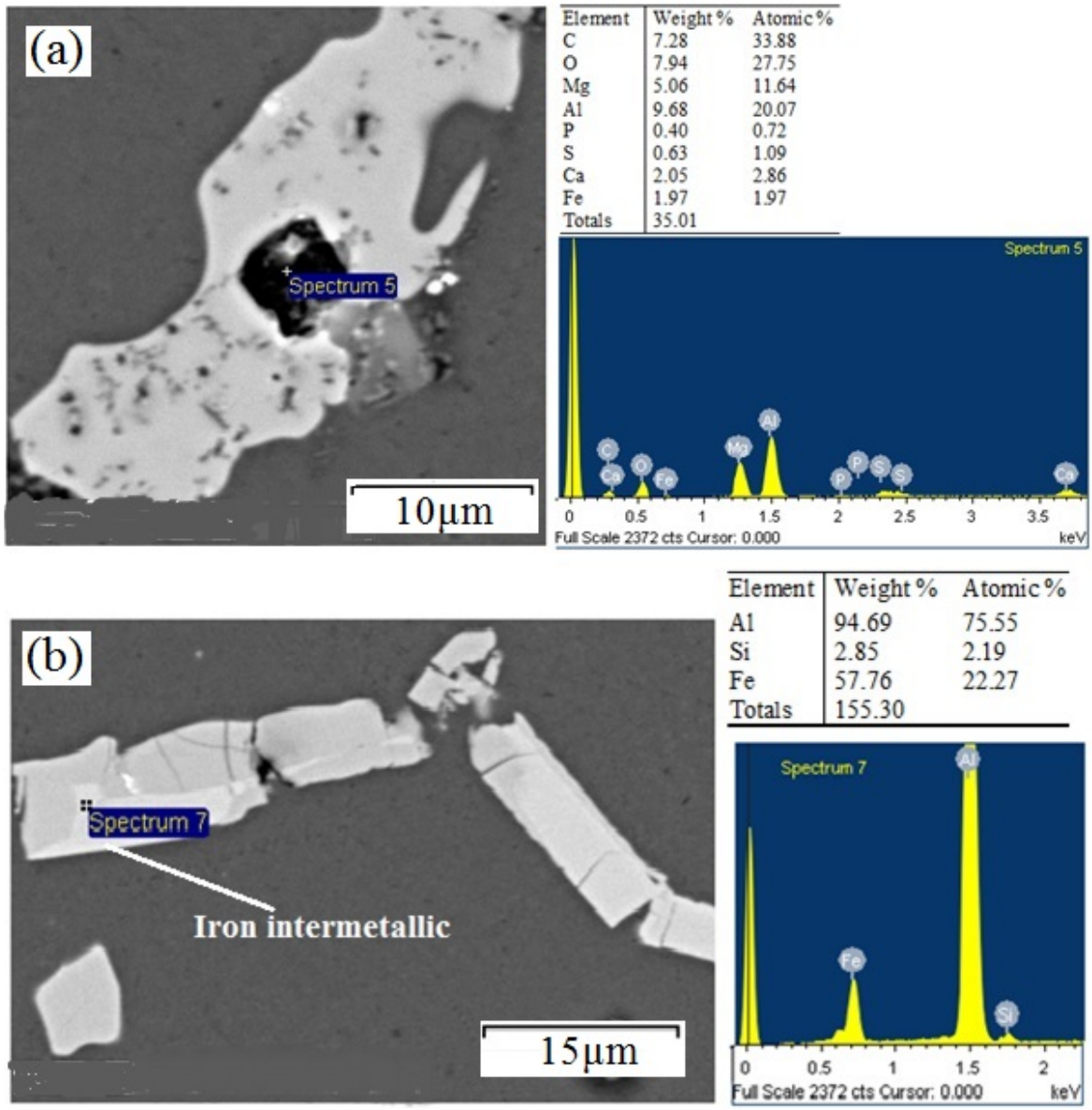

Figure 4.13: Micrographs of Extruded Material: (a) Mg and Traces of Ca in Second Phase Particles; (b) Brittle Iron Intermetallics in Second Phase Particles.

Results of the tensile test conducted on the non extruded (cast) and extruded specimens at a test speed of 0.1 kN/sec were as shown in Figure 4.14. The ultimate tensile strength, breaking stress and % elongation of the cast specimen changed from 84 MPa, 53 MPa and 2.4 % to 214 MPa, 175 MPa and 4.8% respectively.

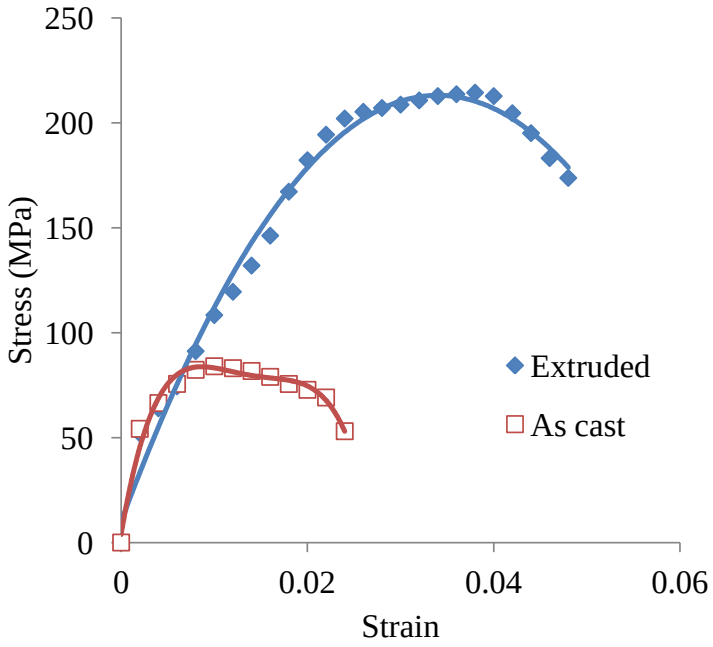

Figure 4.14: Stress versus strain curve of the non extruded (as cast) and extruded alloy 6061.

4.4.2 Discussions

The reduction of the diameter from 50 mm to 14 mm gave an acceptable extrusion ratio of 13, which is below the normal ratio of 35. On the other hand it was observed that extrusion temperature had a significant impact on extrusion force and length of extruded rod. Temperature was inversely proportional the force and directly proportional to the length. Theoretical force required for extrusion at room temperature was calculated as 0.035 MPa. A rise in temperature made the force to reduce. At a temperature of 350 ^{0}C a force of 0.020 kN/m^2 extruded the material for a length of 50 mm as shown in Figure 4.9 (a). When temperature was between 400 - 500 ^{0}C, a lower force of up to 0.015 MPa was required to extrude the material to a length of 0.5 m. For temperature above 500 ^{0}C, the applied pressure was 0.009 MPa; but, the material suffered from hot shortness and cracked on the surface as shown in Figure 4.9 (c). Therefore, extrusion ratio of 13, force of about 0.015 MPa and average temperature of 450 ^{0}C were recommended for extruding the alloy.

Four challenges were encountered during extrusion. First, there was an abrupt drop in temperature since the die and container were not insulated against heat loss. In future they need to be guarded against heat loss by either lagging or incorporating a heater. The heater will be capable of maintaining the parts at the required extrusion temperature; and stop heating them eternally in a furnace. This will ensure that the material is extruded at the optimal temperature. Secondly, piston travel should be kept parallel to the container wall, in order to prevent container wall from being damaged. Third, an increase of extrusion force should be considered. Finally, removal of the remaining billet from the container was difficult. A quick and easy billet extraction mechanism need to be incorporated in a future design to overcome this challenge.

Extrusion eliminated porosity, reduced the grain size, broke down the second phase particles and spheroidized the silicon plates. Gas pores closed when the material was deformed while flowing through the extrusion die; and thus, eliminating the defects. Due to heating and deformation the grains were recrystallized to form grains which were 3 times smaller than the original size in the non processed alloy. Second phase particles in the extruded material were found to be shorter and more homogenous. Second phase particles were smaller because of simultaneous breakdown of silicon plates and the iron intermetallics into smaller pieces. Deformation homogenized the phases in the aluminum matrix. Heating the material in the furnace made the silicon particles to change from the plate-lets into a globular (spheroidal) form. Therefore, heating spheroidized the silicon plates. The effects of extrusion on the microstructure of the material were beneficial to its mechanical properties.

Consequently, extrusion improved mechanical properties of the cast material as evidenced by the tensile results. Ultimate tensile strength, breaking stress and % elongation increased 2.55, 3.30 and 2.00 times respectively. Improvement in mechanical properties resulted from changes in the microstructure including grain refinement, elimination of porosity and second phase fragmentation which

contributed significantly to drastic increase in strength and ductility. Silicon plates and Iron intermetallics were broken down and homogenized within the extruded structure. The tensile strength of standard 6061 alloy ranges from 124 - 290 MPa; and is comparable to 214 MPa of the recycled extruded alloy. Strength of the alloy can be increased further by heat treatment. Consequently the alloy is suitable for structural applications.

4.5 High Pressure Torsion

4.5.1 Results

Radial distance measured from the centre of a specimen during optical microscopy was divided into two equal sections namely: core (0 - 2.5 mm), and periphery (2.5 - 5.0 mm). Second phase particles in $\frac{1}{4}$T, $\frac{1}{2}$T and 10T specimens were as shown in Figure 4.15. Distribution of particles in 1T and 5T specimens was similar to $\frac{1}{2}$T and 10T respectively. Size of the particles reduced from the core towards the periphery. Particle size also decreased gradually with increase in the number of turns. The rate and intensity of breakdown of second phase particles increased with rise in radial distance from core and number of turns.

Micrographs of etched specimens periphery indicated that break down of the phases was also affected by their shape and size as shown in Figure 4.16. At 5 turns large blocky particles were left in the periphery while elongated particles were present in the core as shown in Figure 4.17.

Particles in the specimens' micrographs were analyzed using Image J software. Analysis for perimeter and circularity against feret diameter was conducted at the core and periphery of 0.5T specimens as shown in Figure 4.18. Mean perimeter at the core and periphery were 0.05 and 0.04 mm respectively. Circularity was found to increase from 0.451 at the core to 0.548 at the periphery. Summary of the analysis

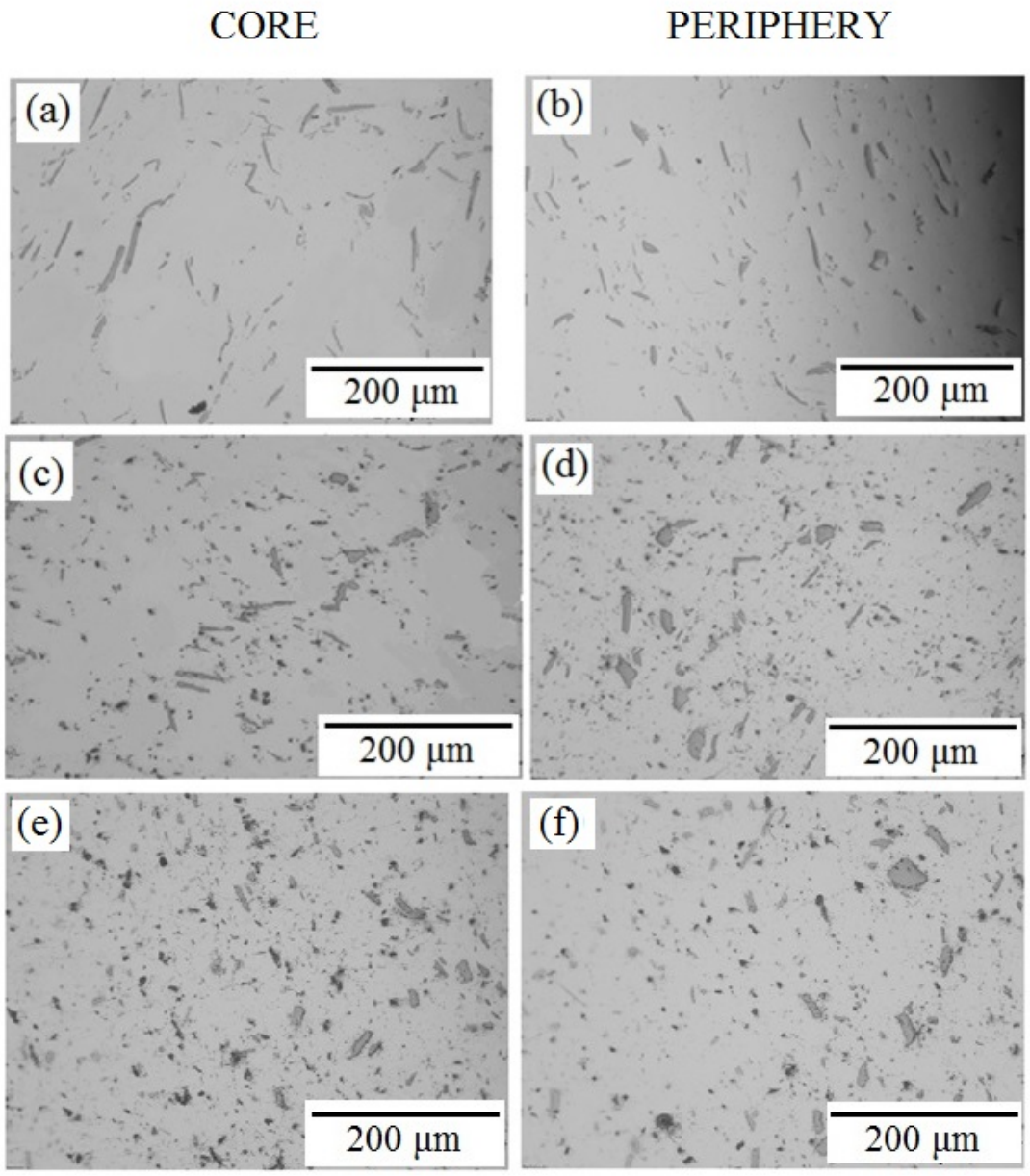

Figure 4.15: Micrographs of HPT Processed Material at the Core and Periphery After (a-b)$\frac{1}{4}$T; (c-d) $\frac{1}{2}$T and (e-f) 10T.

of number of particles; and average perimeter, area and circularity for the different specimens was as shown in Figure 4.19. The number and circularity of particles increased with the number of turns, while their perimeter and area decreased.

Further the specimens were tested for microhardness along the diameter; and results

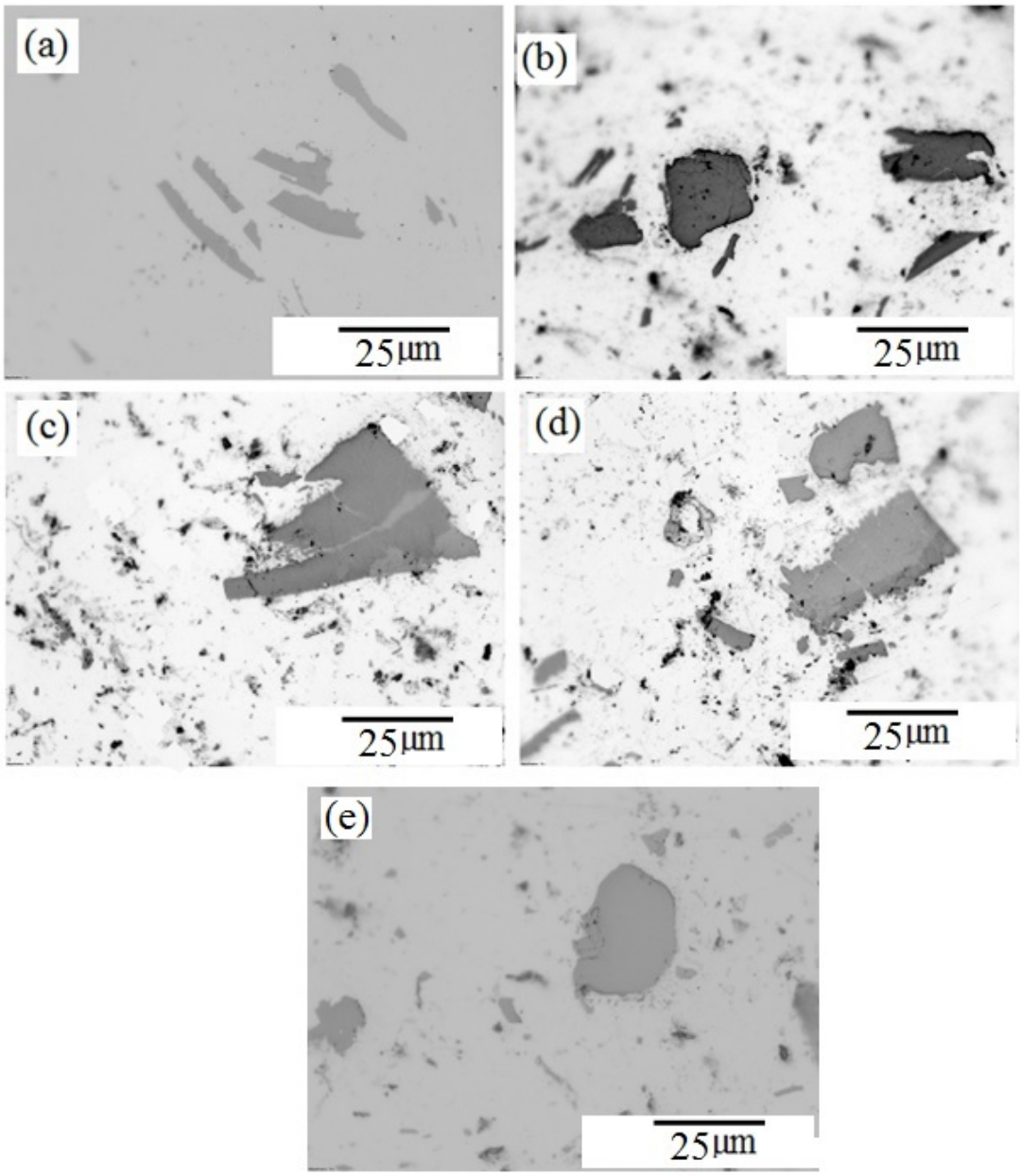

Figure 4.16: Micrographs of Etched HPT Specimens Periphery After : (a) $\frac{1}{4}$T; (b) $\frac{1}{2}$T (c) 1T (d) 5T and (e) 10T.

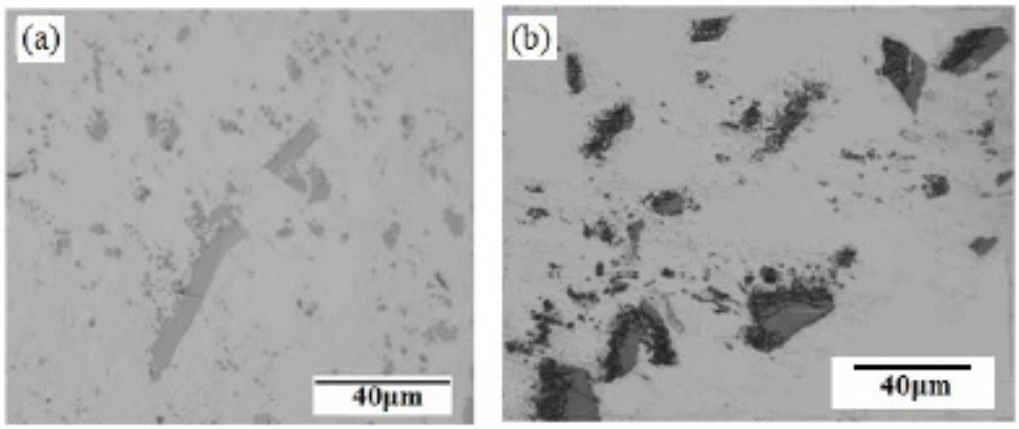

Figure 4.17: Micrographs of a Specimen after 5 HPT Turns, at: (a) Core; and (b) Periphery.

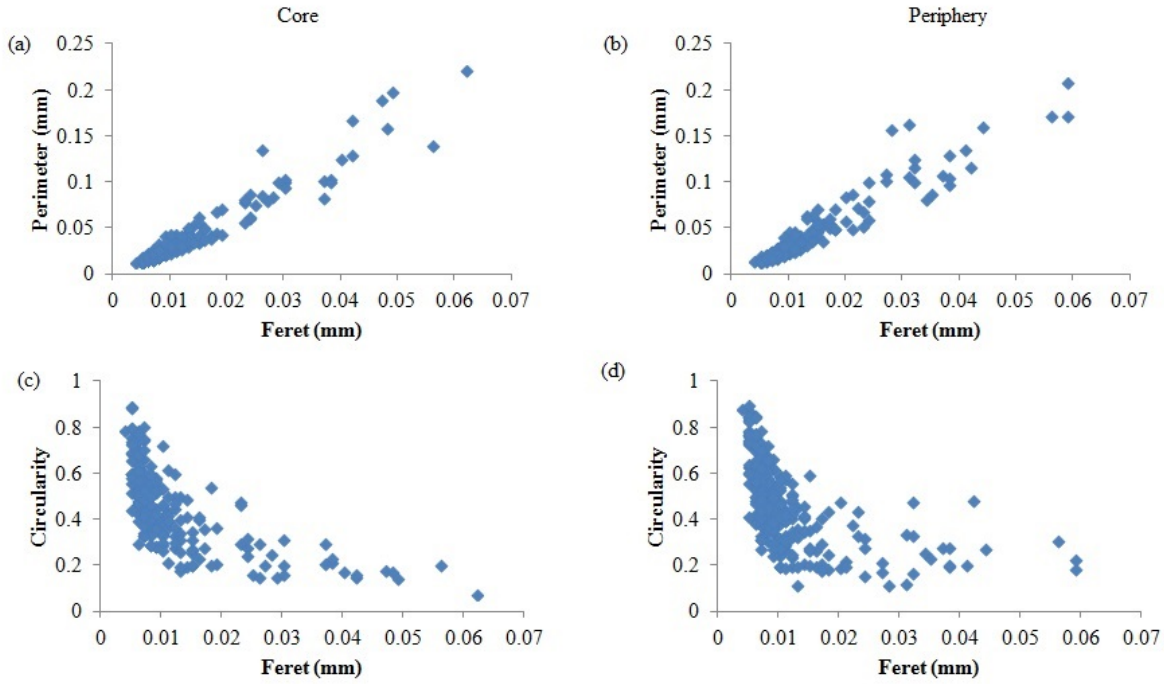

Figure 4.18: Perimeter and Circularity of a Specimen After 0.5 HPT Turns, at: (a)Perimeter at the Core; (b) Perimeter at the Periphery; (c) Circularity at the Core; and (d) Circularity at the Periphery.

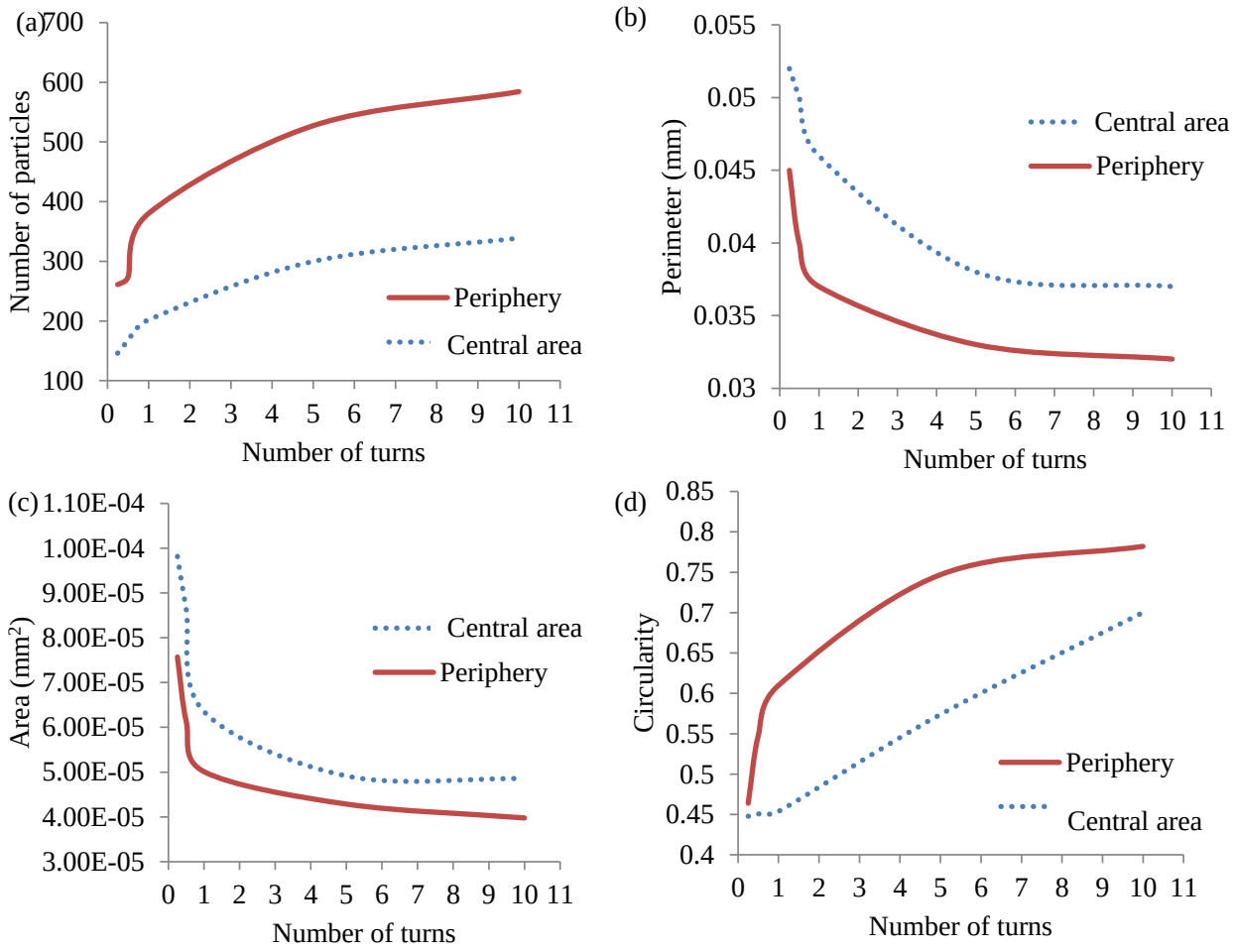

Figure 4.19: Summary of the Analysis of the Specimens' Particles Subjected to Varying Number of HPT Turns : (a) Number of Particles; (b) Average Perimeter; (c) Average Area; and (d) Average Circularity.

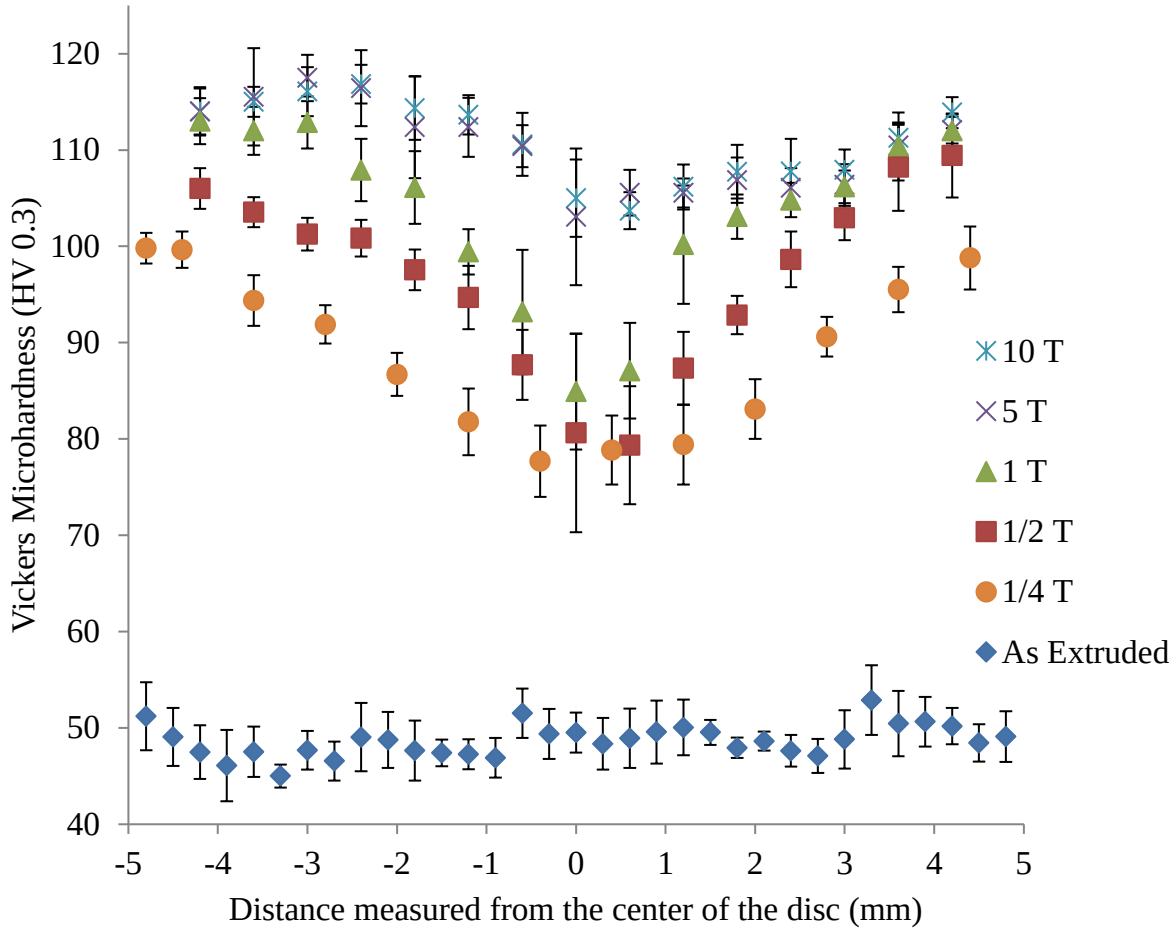

Figure 4.20: Microhardness of HPT Specimens From Alloy 6061.

were as shown in Figure 4.20. Average microhardness of the specimens was as shown in Figure 4.21. There was 81% increase in average hardness from specimens without HPT to $\frac{1}{4}$T. Increase in hardness between successive specimens among $\frac{1}{4}$T, $\frac{1}{2}$T, 1T and 5T specimens was 16.5, 13.9 and 13.8 % respectively. Increase in hardness between 5T and 10T specimens was 1.3%. Therefore, the average microhardness at 5T turns was optimal. Increasing turns from 5T to 10T had minimal effect on the hardness.

Microhardness was found to vary with equivalent strain as shown in Figure 4.22. In section (a - b) a steep increase of microhardness with increase in equivalent strain was observed. Thereafter the hardness increased gradually with straining in section

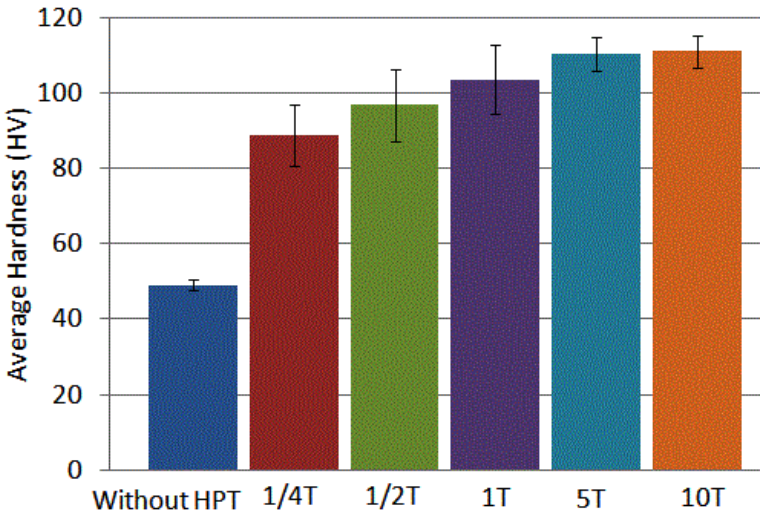

Figure 4.21: Average Microhardness of HPT Specimens From Alloy 6061.

(b - c) up to a maximum of about 105 HV at an equivalent strain of $\sim$ 3.5. At point (c) hardness hand reached a maximum. Further straining did not increase the hardness of the specimens. When average microhardness was plotted against equivalent strain the curve had 4 distinct sections as shown in Figure 4.23. Hardness dropped between a-b, then increased sharply between b-c, onset of steady state was noted between c-d and a steady state was attained between d-e.

4.5.2 Discussions

Average size of second phase particles in specimens without HPT was bigger than in HPT processed specimens. The few smaller particles surrounding them did not appear to be ordered in any manner. However, micrographs of HPT processed specimens showed that second phase particles were broken as shown in Figure 4.15. Rate of breakdown of the particles was directly proportional to radial distance measured from the core of the specimen. For $\frac{1}{4}$ and $\frac{1}{2}$T specimens breakdown was more pronounced in the periphery as shown in Figure 4.15. Broken particles seemed to originate from long needle shaped particles as they were dispersed in the aluminum matrix behind the particles. The dispersed particles appeared like they were rotated

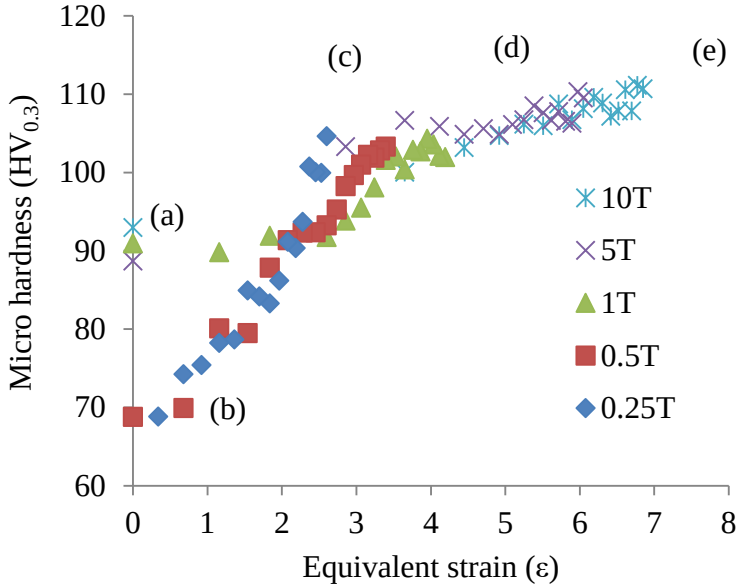

Figure 4.22: Variation of Microhardness with Equivalent Strain of HPT Specimens From Alloy 6061.

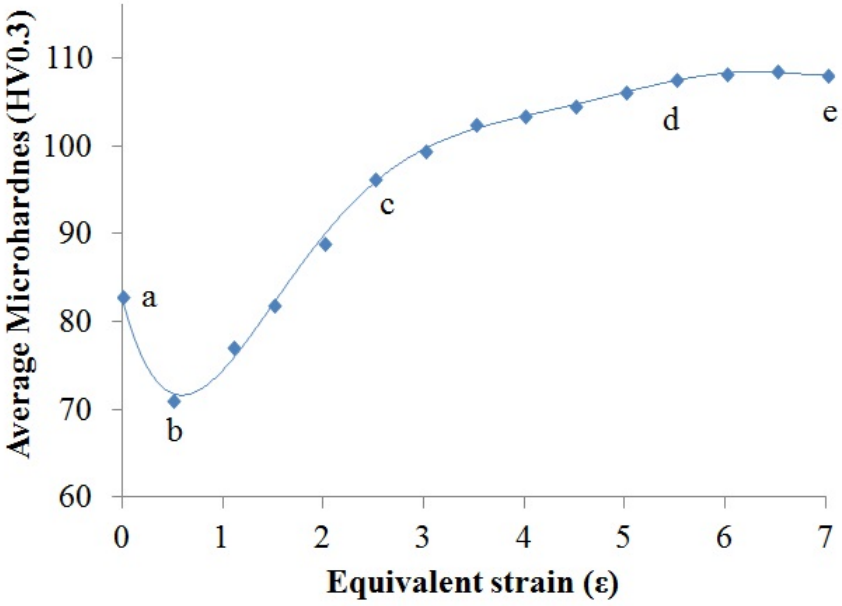

Figure 4.23: Variation of Average Microhardness with Equivalent Strain of HPT Specimens From Alloy 6061.

radially and thus formed a whirlpool like pattern. In 1T specimens the whirlpool spread from periphery to middle section. Whirlpool in the 5T and 10T specimens was clearly visible in all sections. However the small particles were occasionally punctuated by few large particles; an indication that not all particles were fully broken.

Bigger particles that were breaking starting from $\frac{1}{4}$T - 10T specimens varied in shape from needle shaped, blocky shaped to equiaxed as shown in Figures 4.16 and 4.17 . This means that particles that were needle shaped were broken easily; and that is why they disappeared in the pheriphery at lower number of turns. However equiaxed particles were visible after 10T, since they were more resistant to cracking. This means that heat treatment prior to HPT can spheroidize silicon hardening phases hence render them resistant to breaking. However, brittle iron intermetallics which are needle or plate shaped can be broken down and homogenized in the aluminum matrix. As a result hardness of the material is improved.

Image J software was used to analyze the processed particles with respect to their number, perimeter, area and circularity as shown in Figure 4.18. The number of particles in the core and periphery of 0.5T specimens were 167 and 273 respectively. Initially, the second phase partcles were uniformly distributed throughout the unprocessed specimen. However processing broke the specimens more at the pheriphery than at the core. In all processing levels the particles increased with the number of turns as shown in Figure 4.19 (a). Increase in the number of second phase particles was as a result of their breakage. The curves were leveling off between 5 and 10 turns. This means that the rate of breakage of particles was slowing down. Average perimeter and area of the particles were inversely proportional to number of turns; and hence strain as shown in Figure 4.19 (b) and (c). As the size of particles reduced, the perimeter and area of the particles also reduced. At lower turns circularity was about 0.45 and increased to about 0.85 as shown in Figure 4.19 (d). Rise in circularity means that the particles were breaking from large needle shaped

particles into smaller equiaxed particles that were homogenized in the metal matrix. Breakage and homogenization of the particles have been found to be beneficial to mechanical properties including hardness, tensile strength and fatigue (Sakai et al., 2005; Xu et al., 2008). the breakage of the particles was indicated by rise in number of particles, decraese in their size as indicated by reduction in area and perimater, and rise in circularity.

Microhardness after HPT processing varied along the diameter of a specimen and also from one specimen to another as the number of turns increased as shown in Figure 4.20. Extruded material, prior to HPT processing had average hardness 49±1.4 $HV_{0.3}$. Minimal standard deviation in hardness was due to presence of second phase particles in the aluminum matrix.

HPT processing at a constant pressure of 6 GPa and varying number of turns increased the average hardness of the specimens as shown in Figure 4.21. For $\frac{1}{4}$T average hardness was recorded as 88.6±8.15 $HV_{0.3}$. Compared to the unprocessed specimens this was 80.8% increase. Such increase can be attributed to combined effect of pressure and torsion on the material. Processing broke down the second phase particles, distributed the broken particles and minimized defects like porosity. Additionally, torsion contributed to strain hardening of the material; and thus increasing hardness. However; variation in hardness from a minimum at the core, a sharp rise in the middle and a maximum at the periphery resulted to the high standard deviation. The curve was not smooth as particles were not of uniform size. Variation was highest at the core, where particles had minimal breakage.

Variation of average hardness between any successive specimens from $\frac{1}{4}$ - 10 T was 16.5, 13.9, 13.8 and 1.3 % respectively. Therefore, it was inversely proportional to the number of turns. A rise in number of turns increased strain in the specimen; and hence strain hardness. Therefore increase in strain resulted to rise in hardness. Increase in strain was proportional to the radial distance from the core and the

number of turns. This explains reason as to why hardness was higher at the periphery than at the core. However a maximum hardness was attained at periphery followed by an increase towards core through middle section as the number of turns increased as shown in Figure 4.20.

A curve of average microhardness versus equivalent strain show that maximum hardness of ∼110 $HV_{0.3}$ was acquired at an equivalent strain of ∼5 as shown in Figure 4.22. Microhardness of pure aluminum has been shown to be related to equivalent strain by dividing the curve into sectionsIto and Horita (2009). The curve was divided into 4 sections, namely; (a-b), (b-c), (c-d) and (d-e). In section (a-b) hardness was decreasing up to a minimum at (b). Large variation of core hardness of the specimens lowered their average equivalent strain to a minimum at b. The region was usually marked by accumulation of dislocations to form subgrain boundaries. The boundaries blocked the dislocation motion. As a result low angle grain boundaries were formed in section (b-c). The formation of the grains was marked by sharp rise in hardness. Further straining in section (c-d) destroyed the dislocations in the grains and increased the angle of misorientation, to produce high angle grains. Hardness was observed to rise gradually. This marked the onset of steady state condition. In section four (d-e), hardening due to dislocation absorption was in equilibrium with softening due to dislocation accumulation. Consequently, hardness remained constant with increase in equivalent strain. HPT at 10T improved significantly the strength and microhardnes of the extruded material as shown in Table 4.6.

Table 4.6: A Summary of the properties of Samples at Different Processing Levels

property	standard alloy	Cast alloy	Extruded alloy	HPT processes
Strength (MPa)	190 - 240	84	214	381
Microhardness ($HV_{0.3}$)	160 - 100	50	49	110

Therefore HPT grain refinement process included accumulation of dislocations, formation of low angle grain boundaries, destruction of dislocations to increase misorientation angles and finally establishing an equilibrium between accumulation and annihilation of dislocations. The second phase particles were also broken down and homogenized. This resulted in ultra fine and equiaxed grains with high angle boundaries.The processing enhanced the hardness of the material as well as strength.

4.6 Friction Stir Welding

The Al 6061 alloy was friction stir welded at spindle speeds ranging from 530 - 1320 rev/min and feed rate of between 40 - 100 mm/min. Microstructure, tensile and microhardness results of the welded material are discussed in this section.

4.6.1 Results

Metallography specimens of the extruded alloy were sectioned along the Y - axis as shown in Figure 3.11 and etched. Macrograph and micrographs of a section welded at 530 RPM and a feed rate of 100 mm/min were as shown in Figure 4.24. Macro examination of the specimen revealed a bright and tapered stirred zone (SZ); whose top and bottom width were equal to tool shoulder diameter and pin diagonal respectively. Microscopic observation of the section, at a low magnification revealed three distinct zones including the brighter middle zone, transition zone and a zone with pancaked grains. At a higher magnification the zones increased to four based on average grain size as shown in Figure 4.25. Average grain size of stirred zone (SZ), heat affected zone (HAZ), and base metal (BM); were 7, 183, 93 μm respectively. The transition phase had partially deformed grains of HAZ and grains of SZ, hence referred to as thermomechanically affected zone (TMAZ).

Tensile strength of welded specimens at a constant feed of 100 mm /min and varying spindle speed was as shown in Figure 4.26; and their ultimate tensile strength was

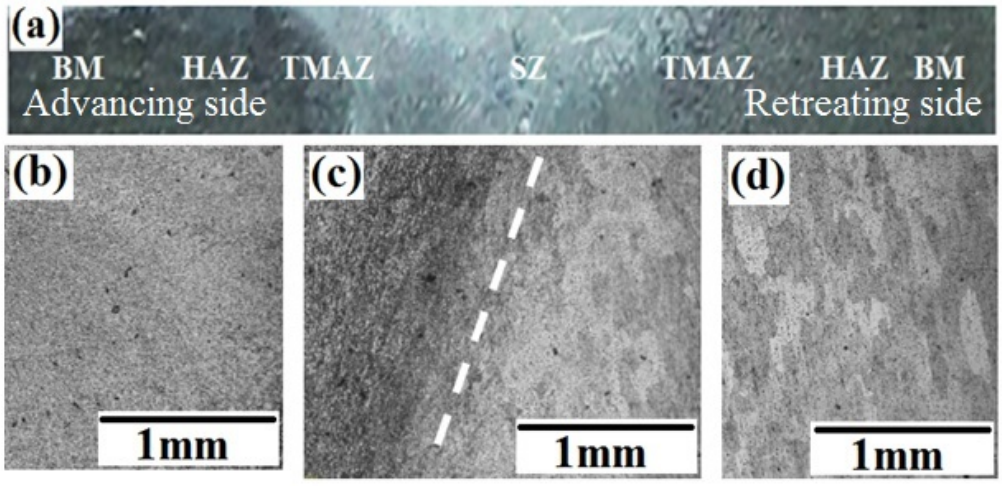

Figure 4.24: Structure of FSW Specimens Processed at 530 rev/min and 100 mm/min: (a) Macrograph of Over Etched section; and (b) Micrographs of (b); Stirred Zone (SZ), (c) Thermomechanically Affected Zone (TMAZ) Shown by Dotted Line; and (d) Heat Affected Zone (HAZ) Together With Base Metal (BM).

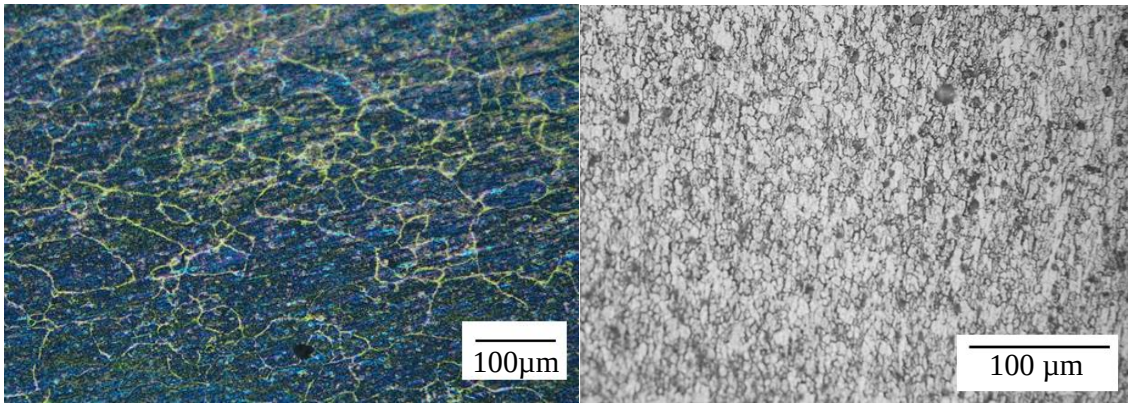

Figure 4.25: Micrographs of FSW Specimens Processed at 530 RPM and 100 mm/min: (a) Base Metal and (b) Stirred Zone.

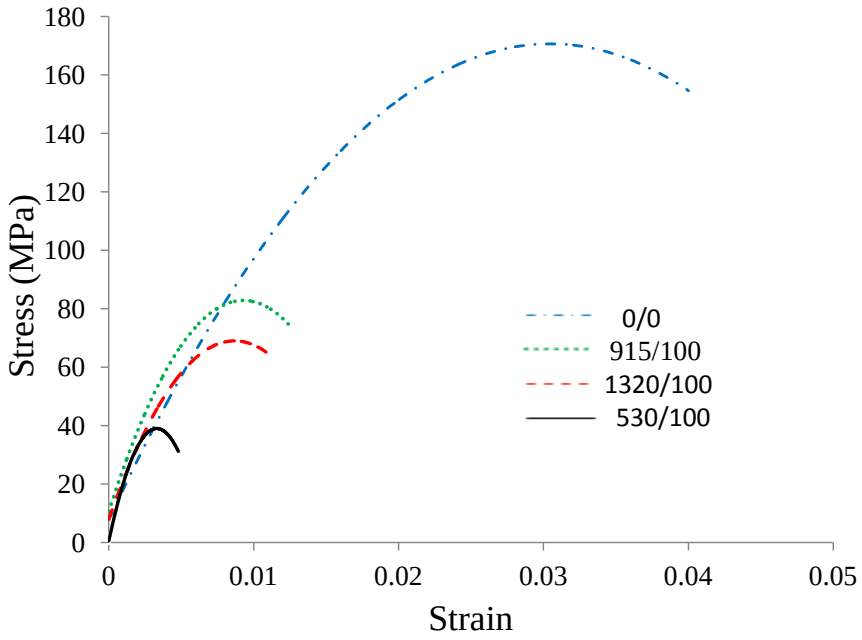

Figure 4.26: Stress Versus Strain of Specimens Processed at Speed of 0 (Unprocessed), 530, 915 and 1320 rev/min and Constant Feed of 100 mm/min.

as shown in Figure 4.27. The unwelded specimen had strength of 170 MPa. Welding the specimen at the lowest speed of 530 rev/min reduced the strength to 40 MPa. However increase in speed to 915 rev/min, increased the strength to 84 MPa. At a speed of 1320 rev/min the strength reduced to 68 MPa.

Strength, yield strength and ductility were lower in the welded materials than in the unprocessed one as shown in Table 4.7.

Table 4.7: Properties of Al 6061 Welded by FSW at a feed rate of 100 mm/min

Speed (RPM)	Strength (MPa)	Yield strength (MPa)	Ductility (%)
Unwelded	170	110	26
530	40	36	6
915	84	60	10
1320	68	50	10

Vickers microhardness distribution along a line M-N on a section cut along the Y -

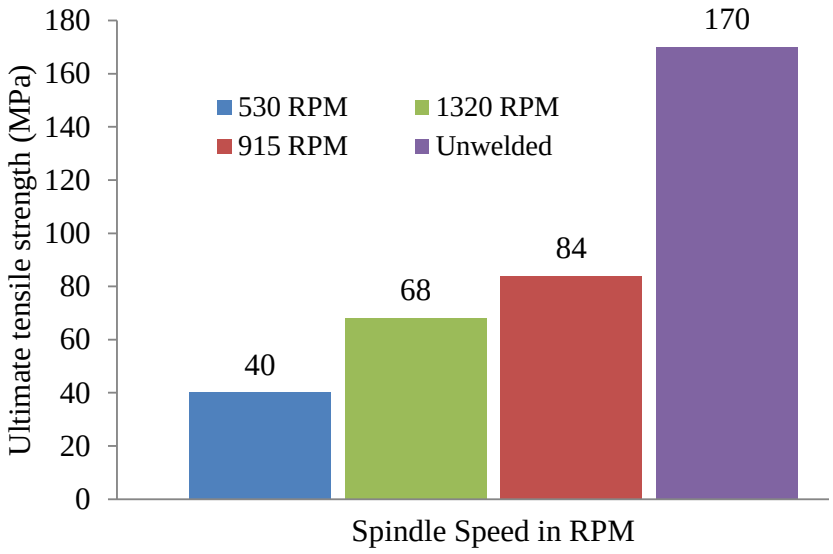

Figure 4.27: Ultimate Tensile Strength of Specimens Welded at Speed of 0 (Unprocessed), 530, 915 and 1320 rev/min and constant feed rate of 100 mm/min.

axis of specimens welded at a constant feed rate of 40 mm/min and spindle speed of 530, 915 and 1320 rev/min was as shown in Figure 4.28. Effect of increasing feed rate to 100 mm/min at the varying spindle speeds on microhardness was as shown in Figure 4.29. The mean microhardness of the stirred zone for spindle speeds of 530, 915 and 1320 rev/min at feed rate of 40 and 100 mm/min was as shown in Figure 4.30

4.6.2 Discussions

Original structure of the extruded material that was welded through FSW had pancaked grains oriented in the direction of extrusion. Their average size was 93 μm.

During welding as shown in Figure 3.11, rotating tool pin and shoulder where in contact with workpiece; and thus produced frictional heat which softened the material. The softened material was stirred by the tool that was simultaneously

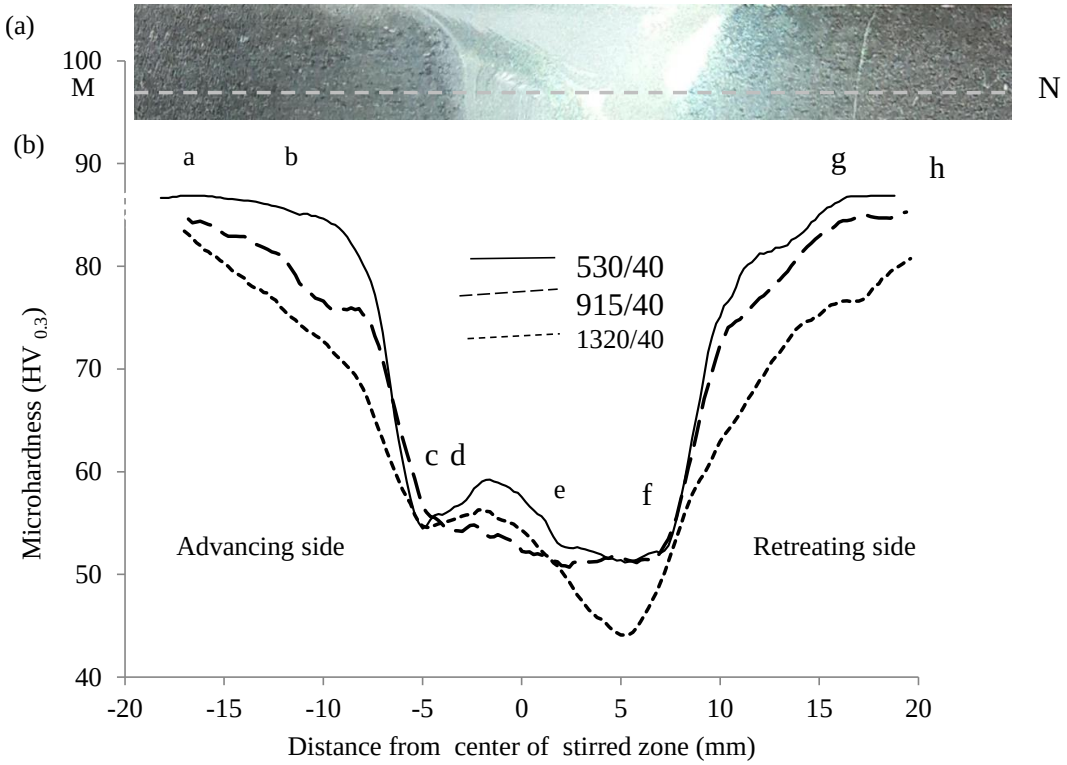

Figure 4.28: Hardness Measurement (a) Measured Along a Section M-N (b) Specimens Welded at a Feed Rate of 40 mm/min and Spindle Speeds of 530, 915 and 1320 rev/min.

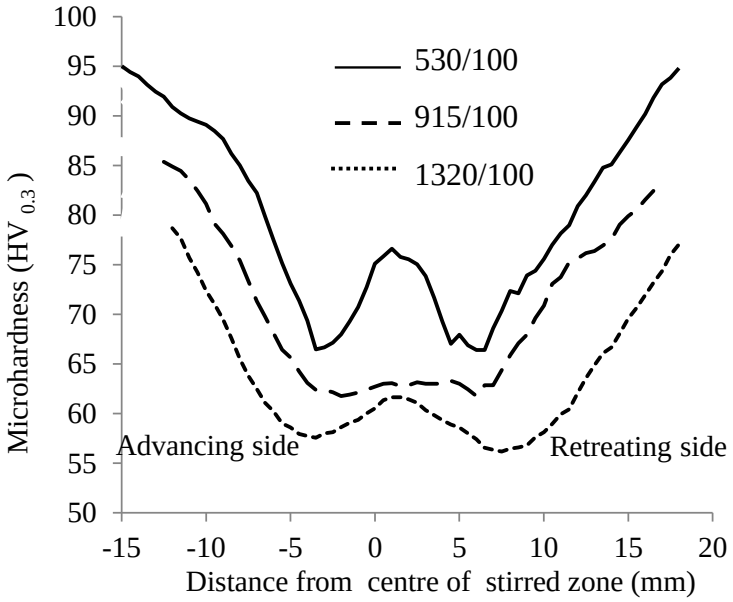

Figure 4.29: Microhardness of Specimens Processed at a Feed Rate of 100 mm/min and Spindle Speeds of 530, 915 and 1320 rev/min.

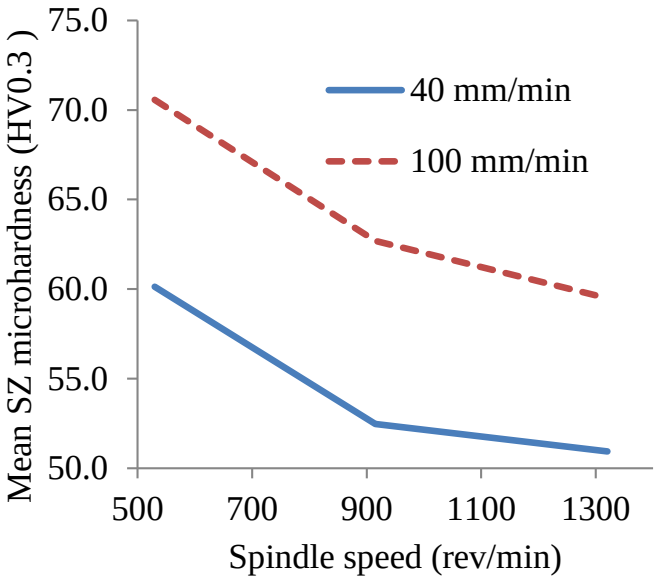

Figure 4.30: Average Microhardness of SZ of FSW Specimens Processed at a Feed Rate of 40 and 100 mm/min and Varying Spindle Speed Measured in rev/min.

advanced through it. Advancing side was characterized by rotation and feed of the tool being in same direction; and in retreating side, rotation and feed were opposite. Material being stirred by pin was moved upward. Eventually the motion was restricted when the material contacted the shoulder. The contact increased frictional heat and surface area.

Stirred zone (SZ) was tapered with the top portion being wider than the bottom as shown in Figure 4.24. The top and bottom portions of the taper were equal to diameter of the shoulder and pin respectively. Macro examination of an over etched friction stir Welded specimen made the zone to appear brighter than the rest. The zone was welded mechanically due to stirring in an elevated temperature; and had an average grain size of 7 μm. This was a reduction from the original size of 93 μm in the base metal (BM). Consequently stirring and frictional heating refined the grain structure of the zone.

The frictional heat has been found to be highest next to the tool pin and shoulder

(Hwang et al., 2008). The temperature gradient was inversely proportional to the distance from the tool. The area next to BM that was affected by heat only was referred to as heat affected zone (HAZ). Grain size in the section increased by 100 % compared to the original structure in base metal (BM). The grain growth was due to heating and slow cooling of the welded material in open air.

A zone existing at the transition from SZ to HAZ had grains that were partially distorted by stirring and heating. Pancaked grains in the zone were oriented in the direction of rotation. The zone was referred to as thermal mechanically affected zone (TMAZ). The TMAZ was narrow and represented transition from SZ to HAZ.

Ultimate tensile strength of the unprocessed material was 170 MPa as shown in Figure 4.27. Welding the material while varying spindle speed and keeping feed rate constant at 100 mm/min affected its ultimate tensile strength. The material processed at 530 rev/min had its strength reduced to 40 MPa and failed in SZ. The the spindle speed and feed rate did not generate frictional heat that was enough to plasticize the material fully. Therefore, the SZ was weak hence failed at a low stress. Raising the speed to 915 rev/min increased the strength to 84 MPa and failure occurred in HAZ. Friction produced heat that plasticized the material fully. This resulted in a SZ with higher strength than HAZ. The point of failure had coarse grains due to rise in frictional heat. In this section the grains coarsened because of exposure to heating above recrystallization temperature and slow cooling. This resulted in softening of the metal especially near the border of TMAZ and HAZ where the effect of temperature was highest. Increasing the speed to 1320 rev/min lowered the strength to 68 MPa and failure occurred in the HAZ. The excess heat coarsened the grains in the HAZ and the SZ, thus softening the zone highly. High spindle speed increased the frictional heat that coarsened the refined grains in the SZ. Optimum tensile properties were obtained at a speed of 915 RPM as shown in Table 4.7.

Measurement of microhardness across FSW processed specimen at a speed of 530 RPM and feed of 40 mm/min showed that the hardness varied from a-h as shown in Fig. 4.28. In the BM (a-b) hardness was maximum at 88 $HV_{0.3}$. Structure of the material was not affected by heat. Hence the zone retained the hardness of the original material. Hardness decreased in HAZ (b-c) from 88 $HV_{0.3}$ to 55 $HV_{0.3}$. The heat was above the material's recrystallization temperature; and consequently coarsened its grains and dissolved the hardening phases. The effect was proportional to the temperature gradient and this made the temperature to be lowest at point c where frictional heat was highest. Hardness rose briefly in TMAZ (c-d) up to 60 $HV_{0.3}$. In this section there was partial straining as it was in the vicinity of the stirred zone.

Hardness levelled off in SZ (d-e) to an average of 58 $HV_{0.3}$. Heat and stirring action made the material to experience solid state welding. The ensuing refined grains were harder and more uniform than the grains in the TMAZ. Temperature in the section was still high, and hence reduced the hardness of the material. Further the second phase particles were mechanically broken down and homogenized by stirring action. The size of this section was approximately 5 mm; and therefore was equal to the diameter of tool pin.

Lowest hardness of 52 $HV_{0.3}$ was recorded at (f). The hardness was on TMAZ of retreating side that was lower than that of advancing side. It could have resulted from increased temperature due to the opposite motion of feed and rotation of the tool on that side. Mechanical forces that resulted in distortion of grains were quite high in the vicinity of the pin surface. Finally hardness rose to a maximum of 88 $HV_{0.3}$ in the HAZ of the retreating side (f-g) and levelled off in the BM (g-h).

When speed was increased from 530 to 915 rev/min and then 1230 rev/min at a constant feed of 40 mm/min as shown in Figure 4.29, average micro hardness of SZ decreased. Hardness of TMAZ and HAZ also decreased. The HAZ also became

wider. Rise in speed increased friction between tool and material. Consequently, there was rise in heat in SZ. The increased heat was conducted to the other zones. Inevitably heat lead to grain growth and softened the hardening phases in the material. Therefore hardness was inversely proportional to speed of tool rotation. Rise of feed from 40 mm/min to 100 mm/min as shown in Figure 4.30, reduced the period of contact between tool and material, thus lowering frictional heat. Rise in feed rate was directly proportional to rise in hardness.

CHAPTER FIVE

CONCLUSIONS AND RECOMMENDATIONS

5.1 Concluding Remarks

Mass balance analysis and meticulous scrap sorting identified four secondary structural aluminium alloys equivalent to Al 6005, 6063, 6061 and 6070 in the 6000 series alloys. Al 6061 secondary alloy was selected for further analysis because it has broad structural applications and its composition marched that of a standard 6061 alloy. Characterization of secondary 6061 Al alloy after melting, extrusion, HPT and FSW showed that it was suitable for structural applications and it behaviour could be genaralized to the other 3 since they are from a similar series. The following conclusions can be drawn from this work:

1. Mass balance analysis performed in year 2017 showed that 9950 tons of aluminum scrap was recycled. Structural wrought Aluminium scrap was 23 % of the total scrap, and was enough for the development of a structural alloy.

2. Four batches A, B, C and D of carefully sorted structural scrap, when melt without addition of primary aluminium and adjustment of alloying elements yielded secondary Aluminium 6005, 6063, 6061 and 6070 alloys respectively.

3. Extrusion of the as cast Aluminium 6061 alloy at a temperature of 450 ^{0}C and a pressure of 15 kN/m^2 eliminated porosity and reduced the size of second phase particles; consequently, improving strength from 100 to 214 Mpa. The strength compared to that of standard Al 6061 alloy Which range from 124 - 290 MPa.

4. HPT of extruded Al 6061 alloy at 10T broke down and homogenized the second

phase particles. Consequently, strength and microhardness of the alloy was increased from 214 - 381 MPa and from 50 - 110 $HV_{0.3}$ respectively.

5. FSW processed extruded Al 6061 alloy had highest strength of 84 Mpa at 915 rev/min and 100 mm/min; and highest micro hardness of 70 $HV_{0.3}$ at 530 rev/min and 100 mm/min.

5.2 Recommendations for Future Research

- The extrusion die need to be improved by incorporating billet extraction mechanism, a heater, insulating the cylinder body to prevent heat loss and increase the extrusion force.

- There is a need for development of tools for HPT and FSW processing of aluminum alloys.

- A study of heat distribution across the FSW processed zone need to be conducted.

5.3 Benefit of the Research

This research findings are vital for local players in the aluminum industries processing structural materials using scrap aluminum. Adoption of meticulous scrap sorting techniques will eliminate use of costly primary aluminium and adjustment of alloying elements. The cheaper structural Aluminium alloys with enhanced properties and weldability through HPT and FSW will compete with costly standard alloys in the manufacture of engineering structures.

5.4 Outputs from the Research

Two papers have been presented in a conference and two papers have been published in a journal. The papers include:

- Wang'ombe D. N., Mose B. R., Maranga S. M. and Mbuya T. O.; "Effects of Friction Stir Welding on Microstructure and Mechanical Properties of Extruded Secondary Aluminium 6061 Alloy"; Materialwiss Werkstofftech Vol. 52, pp 270 - 278; 2021.

- Wang'ombe D. N., Mose B. R., Maranga S. M., Ng'ang'a S. P. and Mbuya T. O.; "Recycling of Aluminium scrap in Kenya: A Survey of Foundry Enterprises and Mechanical Properties of Resultant Alloys"; Journal of Sustainable Research in Engineering Vol. 5 (1), pp 25 - 33; 2019.

- Wang'ombe D. N., Maranga S. M., Mose B. R. and Mbuya T. O.; "Advances in Friction-stir Processing of Aluminum Alloys"; Proceedings of the Sustainable Research and Innovation Conference, JKUAT Main Campus, Kenya; pp 196 - 202; 2018.

- Wang'ombe D. N., Maranga S. M., Mose B. R. and Mbuya T. O.; "The Status of Kenyan Aluminum Recycling Industry"; Proceedings of the Sustainable Research and Innovation Conference, JKUAT Main Campus, Kenya; pp 194 - 199; 2017.

REFERENCES

Agamuthu, P., Mahendra, V., & Mohd, A. (2011). Material flow analysis of aluminium in a dynamic system: Jeram sanitary landfill. *Malaysian Journal of Science*, *30*(1), 16–27.

Alhamidi, A., & Horita, Z. (2015). Grain refinement and high strain rate superplasticity in alumunium 2024 alloy processed by high-pressure torsion. *Materials Science and Engineering: A*, *622*, 139–145.

Ammar, H., Samuel, A., & Samuel, F. (2008). Porosity and the fatigue behavior of hypoeutectic and hypereutectic aluminum–silicon casting alloys. *International journal of Fatigue*, *30*(6), 1024–1035.

An, X. H., Lin, Q. Y., Wu, S. D., Zhang, Z. F., Figueiredo, R. B., Gao, N., & Langdon, T. G. (2011). The influence of stacking fault energy on the mechanical properties of nanostructured cu and cu–al alloys processed by high-pressure torsion. *Scripta Materialia*, *64*(10), 954–957.

Askeland, D. R., Phulé, P. P., Wright, W. J., & Bhattacharya, D. K. (2003). *The science and engineering of materials*. Springer, New York.

Ayogu, P. C., & Eze, F. I. (2019). Colorimetric determination of chromium in aluminium alloys by diphenylcarbazide method. *Open Journal of Chemistry*, *5*(1), 009–012.

Azushima, A., Kopp, R., Korhonen, A., Yang, D.-Y., Micari, F., Lahoti, G., ... others (2008). Severe plastic deformation (spd) processes for metals. *CIRP annals*, *57*(2), 716–735.

Bahrami, M., Dehghani, K., & Givi, M. K. B. (2014). A novel approach to develop aluminum matrix nano-composite employing friction stir welding technique. *Materials & Design*, *53*, 217–225.

Bell, S., Davis, B., Javaid, A., & Essadiqi, E. (2003). Final report on scrap

management, sorting and classification of aluminum. *Natural Resources Canada Report*, *22*, 2003–22.

Billy, R. (2012). *Material Flow Analysis of Extruded Aluminium in French Buildings: Opportunities and Challenges for the Implementation of a Window-to-Window System in France* (Unpublished master's thesis). Department of Hydraulic and Environmental Engineering, Norwegian University of Science and Technology.

Boin, U., & Bertram, M. (2005). Melting standardized aluminum scrap: A mass balance model for europe. *JOM*, *57*(8), 26–33.

Brunner, P. H., & Rechberger, H. (2016). *Handbook of material flow analysis: For environmental, resource, and waste engineers*. CRC press, Boca Raton.

Bussu, G., & Irving, P. E. (2003). The Role of Residual Stress and Heat Affected Zone Properties on Fatigue Crack Propagation in Friction Stir Welded 2024-T351 Aluminium Joints. *International Journal of Fatigue*, *25*, 77-88.

Callister, W. D. (2007). *Materials science and engineering: An introduction*. John Wiley and Sons, Inc., United States of America.

Cam, G., & Mistikoglu, S. (2014). Recent Developments in Friction Stir Welding of Al-Alloys. *Journal of Materials Engineering and Performance*, *23*, 1936–1953.

Central Bureau of Statistics. (2001). *Statistical Abstract 2000* (Tech. Rep.). Ministry of Finance and Planning, Kenya.

Ceschini, L., Boromei, I., Minak G., M. A., & F., T. (2007). Effect of Friction Stir Welding on Microstructure, Tensile & Fatigue Properties of the AA7005/10%Al_2O_3 Composite. *Composites Science and Technology*, *67*, 605-615.

Charit, I., & MishraLow, R. S. (2005). Temperature Superplasticity in a Friction-Stir-Processed. *Acta Materialia*, *53*, 4211-4223.

Commin, L., Dumont, M., Masse, J. E., & Barrallier, L. (2009). Friction Stir Welding of AZ31 Magnesium Alloy Rolled Sheets: Influence of Processing Parameters. *Acta Materialia*, *57*, 326-334.

Dahlström, K., Ekins, P., He, J., Davis, J., & Clift, R. (2004). Iron, steel and

aluminium in the uk: Material flows and their economic dimensions. *London: Policy Studies Institute*.

Das, S. K. (2006). Designing aluminium alloys for a recycling friendly world. In *Materials science forum* (Vol. 519, pp. 1239–1244).

Das, S. K., Green, J., & Kaufman, J. G. (2007). The development of recycle-friendly automotive aluminum alloys. *Jom*, *59*(11), 47–51.

Das, S. K., Green, J. A. S., & Kaufman, J. G. (2010). Aluminum Recycling: Economic and Environmental Benefits. *Light Metal Age*, *68*(1), 42.

Davis, J. R. (1993). *Aluminum and aluminum alloys*. ASM international, United States of America.

Dobatkin, S. V., Bastarache, E. N., Sakai, G., Fujita, T., Horita, Z., & Langdon, T. G. (2005). Grain Refinement and Superplastic Flow in an Aluminium Alloy Processed by High-Pressure Torsion. *Materials Science and Engineering*, *A4008*, 141-146.

EAA. (2011). *Power train - Engine blocks, the Aluminium Automotive Manual* (Tech. Rep.). European Aluminium Association.

Edalati, K., Fujioka, T., & Horita, Z. (2008). Microstructure and Mechanical Properties of Pure Cu Processed by High-Pressure Torsion. *Materials Science and Engineering*, *A497*, 168-173.

Edalati, K., & Horita, Z. (2009). Scaling-up of high pressure torsion using ring shape. *Materials Transactions*, *50*(1), 92–95.

Edalati, K., & Horita, Z. (2011). Significance of Homologous Temperature in Softening Behavior and Grain size of Pure Metals Processed by High Pressure Torsion. *Material Science and Engineering*, *A528*, 7514-7523.

Edalati, K., Lee, S., & Horita, Z. (2012). Continuous high-pressure torsion using wires. *Journal of Materials Science*, *47*(1), 473–478.

Elangovan, K., & Balasubramanian, V. (2008a). Influences of Tool Pin Profile and Tool Shoulder Diameter on the Formation of Friction Stir Processing Zone in AA6061 Aluminium Alloy. *Materials and Design*, *29*, 362-373.

Elangovan, K., & Balasubramanian, V. (2008b). Influences of Tool Pin Profile and Welding Speed on The Formation of Friction Stir Processing Zone in AA2219 Aluminium Alloy. *Journal of Materials Processing Technology*, *200*, 163-175.

Elgallad, E. M., Samuel, A. M., Samuel, F. H., & Doty, H. W. (2010). Effects of additives on the microstructures and tensile properties of a new al-cu based alloy intended for automotive castings (10-042). *Transactions of the American Foundrymen's Society*, *118*, 39.

El-Rayesa, M. M., & El-Danafa, E. A. (2012). The Influence of Multi-Pass Friction Stir Processing on the Microstructural and Mechanical Properties of Aluminum Alloy 6082. *Journal of Materials Processing Technology*, *212*, 1157-1158.

Gao, Y. X., Yi, J. Z., Lee, P. D., & Lindley, T. C. (2004). The effect of porosity on the fatigue life of cast aluminium-silicon alloys. *Fatigue & Fracture of Engineering Materials & Structures*, *27*(7), 559–570.

Gaustada, G., Olivetti, E., & Kirchain, R. (2012). Improving Aluminum Recycling: A survey of Sorting and Impurity Removal Technologies. *Resources, Conservation and Recycling*, *58*, 79-87.

Gilstad, G., & Hammervold, J. (2014). Life cycle assessment of secondary aluminium refining. In *Light metals 2014* (pp. 901–906). Springer.

Green, J. A. S. (2007). *Aluminum recycling and processing for energy conservation and sustainability*. ASM International, United States.

Hofmann, D. C., & Vecchio, K. S. (2005). Submerged Friction Stir Processing (SFSP): An Improved Method for Creating Ultra-Fine-Grained Bulk Materials. *Journal of Materials Processing Technology*, *A402*, 234-241.

Horita, Z., & Langdon, T. G. (2005). Microstructures and Microhardness of an Aluminium Alloy and Pure Copper After Processing by High-Pressure Torsion. *Materials Science and Engineering*, *A410-411*, 422-425.

Horita, Z., & Langdon, T. G. (2008). Achieving Exceptional Superplasticity in a Bulk Aluminium Alloy Processed by High-Pressure Torsion. *Scripta Materialia*, *58*, 1029-1032.

Hwang, Y. M., Kang, Z. W., Chiou, Y. C., & Hsu, H. H. (2008). Experimental Study on Temperature Distributions Within the Workpiece During Friction Stir Welding of Aluminum Alloys. *International Journal of Machine Tools and Manufacture*, *48*, 778-787.

Intan, F. M., Lee, S. W., & Horita, Z. (2013). Strengthening of Al 6061 Alloy by High-Pressure Torsion Through Grain Refinement and Aging. *Materials Science Forum*, *765*, 408–412.

Ito, Y., & Horita, Z. (2009). Microstructural evolution in pure aluminum processed by high-pressure torsion. *Materials Science and Engineering: A*, *503*(1-2), 32–36.

Jata, K. V., & Semiatin, S. L. (2000). Continuous Dynamic Recrystallization During Friction Stir Welding of High Strength Aluminum Alloys. *Scripta mater.*, *43*, 743-749.

Jiang, D. S., Lui, T. S., & Chen, L. H. (1999). Crack Propagation Behaviour of A356 and Al-1Si-0.3Mg Aluminium Alloys Under Resonant Vibrations. *Materials Transactions*, *40*, 283-289.

Jiang, H., Zhu, Y. T., Butt, D. P., Alexandrov, I. V., & Lowe, T. C. (2000). Microstructural Evolution, Microhardness and Thermal Stability of HPT-Processed Cu. *Materials Science and Engineering*, *A290*, 128-130.

Kalpakjian, S., & Schmid, S. R. (2010). *Manufacturing engineering and technology.* Pearson etext, New York, 6th Edition.

Kashyap, K. T., & Chandrashekar, T. (2001). Effects and Mechanisms of Grain Refinement in Aluminium Alloys. *Bull. Mater. Sci.*, *24*, 345-352.

Kaufman, J. G. (2006). *Mechanical Engineers Handbook: Materials and Mechanical Design, Volume 1.* John Wiley and Sons, Inc., United States.

Kaufman, J. G., & Rooy, E. L. (2004). *Aluminium alloy castings, properties, processes and applications.* American Foundry Scociety, United States of America.

Kawasaki, M., Ahn, B., & Langdon, T. G. (2010). Microstructural Evolution in

a Two-phase Alloy Processed by High-Pressure Torsion. *Acta Materialia*, *58*, 919-930.

Kemal, M., Kulekci, E. U., & Buldum, B. (2015a). Critical Analysis of Friction Stir-Based Manufacturing Processes. *Int J Adv Manuf Technol*, *2*, 1-5.

Kemal, M., Kulekci, E. U., & Buldum, B. (2015b). Critical Analysis of Friction Stir-Based Manufacturing Processes. *Int J Adv Manuf Technol*.

Kevorkijan, V. (2010). Advances in Recycling of Wrought Aluminium Alloys for Added Value Maximisation. *Association of Metallurgical Engineers of Serbia*, *16*, 103-114.

Kevorkijan, V. (2013). Challenges and Advantages of Recycling Wrought Aluminium Alloys From Lower Grades of Metallurgically Clean Scrap. *Materials and Technology*, *47*, 13-23.

King, F. (1987). *Aluminium and its alloys*. Ellis Horwood Limited, England.

KNBS. (2012). *Economic Survey 2012* (Tech. Rep.). Kenya National Bureau of Statistics, Kenya.

KNBS. (2013). *Statistical Abstract 2013* (Tech. Rep.). Kenya National Bureau of Statistics, Kenya.

KNBS. (2015a). *Economic Survey 2015* (Tech. Rep.). Kenya National Bureau of Statistics, Kenya.

KNBS. (2015b). *Statistical Abstract 2015* (Tech. Rep.). Kenya National Bureau of Statistics, Kenya.

KNBS. (2016). *Economic Survey 2016* (Tech. Rep.). Kenya National Bureau of Statistics, Kenya.

Kraisat, W., & Jadyil, W. A. (2010). Strengthening Aluminium Scrap by Alloying with Iron. *Jordan Journal of Machanical and Industerial Engineering*, *4*, 372-377.

Krishnan, K. N. (2002). On the Formation of Onion Rings in Friction Stir Welds. *Materials Science and Engineering*, *A327*, 246-251.

Kumar, K., & Kailas, S. V. (2008). The Role of Friction Stir Welding Tool on

Material Flow and Weld Formation. *Materials Science and Engineering*, *A485*, 367-374.

Kumari, S. S., Pillai, R. M., Nogita, K., Dahle, A. K., & Pai, B. C. (2006). Influence of calcium on the microstructure and properties of an al-7si-0.3mg-xfe alloy. *Metallurgical and Materials Transactions A*, *37*, 2581-2587.

Kwon, Y. J., Saito, N., & Shigema, I. (2002). Friction stir process as a new manufacturing technique of ultrafine grained aluminum alloy. *Journal of materials science letters*, *21*, 1473-1476.

Lakshmanan, A. N., Shabestari, S. G., & Gruzleski, J. E. (1995). Microstructure Control of Iron Intermetallics in Al-Si Casting Alloys. *Z.Metallkd*, *86*, 457-464.

Lesniak, D., & Woznicki, A. (2012). Extrusion of Al-Cu-Mg Alloys with Simultaneous Solution Heat Treatment. *Archives of Metallurgy and Materials*, *57*, 19-31.

Li, Y., Murr, L. E., & McClure, J. C. (1999). Flow Visualization and Residual Microstructures Associated with the Friction-Stir Welding of 2024 Aluminum to 6061 Aluminum. *Materials Science and Engineering*, *A271*, 213-223.

Li, Z., Samuel, A. M., Samuel, F. H., Ravindran, C., Doty, H. W., & Valtierra, S. (2004). Parameters controlling the performance of aa319-type alloys: Part ii. impact properties and fractography. *Materials Science and Engineering: A*, *367*(1-2), 111–122.

Liu, G., Murr, L. E., Niou, C.-S., McClure, J. C., & Vega, F. R. (1997). Microstructural Aspects of The Friction-Stir Welding of 6061-T6 Aluminum. *Scripta Materialia*, *37*, 355-361.

Lui, L., Samuel, A. M., & Samuel, F. H. (2003). Influence of Oxides on Porosity Formation in Sr-treated Al-Si Casting Alloy. *Journal of Material Science*, *38*, 1255-1267.

Lumley, R. (2011). *Fundamentals of aluminum metallurgy.* Woodhead Publishing Limited, Cambridge.

Ma, Z. Y., Sharma, S. R., & Mishra, R. S. (2006). Effect of Friction Stir Processing on the Microstructure of Cast A356 Aluminum. *Materials Science*

and Engineering, *433*, 269-278.

Mbuya, T. O., Bruno, R. M., Ng'ang'a, S. P., & Maranga, S. M. (2010). Improving the Mechanical Performance of a Secondary Cast Aluminium Piston Alloy Through Addition of Minor Elements. *Proceedings of the 12th International Conference on Aluminium Alloys, Yokohama ,Japan*.

Mohamed, A. M. A., Samuel, F. H., & Kahtani, S. A. (2013). Microstructure,Tensile Properties and Fracture Behavior of High Temperature Al-Si-Mg-Cu Cast Alloys. *Materials Science and Engineering*, *A577*, 64-72.

Moreira, P. M. G. P., Santos, T., Tavares, S. M. O., Richter-Trummer, V., Vilaça, P., , & de Castro, P. M. S. T. (2009). Mechanical and Metallurgical Characterization of Friction Stir Welding Joints of AA6061-T6 with AA6082-T6. *Materials and Design*, *30*, 189-187.

Mose, B. R. (2009). *Effect of Minor Elements on Castability, Microstructure and Mechanical Properties of Recycled Aluminium Alloys* (Unpublished master's thesis). Department of Mechanical Engineering, Jomo Kenyatta University of Agriculture and Technology.

Mrówka-Nowotnik, G., Sieniawski, J., & Wierzbiñska, M. (2007). Intermetallic Phase Particles in 6082 Aluminum Alloy. *Archives of Materials Science and Engineering*, *28*, 69-76.

Muller, U. (2011). *Introduction to structural aluminium design*. Whittles Publishing, United Kingdom.

Murali, S., Arvind, T. S., & Raman, K. S. (1997). Fatigue Properties of Sand Cast, Stircast and Extruded Al-7Si-0.3Mg Alloy with Trace Additions of Be and Mn. *Materials Tractions, JIM*, *38*, 28-36.

Nandan, R., DebRoy, T., , & Bhadeshia, H. K. D. H. (2008). Recent Advances in Friction-Stir Welding - Process, Weldment Structure and Properties. *Progress in Materials Science*, *53*, 980-1023.

Ng'ang'a, S., Odera, B., Mbuya, T., & Oduori, F. (2010). Effective recycling of cast aluminium alloys for small foundries. , *12(2)*, 162-181.

Njuguna, M. (2007). *Influence of Modifiers and Heat Treatment on the Fatigue Life and Mechanical Properties of Recycled Aluminium Alloys* (Unpublished master's thesis). Department of Mechanical Engineering, Jomo Kenyatta University of Agriculture and Technology.

Nturanabo, F., Masu, L., & Kirabira, J. B. (2019). Aluminum alloys and composites. *Novel Applications of Aluminium Metal Matrix Composites*, 3 - 41.

OECD, O. (2008). Measuring material flows and resource productivity. *The OECD guide*, *1*.

Olabode, M., Kah, P., & Martikainen, J. (2013). Aluminium alloys welding processes: Challenges, joint types and process selection. *Proceedings of the Institution of Mechanical Engineers, Part B: Journal of Engineering Manufacture*, *227*(8), 1129–1137.

Omranpour, B., Kommel, L., Sergejev, F., Ivanisenko, J., Antonov, M., Hernandez-Rodriguez, M. A., & Garcia-Sanchez, E. (2021). Analysis of the Reciprocal Wear testing of Aluminum AA1050 Processed by a Novel Mechanical Nanostructuring Technique. *IOP Conference Series: Materials Science and Engineering*, *1140*(1), 540–548.

Ouyang, J., Yarrapareddy, E., & Kovacevic, R. (2006). Microstructural Evolution in the Friction Stir Welded 6061 Aluminum Alloy (T6-Temper Condition) to Copper. *Journal of Materials Processing Technology*, *172*, 110-122.

Peel, M., Steuwer, A., Preuss, M., & Withers, P. J. (2003). Microstructure, Mechanical Properties and Residual Stresses as a Function of Welding Speed in Aluminium AA5083 Friction Stir Welds. *Acta Materialia*, *51*, 4791-4801.

Ramachandran, T. R., Sharma, P. K., & Balasubramanian, K. (2008). Grain Refinement of Light Alloys. *WFC - World Foundry Congress*, *68*, 189-193.

Rana, R. S., Purohit, R., & Das, S. (2012). Reviews on the Influences of Alloying Elements on the Microstructure and Mechanical Properties of Aluminium Alloys and Alloy Composites. *International Journal of Scientific and Research Publications*, *2*, 1-7.

Ravi, K. R., Pillai, R. M., Amaranathan, K. R., Pai, B. C., & Chakraborty, M. (2008). Fluidity of Aluminum Alloys and Composites: A review. *Journal of Alloys and Compounds*, *456*, 201-210.

Rhodes, C. G., Mahoney, M. W., H., B. W., & Calabrese, M. (2003). Fine-Grain Evolution in Friction-Stir Processed 7050 Aluminum. *Scripta Materialia*, *48*, 1451-1455.

Sabatino, M. D., & Arnberg, L. (2009). Castability of Aluminium Alloys. *Transactions of The Indian Institute of Metals*, *Vol. 62*, 321-325.

Saito, Y. (1998). Ultra-fine grained bulk aluminum produced by accumulative roll-bonding (arb) process. *Scripta mater.*, *39*(9), 1221–1227.

Sakai, G., Horita, Z., & Langdon, T. G. (2005). Grain refinement and superplasticity in an aluminum alloy processed by high pressure torsion. *Materials Science and Engineering*, *A393*, 344-351.

Santella, M. L., Engstrom, T., Storjohann, D., & Pan, T. Y. (2005). Effects of Friction Stir Processing on Mechanical Properties of the Cast Aluminum Alloys A319 and A356. *Scripta Materialia*, *53*, 201-206.

Schlesinger, M. (2007). *Aluminium recycling*. CRC Press, United States of America.

Sen, U., & Sharma, K. (2016). Friction stir processing of aluminum alloys: A literature survey. *IJSRSET*, *2*, 771-774.

Smallman, R. E., & Bishop, R. J. (1999). *Modern physical metallurgy and materials engineering*. Butterworth-Heinemann, United Kingdom.

Su J, Q., Nelson, T. W., Mishra, R., & Mahoney, M. (2003). Microstructural Investigation of Friction Stir Welded 7050- T651 Aluminium. *Acta Materialia*, *51*, 713-729.

Taghaddos, E., Hejazi, M. M., Taghiabadi, R., & Shebestari, S. G. (2009). Effect of Iron Intermetallics on the Fluidity of 413 Aluminium Alloy. *Journal of Alloys and Compounds*, *468*, 539-545.

Tan, E., & Ogel, B. (2007). Influence of Heat Treatment on the Mechanical Properties of AA6066 Alloy. *Turkish Journal of Engineering and Environmental Sciences*,

31, 53-60.

Taylor, J. A. (2004). The effect of Iron in Al-Si Casting Alloys. In *35th australian foundry institute national conference* (Vol. 148, p. 157).

Thomas, W. M., & Nicholas, E. D. (1997). Friction Stir Welding for the Transportation Industries. *Materials and Design*, *18*, 269-273.

Troeger, L. P., & Starke, E. A. (1999). Statistical Analysis of Metal Scrap Generation: The Case of Aluminum in Germany. *Resources, Conservation and Recycling*, *26*, 91-113.

Vargel, C. (2004). *Corrosion of aluminium*. Elsevier Ltd., United Kingdom.

Vimalraj, C., & Kah, P. (2021). Experimental review on friction stir welding of aluminium alloys with nanoparticles. *Metals*, *11*(3), 390.

Vorhauer, A., & Pippan, R. (2004). On the Homogeneity of Deformation by High Pressure Torsion. *Scripta Materialia*, *51*, 921-925.

Wang, Q. G., Jones, P. E., & Osborne, M. (2003). Effect of Iron on the Microstructure and Mechanical Properties of an Al-7Si-0.4Mg Casting Alloy. *Society of Automotive Engineers, Inc, United States of America*.

Wangombe, D. N. (2014). *Effects of Porosity and lntermetallics on Fatigue and Impact Properties of Recycled Aluminium-Silicon Alloys* (Unpublished master's thesis). Department of Mechanical Engineering, Jomo Kenyatta University of Agriculture and Technology.

Wen, K. Y., Hu, W., & Gottstein, G. (2003). Intermetallic Compounds in Thixoformed Aluminium Alloy A356. *Material Science and Technology*, *19*, 762 - 768.

Weramwanja, P. M. (2010). *Aluminium Material Flow and Value Chain Analysis in the Kenyan Industry* (Unpublished master's thesis). Department of Mechanical Engineering, Jomo Kenyatta University of Agriculture and Technology.

Xu, C., Horita, Z., & Langdon, T. G. (2008). The evolution of homogeneity in an aluminum alloy processed using high-pressure torsion. *Acta materialia*, *56*(18), 5168–5176.

Xu, C., Horita, Z., & Langdon, T. G. (2010). Microstructural Evolution in Pure Aluminum in the Early Stages of Processing by High-Pressure Torsion. *Materials Transactions*, *51*, 2-7.

Zeru, G. T. (2014). *Development of Recycle-friendly Secondary Cast Aluminium Alloy for Cylinder Head Applications* (Unpublished master's thesis). Department of Mechanical Engineering, Jomo Kenyatta University of Agriculture and Technology.

Zhang, B., Chen, W., & Poirier, D. R. (2000). Effect of Solidification Cooling Rate on the Fatigue Life of A356.2-T6 Cast Aluminium Alloy. *Fatigue Fract Engng Mater Struct*, *23*, 417 - 423.

Zhilyaev, A. P., & Langdon, T. G. (2008). Using high-pressure torsion for metal processing: Fundamentals and applications. *Progress in Materials science*, *53*(6), 893–979.

Zhilyaev, A. P., McNelley, T. R., & Langdon, T. G. (2007). Evolution of Microstructure and Microtexture in fcc Metals During High Pressure Torsion. *Journal of Material Science*, *42*, 1517-1528.

Zhu, A. W., Gable, B. M., Shiflet, G. J., & Starke Jr, E. A. (2002). The intelligent design of age hardenable wrought aluminum alloys. *Advanced Engineering Materials*, *4*(11), 839–846.

Zhu, Y. T., & Lowe, T. C. (2000). Observations and Issues on Mechanisms of Grain Refinement During ECAP Process. *Materials Science and Engineering*, *A291*, 46-53.

Appendices

LIST OF APPENDICES

APPENDIX A

Aluminium Scrap (tons/month) Collected by Dealers

Town	Code	Name	Automotive	Construction	Household	Electrical	Total
	01Ms	Makupa steel	1.5	1.5	1	-	4
Mombasa	02Ms	Mugo Scrap	3.2	1.3	0.5	-	5
	03Ms	Gupta Scrap	0.6	0.2	0.8	-	2.5
	04Ns	Dama Scrap	13	12	10	-	39
	05Ns	Frank Scrap	10	2	1	-	13
	06Ns	Shallion Scrap	55	8	7	-	70
	07Ns	Shiva Scrap	14	10	10	-	34
	08Ns	Macharia Traders	70	75	30	10	185
	09Ns	Metal Merchant	60	60	25	5	150
	10Ns	Jema Scrap	3	0.5	0.5	-	4
Nairobi	11ts	Jua Kali	0.5	0.5	0.1	-	1.1
	12ts	Washiru Scrap	0.2	0.05	0.15	-	0.4
	13ts	Metallic Enterprise	1.5	0.5	0.5	-	2.5
	14ts	Herman Scrap	2.5	0.5	1	-	4
	15ts	Gichanja Scrap	0.1	0.05	0.05	-	0.2
	16ts	Kamau Scrap	0.5	0.2	0.3	-	1.1
	17ts	Metal Traders	0.2	0.2	0.1	-	0.5
	18ns	Machira Scrap	5	2.0	3	-	10
	19ns	Wagura Scrap	1.1	0.6	1.3	-	3
Nakuru	20ns	Kanyoni Scrap	4.3	1.7	1.0	0.2	7
	21ns	Tanzanite Scrap	0.6	0.5	0.4	-	1.5
	22ns	Wadaka Scrap	0.1	0.1	0.1	-	0.2

APPENDIX B

Aluminium (tons/month) Consumed by Foundries

Town	Code	Name	Cast	Wrought	primary Al	new scrap	Recovery	Total	Export
Mombasa	Mf03	Kaluworks KARM		210	70	3	3	280	112
	Mf04	Narcol ARM		50	80	2	1.5	130	32.5
	Mf05	Kitchen King		80		1.5	1	80	
	tf06	Booth Extrusions		100	20	20	0.9	120	40
Nairobi	tf07	Mutua Foundry	5			0.048	0.01	5	
	tf08	Njoroge Foundry	3			0.05	0.02	3	
	Nf09	E.A. Foundry Works	7					7	
	Nf10	Numerical Machining Complex	6					6	
	Nf11	Kens Metal Ltd	10					10	
	Nf12	Edward's Foundry	0.8			0.06	0.03	0.8	
	Nf13	Shemba Casting	1			0.07	0.01	1	
	Nf14	4M Casting	3	1.5		0.05	0.12	4.5	
	Nf15	Smarter Casting	1.3	0.6		0.2	0.05	1.9	
	Nf16	Nafuu Casting	1.5			0.063	0.03	1.5	
	Nf17	Nafuu Foundry	0.3	0.08		0.05	0.02	0.4	
	Nf18	General Aluminium Fabricators		60		5	0.5	60	30
	Nf19	Crystal Industries		80				80	
	Nf21	East African Cables		30	40	4	1	70	
Nakuru	nf25	Maina Foundry	4	2		0.15		6	
	nf27	Hakika Engineering	2	1				3	
	nf28	Nakuru Moulding	3	1				4	
	nf29	Sunshine Engineering	0.5					0.5	

APPENDIX C

Questionnaire

1. **Preamble**:

   The department of mechanical engineering in JKUAT has been working on the aspects of foundry practice since year 2001. Sand, investment and gravity die casting have been used. Research has been done on natural and artificial moulding sand. Scrap from cylinder heads, engine blocks, pistons and car wheels have been used to develop secondary aluminium alloys. In collaboration with the local foundries, studies have been conducted with an aim of improving their quality control and performance.

   This questionnaire has been structured in such a way that the information gathered can form a basis for the development of recycled friendly aluminium alloys for automotive and structural applications. This study aims to determine aluminium scrap sources, categories, and to examine its flow within Kenya. It is anticipated that our local aluminium scrap dealers and foundries will use the findings of this research to make excellent aluminium products from recycled friendly alloys.

   The information obtained will be treated in confidence and will not be in any form used to identify the organization. The data will be used only for this research.

   Please return the completed questionnaire to: Mr. Daniel Ng'era Wang'ombe, Department of Mechanical Engineering, JKUAT, P.O Box 62 000 - 00200, Nairobi. Telephone: 0722- 283 492; E-mail: wangombedanielngera@tum.ac.ke

2. **General Company Information**

Name: .....

Location: ..... Tel No: ..... Email: .....

Contact person ..... Postal address: .....

3. **Guided questions**

(a) Aluminium scrap received (*to be filled by scrap dealers and foundries*)

i. Do you handle aluminum scrap? Yes [ ] No [ ]

ii. If yes select the type of the scrap you handle.

Soft (wrought) alloy [ ] hard (cast) alloy [ ]

iii. Select the local suppliers of your scrap. Scrap collecters [ ] garages [ ] organizations [ ] any other .....

iv. Select your approximate average monthly receipts of local scrap.

Quantity (tonnes)	Soft	Hard
>10	[ ]	[ ]
7.1-10	[ ]	[ ]
3.1-7.0	[ ]	[ ]
1.1-3.0	[ ]	[ ]
0.5-1.0	[ ]	[ ]
< 0.5	[ ]	[ ]

Quantities >10 tonnes specify.....

v. Estimate the % composition of each of the following categories in your scrap.

automotive [ ] building [ ] household [ ]

packaging [ ] engineering [ ] electrical [ ]

any other (specify) .....

vi. State where applicable the buying price in shillings/kg of local scrap.

Soft ..... hard .....

vii. Do you import aluminium scrap? Yes [ ] No [ ]

viii. If yes select the sources.

East African Community [ ] Rest of Africa [ ]

Europe [ ] America [ ] Asia [ ]

any other (specify) .....

ix. Select your approximate average monthly aluminum import.

Quantity (tonnes)	Soft	Hard	primary aluminium
>10	[ ]	[ ]	[ ]
7.1-10	[ ]	[ ]	[ ]
3.1-7.0	[ ]	[ ]	[ ]
1.1-3.0	[ ]	[ ]	[ ]
0.5-1.0	[ ]	[ ]	[ ]
< 0.5	[ ]	[ ]	[ ]

Quantities >10 tonnes specify .....

x. State where applicable the buying price in shillings/kg of imported aluminum.

Soft ..... hard ..... primary aluminum .....

(b) Scrap processing *(This section should be filled only by the scrap dealers).*

i. Do you perform value added activities to your scrap?

Yes [ ] No [ ]

ii. If yes select from the activities given below:

Sorting [ ] cleaning [ ] balling [ ]

Casting ingots [ ] any other (specify) .....

(c) Scrap consumers *(This section should be filled only by the scrap dealers)*

i. Select the categories of your customers

Large scrap dealers [ ] second hand dealers [ ]

Foundries[ ] Casting ingots [ ] any other (specify).....

ii. Select the location of your customers:

Local [ ] East African Community [ ] Rest of Africa [ ]

Europe [ ] America [ ] Asia [ ]

any other (specify) .....

iii. If you have local customers, list them:

(a) ..... (b) ..... (c) .....

(d) ..... (e) ..... (f) .....

iv. Fill the scrap sales information

Customer	soft (tonnes)	hard (tonnes)	Price(shs)/kg
Local	[ ]	[ ]	[ ]
East African Community	[ ]	[ ]	[ ]
Rest of Africa	[ ]	[ ]	[ ]
Europe	[ ]	[ ]	[ ]
America	[ ]	[ ]	[ ]
Asia	[ ]	[ ]	[ ]

(d) Preparation of the scrap *(this section should be filled only by the foundries).*

i. Do you perform scrap cleaning? Yes [ ] No [ ]

ii. Do you perform scrap sorting? Yes [ ] No [ ]

iii. If yes state the various categories the scrap is sorted into.

A. .....

B. .....

C. .....

(e) Processing of the scrap *(this section should be filled only by the foundries).*

i. Do you perform scrap melting Yes [ ] No [ ]

ii. If yes, select the products you cast:

Ingots [ ] billets [ ] slabs [ ] components [ ]

any other (specify) .....

iii. State your average monthly consumption of scrap ..... Kgs.

iv. During the melting of the scrap do you add pure aluminum?

Yes [ ] No [ ]

v. If yes, state your average monthly consumption; .....kg/month.

vi. Select the source of the pure aluminum used.

local [ ] import [ ]

(f) By-Products *(this section should be filled only by the foundries).*

i. Do you generate any by-products during melting and casting?

Yes [ ] No [ ]

ii. If yes, select the by-products you generate:

dross [ ] in-house scrap [ ]

any other (specify) .....

iii. If dross is generated, do you recover aluminium from it?

Yes [ ] No [ ]

iv. If yes, state the approximate quantity of aluminum recovered from the dross ..... Kg/month.

v. If in-house scrap is generated, approximate the quantity ..... Kg/month.

(g) Post casting processes *(this section should be filled only by the foundries).*

i. Do you perform any post casting process? Yes [ ] No [ ]

ii. If yes, select the processes you perform:

Rolling [ ] drawing [ ] extrusion [ ]

forging [ ] any other (specify) .....

iii. During post casting processes, do you generate any in-house scrap?

Yes [ ] No [ ]

iv. If yes, approximate the quantity of in-house scrap ..... Kg/month.

(h) Products *(this section should be filled only by the foundries).*

i. Approximate the weight of the finished ..... Kg/month.

ii. Select the market for your products. Local [ ] Export [ ]

iii. Approximate the proportion of products consumed locally .....%.

iv. Approximate the value in shs/kg of the finished products:

A. consumed locally .....shs/kg

B. exported ..... shs/kg

(i) Research Interest *(this section should be filled by scrap dealers and foundries).*

i. Are you interest in obtaining the research findings?

Yes [ ] No [ ]

APPENDIX D

Drawing of Extrusion Assembly

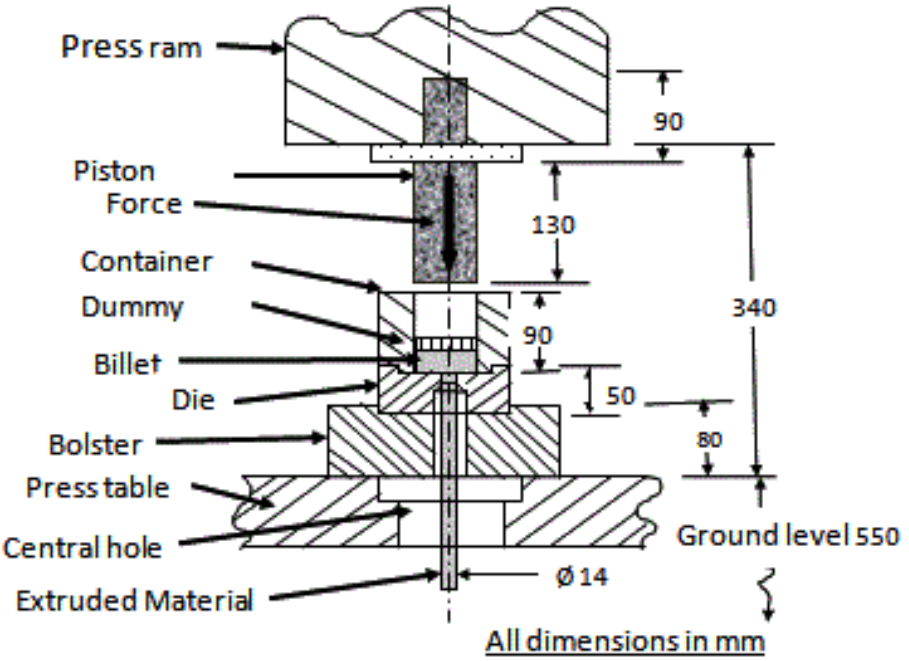

APPENDIX E

Parts of Extrusion Assembly

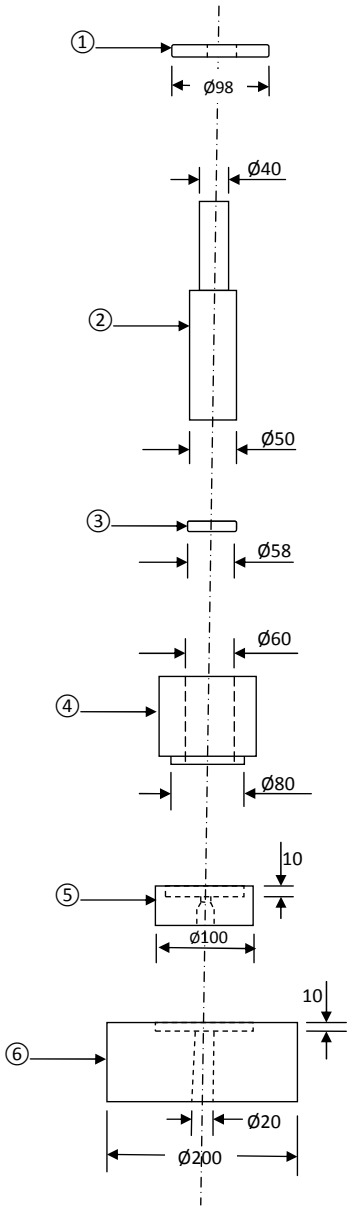

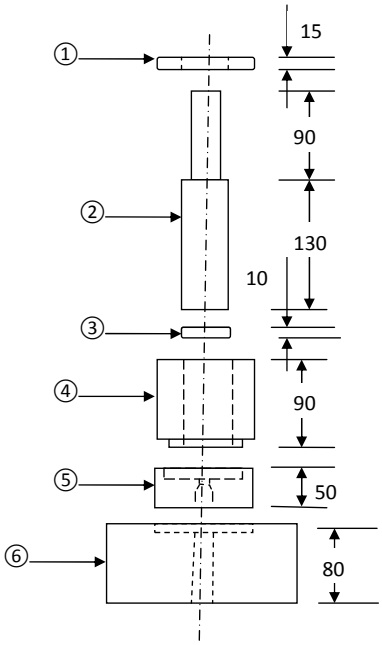

6	Bolster	MS	Ø200	80
5	Die	MS	Ø100	50
4	Container	MS	Ø100	90
3	Dummy	MS	Ø50	10
2	Piston	MS	Ø50	220
1	Washer	Ms	Ø100	15
No.	Part	Material	Width	Length
THE EXTRUSION ASSEMBLY				

MS- Mild steel;

All Dimensions in millimetres

APPENDIX F

Friction Stir Welding Fixture

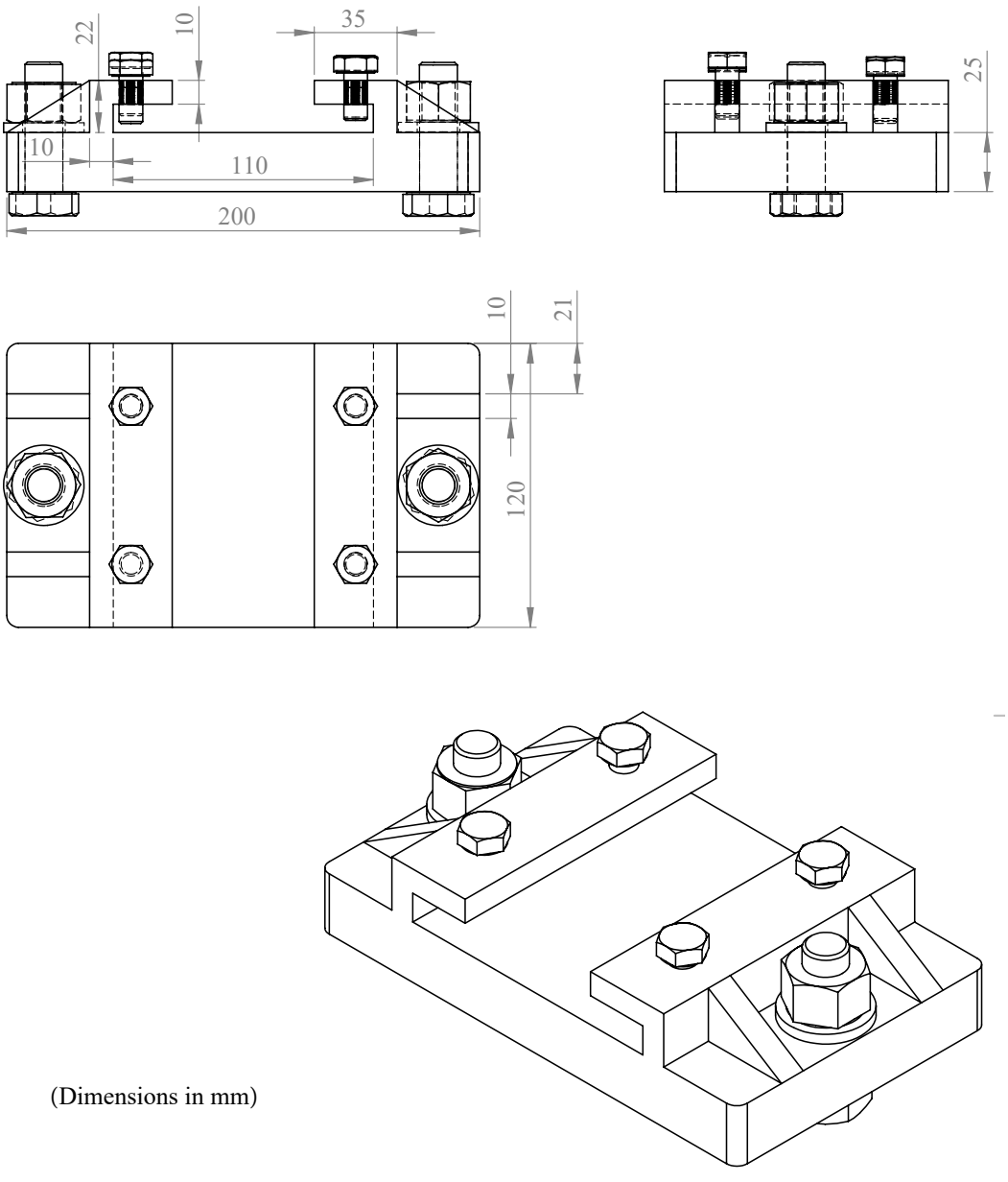

(Dimensions in mm)